THEORETICAL STUDIES OF FUEL CELL REACTION MECHANISMS:

H_2 AND O_2 ON PLATINUM ELECTRODES

by

TIANHOU ZHANG

Submitted in partial fulfillment of the requirements

For the degree of Doctor of Philosophy

Dissertation Advisor: Professor Alfred B. Anderson

Department of Chemistry

CASE WESTERN RESERVE UNIVERSITY

August, 2008

CASE WESTERN RESERVE UNIVERSITY

SCHOOL OF GRADUATE STUDIES

We hereby approve the thesis/dissertation of

Tianhou Zhang

candidate for the Ph. D. degree *.

(signed) Clemens Burda
(chair of the committee)

John E. Stuehr

Anthony J. Pearson

Heidi B. Martin

Alfred B. Anderson

(date) June 30th, 2008

*We also certify that written approval has been obtained for any proprietary material contained therein.

Table of Contents

List of Tables

List of Figures

Acknowledgements

Foremost I gratefully acknowledge my advisor, Professor Alfred Anderson, who shared with me a lot of his expertise and deep insight in science. He inspired me and gave me great motivations in this field and set up an academic role model with passions for me. Without his instructions and patient work with me, this thesis cannot be done. It is hard to overstate Professor Anderson's advice, help and supporting for me.

I have to also thank Dr. Aryanpour and Professor Pitsch of Department of Mechanical Engineering of Stanford University for their great help and making my visiting them a wonderful time.

My thanks and appreciations also go to my committee members, Professor Burda, Professor Stuehr, Professor Pearson, and Professor Martin, for their time and work to make my thesis work through.

Thanks also owed to the Multi-University Research-Institutions (MURI) grant DAAD 19-03-1-0169 from the Army Research Office and the National Science Foundation to Case Western Reserve University fund my PhD project.

I would also like to thank all my friends who make my life that enjoyable. With laughter, smiles, tears, friends are always there for me. Thank you for standing and sharing all the time, especially Xiaoyan, Zhuo, Xin, Jun, Xuefeng.

I also really want to give my gratitude to Miss Barbara Brennan, my land lady. During the past years when I pursuing my PhD study in the United States far from home, she took me like a son making me feel have another family.

Finally, I want to say thanks to my parents, but it is impossible for me to thank them enough. My father, Xiping Zhang, and my mother, Xiulan Lu have been giving me their boundless great love ever since they gave my life. Their caring and encouraging made my life shining in any circumstances. I dedicate this thesis to my parents. I love you.

List of Abbreviations

B3LYP	The Hybrid Density Functional Including Beck's Three Parameter Exchange Functional and Lee-Yang-Parr's Correlation Functional
DFT	Density Functional Theory
e	Charge of an Electron, 1.602×10^{-19} Coulombs
EA	Electron Affinity
GGA	Generalized Gradient Approximation
GTO	Gaussian-Type Orbitals
HER	Hydrogen Evolution Reaction
HF	Hartree-Fock Method
HOR	Hydrogen Oxidation Reaction
IP	Ionization Potential
LANL2DZ	Los Alamos Double Zeta Basis Set Including an Effective Core Potential
LDA	Local Density Approximation
LGER	Linear Gibbs Energy Relationship
LRC	Local Reaction Center Model
MP2	Second Order Møller-Plesset Perturbation Theory

MPB	Modified Poisson-Boltzmann Theory
ORR	Oxygen Reduction Reaction
RHE	Reversible Hydrogen Electrode
RPBE	Revised Perdew-Burke-Ernzerhof Functional
SHE	Standard Hydrogen Electrode
STO	Slater-Type Orbitals

Theoretical Studies of Fuel Cell Reaction Mechanisms:

H_2 and O_2 on Platinum Electrodes

Abstract

by

TIANHOU ZHANG

A quantum-chemistry based constrained variation theory and a local reaction center model were applied to analyze the mechanisms for electron transfer reactions on platinum electrode surfaces in fuel cells. Electrode potential-dependent electron transfer activation energies and transition state structures were calculated, as well reversible potentials for reactions of reaction intermediates.

In the mechanistic study of hydrogen oxidation and evolution on platinum electrodes in basic electrolyte, the Tafel step, Volmer step and Heyrovsky step were studied.

Tafel step: $2H(ads) \rightleftharpoons H_2(g)$

Volmer step: $H^+(aq) + e^- \rightleftharpoons H(ads)$,

Heyrovsky step: $H(ads) + H^+(aq) + e^- \rightleftharpoons H_2(ads)$

The results are consistent with the Tafel-Volmer mechanism for H_2 oxidation and a mixture of Tafel-Volmer and Heyrovsky-Volmer mechanism for H_2 evolution on platinum surfaces in basic electrolyte.

The four one-electron transfer steps were studied for oxygen reduction on platinum in basic electrolyte. The interesting result is that superoxide, O_2^-(ads), forms as the first reduction intermediate in base rather than peroxyl, OOH(ads), which forms in acid electrolyte.

Two- and four-electron O_2 reduction mechanisms in acid were explored using 1-fold and 2-fold Pt adsorption site models. Potentials, for O(ads) and OH(ads) reduction steps were related for acid and base by the Nernst equation plus a constant.

A systematic study of OH(ads) reduction to H_2O in acid electrolyte on platinum and the reverse reaction was carried out in the local reaction center model approach using B3LYP and MP2 calculations employing basis sets with and without diffuse functions. It was found that electrode potential-dependent electron transfer activation energy curves predicted by this method are robust toward shifts caused by changing the external potential.

The potential-dependent conversion of OH(ads) $\cdot\cdot H^+(aq) + e^- \rightleftharpoons OH_2$(ads) on a Pt surface was calculated using a new method combining density functional theory and modified Poisson-Boltzmann theory with a 2-D periodic slab model. The calculated potential corresponding to the structure changing from OH(ads) to H_2O(ads) was close to the experimental reduction potential.

Chapter 1

Introduction of Electron Transfer Theory

Electrochemistry is of great importance especially in the field of energy conversion. Electrochemical cells split every net exergonic chemical reaction into two electrochemical reactions, one at the cathode half-cell and the other at the anode half-cell. In the fuel cells, electrons are the charge carriers that do work in an external circuit and anions or cations are the charge carriers in the electrolyte. Electrochemical reactions happen on the interfaces between the electrolyte and the electrodes. On the cathode, the oxidant species in the electrolyte is reduced by the electrons coming through the external circuit from the anode. On the anode, the reductant species is oxidized and releases electrons to the electrode. The mechanisms of electron transfer reactions at electrode surfaces are poorly understood and have been attracting intense investigations.

The development of electron transfer theory began with Gurney, who proposed the radiationless tunneling mechanism of electron transfer in 1931.[1] During a reduction (or an oxidation), an electron transfers to (or from) the reaction center from (or into) the electrode, without emitting radiation, when its electron affinity, *EA*, (or its ionization potential, *IP*,) matches the electrode's work function, φ, or the negative of the Fermi energy level of the electrode. In 1952, Libby used the tunneling theory, along with the Franck-Condon principle[2,3] to explain the different rates of electron exchange between ferri- and ferrocyanide ions and the electron exchange between ferric and ferrous ions.[4] Libby assumed the electron transfer rate depended only on the Franck-Condon factor. However, such outer sphere reactions had activation energies, typically 0.2 eV - 0.4 eV.[5] That is because the reaction center needs to be reorganized to have the configuration to make the isoergonic (radiationless) electron transfer and then it relaxes to the new equilibrium configuration.[6] R. A. Marcus applied this idea to explaining electron transfer

rates both at electrodes and in solution.[7] The early theoretical work on electron transfer has also been done by Hush,[8] Conway,[9] Bockris.[10] These and other theoretical works dealing with the electron tunneling mechanism were reviewed by Libby.[11]

Later, Anderson developed the atom superposition and electron delocalization molecular orbital (ASED-MO) theory[12,13] and applied it with an electrochemical band shifting technique to address the potential dependencies of CO adsorption sites on Pt and Pd,[14,15] as well as the potential-dependent adsorbate and surface-adsorbate vibrational frequencies for CO on Pt[15-17] and CN^- on Ag.[18] The calculated results successfully predicted that CO shifts to the high-coordinate 3-fold adsorption site as the electrode potential decreases. The shift is due to the weakening of the CO σ donation to Pt and the strengthening of back bonding to the π^* orbital. This is as expected from the Blyholder model,[19] and agrees with experiment.[20,21] The vibrational frequency of C-O on Pt was predicted to increase at higher electrode potentials, a result of weakened back donation from the Pt band to the CO $2\pi^*$ orbitals, the same trend as the experimental observations.[22,23] Holloway and Nørskov estimated the frequency shift for CO adsorbed on a Pt electrode using a model wherein the $2\pi^*$ orbital band of adsorbed CO has a Lorentzian distribution.[24] The electric field at the electrode surface was assumed to be a function of the applied electrode potential and the CO vibrational frequency was calculated using a semiempirical relationship between frequency and the $2\pi^*$ occupation. The CO σ-donation was neglected so the results of Holloway and Nørskov are greater than those of the ASED-MO calculations.[25] These works of Anderson and Nørskov are all non-self-consistent semiempirical which may give significant errors in the energy or structure calculations.

A self-consistent theoretical approach is required by the better accuracy. Ten years ago, Anderson's lab began development of a quantum chemical-based theory employing local reaction center models for calculating the electrode potential dependencies of electron transfer activation energies for adsorbed species. The local reaction center model used for calculating reversible potentials and activation energies for reactions on electrode surfaces relies on the chemical bond as a robust concept. Generally, environmentally induced variations in bond properties, such as strength and vibrational frequency, can be understood as perturbations to a well-defined reference state. A useful representational model for chemical events at the electrochemical interface then needs to include at least enough atoms to represent these bond properties prior to and after introducing an electrochemical perturbation.

The radiationless electron transfer theory of Gurney is adapted to the local reaction center model: the electron transfer takes place when the thermodynamic work function of the electrode, φ, is given by

$$\varphi = eU + 4.6 \text{ eV} \qquad (1.1)$$

where U is the electrode potential on the standard hydrogen electrode (SHE) scale and 4.6 eV is the work function of the standard hydrogen electrode.[26]

The reduction potential for the optimized reaction center is called the reduction precursor potential, U_{rp}. For $U \leq U_{rp}$, the reaction center is reduced without an activation energy on a metal electrode (on a semiconductor electrode $U < U_{rp}$ would be the Marcus inverted region,[27] for which the activation energy is greater than zero) and for $U > U_{rp}$ it

is necessary to overcome an activation energy for reduction because the structure must be distorted so that *EA* increases to a value equal the electrode work function.

For oxidation, the direction of electron transfer is from the local reaction center to the electrode, and it occurs when the ionization potential, *IP*, of the reaction center matches the electrode's work function. An oxidation precursor structure may also be calculated and an oxidation precursor potential, U_{op}, defined. Oxidation is activationless for $U \geq U_{op}$ ($U > U_{op}$ would be the inverted region for semiconductor electrodes) and has an activation energy for $U < U_{op}$. An electron transfer transition state is found by constrained variation theory as the lowest energy structure with the desired *IP* or *EA*. In the very first study using the local reaction center model, the potential of a transferring electron was set to various desired values by adding a lithium complex with adjustable ionization potential to the system and finding the lowest energy structure at which the lithium complex became ionized and the reaction center reduced.[28] The computations did not always converge to the correct electronic state, and so the donor was omitted in subsequent studies. A hydronium ion was the proton source in Ref. 28 and in the subsequent studies of reactions in acid solution, the hydronium ion was given two water molecules of solvation, holding them by hydrogen bonding between an H and a water O. The third H of the hydronium ion was coordinated by a hydrogen bond to the molecule being reduced, forming the reduction precursor (rp). The structure was thus: $\cdots HOH_2(OH_2)_2^+$.[29-31] For the reverse (oxidation) reaction, the conjugate $\cdots OH_2(H_2O)_2$ was hydrogen-bonded to the molecule being oxidized, forming the oxidation precursor (op).

In 1999, Anderson and Albu discovered a linear Gibbs energy relationship (LGER) between the reaction energy and the standard reversible potential for reactions of H_nO_m molecules:[30]

$$U^o = -\Delta E/nF + c \qquad (1.2)$$

In equation (1.2) ΔE is the reaction energy for gas phase species, n is the number of electron transferred, F is the Faraday constant, and c is a constant. This inspired and approach to predicting reversible potentials for surface redox reactions by using using calculated or measured adsorption bond strengths as perturbations to known ΔG^o for the reactions in bulk solutions, as outlined in the following scheme (1.3).[32-38]

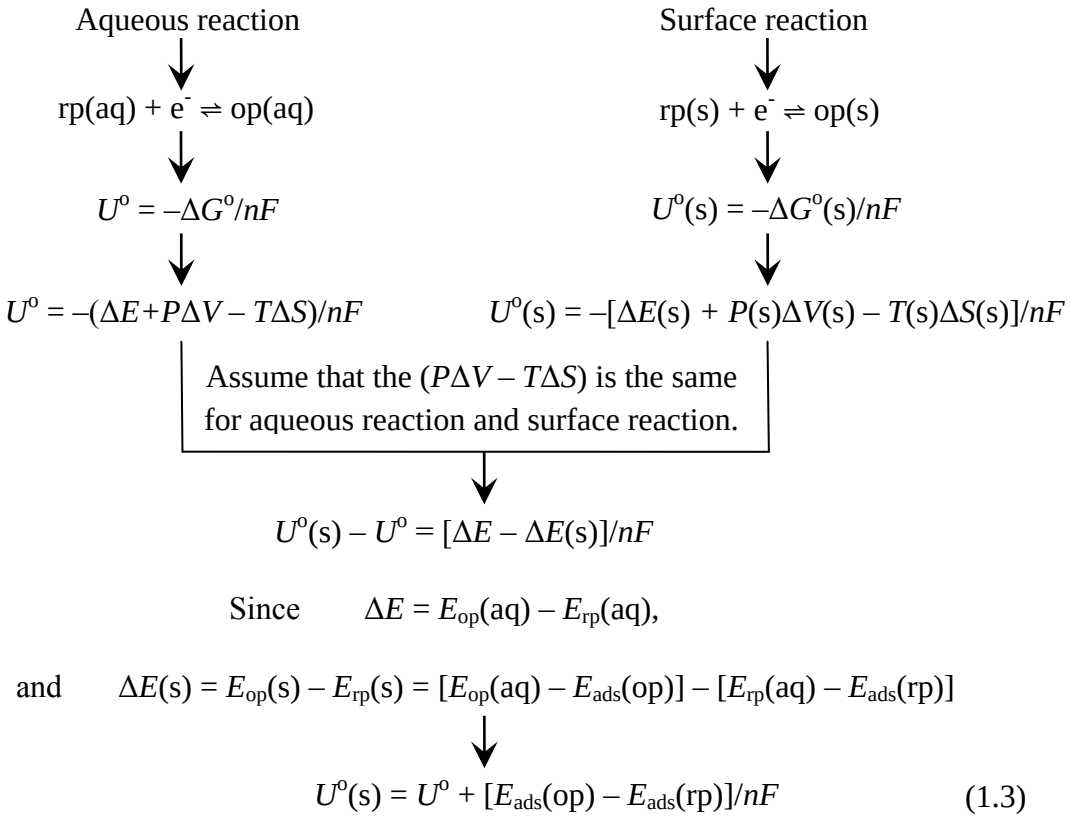

In the above c plays the role of $(-P\Delta V + T\Delta S)/nF$ in solution.

Several interesting applications have been made using this model. The very low overpotential of oxygen reduction reaction on copper laccase was explained.[35,36] Of particular note the active site was not blocked by water molecules and O_2 did not bond strongly to the site. The predicted 0.545 V reversible potential of the OOH(ads) reduction to H_2O_2(ads) on nitrogen-doped graphite by the model matched the observed ~0.55 V current onset potential for H_2O_2 generation on nitrogenated graphite.[38] For cobalt selenide cathodes the linear Gibbs energy relationship predicted 0.61 V as the reversible potential for O_2(ads) reduction to OH(ads) + O(ads) and 0.58 V as the reversible potential for OH(ads) reduction to H_2O(ads). Both were in agreement with the experimental onset potential for oxygen reduction on cobalt selenide, ~0.5 V.[39]

Instead of using the internal energy of the reactions, Nørskov et al. predicted the overpotential of catalyzed oxygen reduction reaction using approximate Gibbs energies.[40] The Gibbs energies were determined using internal energies from slab-band density functional calculations and the entropies from the measurements and calculational models.

As mentioned before, the transition state of an electron transfer reaction is defined as the structure which has the electron affinity, *EA*, in a reduction reaction (or ionization potential, *IP*, in an oxidation reaction) matching the thermodynamic work function of the electrode. This changing structure requires the input of energy, but there are many structures with the requisite *IP*, and the structure with the lowest energy, $E^*(U)$, is sought for the transition state. The activation energy, E_a, at potential U is given by:

$$E_a(U) = E^*(U) - E(U_{op}) \qquad (1.4)$$

A similar situation holds for reduction as the electrode potential is increased from the U_{rp} value. The resulting activation energy for reduction is

$$E_a(U) = E^*(U) - E(U_{rp}) \quad (1.5)$$

$E^*(U)$ is the energy of the transition state structure at potential U. The potential-dependent activation energy is calculated using constrained variation theory. The transition states for the electron transfer reaction were, at first, found by trial and error structure changes, and the energy and *IP* or *EA* were mapped out and the search was done by hand.[28-31,41-47] Later a program was written in the Anderson lab by Kostadinov to do this,[48] and it greatly decreased the time required to find electron transfer transition states in subsequent studies.[49-54] The program employs the Lagrange undetermined multiplier approach, which is a method for finding the extrema of a function of several variables subject to one or more constraints. The Lagrangian function, Λ, for the transition state calculation of an electron transfer reaction is written as:

$$\Lambda(x, \lambda) = \varphi(x) - \lambda[\psi(x) - E_e(U)] \quad (1.6)$$

where x is a vector of structure variables, $\varphi(x)$ is the activation energy, $\psi(x)$ is the electron affinity or ionization potential, $E_e(U)$ is the energy of an electron on the electrode, and λ is the Lagrange multiplier. In seeking the transition state for electron transfer, the constraint condition is that $\psi(x) = E_e(U)$. According to the Lagrangian principle, the transition state is defined as:

$$\nabla_x \Lambda(x^*) = 0 \qquad (1.7)$$

$$\nabla_\lambda \Lambda(x^*) = 0 \qquad (1.8)$$

where x^* is the transition state structure vector.

After the first studies,[28-31,41] which gave suggestive trends, the calculations were made more quantitative by including a potential in the Hamiltonian for the counter ion. This was generated by a negative charge where a hydronium ion was used for acid reactions.[42-55] For reduction reactions in acid, the Coulomb potential field of the counter ion reduced the *EA* of the reaction center and therefore shifted the activation energies and reversible potentials to lower potential. A model with a charge of -1/2*e* located 10 Å from the reaction center or, practically equivalently, -1*e* 20 Å from the reaction center, was chosen, where e stands for the charge of one electron, 1.602×10^{-19} coulombs. The 20 Å spacing represents approximately the average ion spacing in 0.1 M electrolyte. It was proposed that a sum over all electrolyte counter charges, assuming an average rock salt or cesium chloride ionic distribution for the ions in the electrolyte, presented a Madelung potential of the same magnitude, and so the idea of this sum was henceforth used in discussing the addition of a point charge Coulomb potential to the Hamiltonian. The result of this addition was a series of predictions of activation energies, precursor potentials, and reversible potentials for the hydrogen evolution reaction and hydrogen oxidation reaction by the Volmer-Heyrovsky mechanism and for forming under-potential-deposited H atoms on Pt(111) 0.1 M in acid.[47,49,50] These were obtained by MP2 calculations of

structures and internal energies using the Gaussian code with a 6-31G** basis set for the light atoms and an effective core potential with a LANL2DZ basis set for platinum.[56] A single Pt atom was used in the local reaction center model calculations. The Pt-H bond strength was several tenths of an electron-volt higher than for the Pt(111) surface, and so the potential of each potential-dependent activation energy was decreased by V/eV times this quantity. Comparisons with limited experimental data were promising.

Other models have been developed by Savéant[57] and Koper and Voth.[58-60] Savéant developed a simple model describing the kinetics of electron transfer-bond breaking concerted reactions. Koper and Voth extended Savéant's Model by adding the electronic coupling into the model and investigated the solvent effect. Decornez and Hammes-Schiffer presented a theoretical study of proton-coupled electron transfer (PCET) reactions and applied their continuum theory to explain the biological processes.[61-63] Balbuena used internal energy of cluster models and periodic band calculation models to investigate the thermodynamics of adsorptions and reactions on catalysts.[64,65] Neurock also employed band theory to study the catalytic reactions by changing the surface and modeling the counter charge as a uniform charge distribution in the solution region.[66-68]

In this thesis, theoretical studies of the hydrogen evolution and oxidation reactions[53] and the oxygen reduction reaction[54] in base are presented in Chapter 2 and Chapter 3. In these, OH^- solvation was treated by coordinating three water molecules to it. They were held by hydrogen bonding, and each of these water molecules was also given a water molecule coordinated to it, representing a second coordination shell. A diffuse function was added to the O atom basis set to ensure that the reduction precursor structures were reasonable.[32] In Chapter 4, the mechanisms of oxygen reduction reaction in acid is

explored and comparisons with the base results are made. Both 2-fold and 1-fold adsorption models are used. The H^+(aq) is modeled as a hydronium ion in which two hydrogen atoms are hydrogen bonded to one water molecule each. The third hydrogen in the hydronium coordinates to the adsorbed species that is to be reduced on the electrode surfaces. Although the same computational method, B3LYP, and basis set, 6-31+G** are used throughout Chapters 2-4, there are still uncertainties found in the comparisons. A methodological study of OH reduction to H_2O in acid on platinum and the reverse reaction was carried out and is presented in Chapter 5. In this study, the results of the computations using the B3LYP and MP2 methods using the 6-31G** and 6-31+G** basis sets are examined. The electrode potential-dependent electron transfer activation energy curves predicted by this method are found to be robust toward shifts on the potential scale which means one can make useful predictions and explanations by matching one potential point with experimental data. In Chapter 6, an initial study using a newly-developed theoretical method DFT-MPB,[69,70] combined density functional theory and modified Poisson-Boltzmann theory, on liquid-solid interface is presented. The electrode potential dependency of OH adsorption structure on the acid-platinum interface is investigated using this method.

Chapter 2

Hydrogen Evolution on

Platinum Electrodes in Base*

* Based on publication in Ref. 53.

2.1 Background of Hydrogen Oxidation and Hydrogen Evolution Reactions

The hydrogen oxidation reaction (HOR) and hydrogen evolution reaction (HER) have been studied over platinum electrodes since the early 1900s.[1,71-75] Elementary reaction steps for reaction intermediates on electrode surfaces are difficult to determine. It has been suggested recently from Tafel plot (ln*i* vs. *U* where *i* is the current density and *U* is the cathode potential) examinations that hydrogen oxidation in acid solution follows the Heyrovsky-Volmer mechanism on Pt(100) and the Tafel-Volmer mechanism on Pt(111) and (110) surface.[50,76] The reasons for the differences are still unknown. Theoretically predicted activation energies for H_2 oxidation by the Heyrovsky-Volmer mechanism have yielded Tafel plot predictions in agreement with measurements for Pt(100).[50] Over platinum surfaces, the Heyrovsky reaction written in a standard reduction form is

$$H(ads) + H^+(aq) + e^- \rightarrow H_2(g) \qquad (2.1)$$

and Volmer reaction is

$$H^+(aq) + e^- \rightarrow H(ads) \qquad (2.2)$$

In the Volmer-Tafel mechanism for generating H_2, two H(ads) combine by the Tafel reaction:

$$2H(ads) \rightarrow H_2(g) \qquad (2.3)$$

Voltammetric measurements of HER and HOR in base for (100), (111), and (110) platinum electrodes have been analyzed recently.[77] The apparent activation energies for H_2 oxidation at the reversible potential in 0.1 M base are 0.48 eV for the Pt(111) surface and 0.24 eV for Pt(110), but the reasons are unknown and no mechanistic conclusions could be drawn.[77] Non-linearity in both the Tafel and micro-polarization regions prevented the authors of Ref. 77 from estimating an activation energy for the (100) surface. The purpose of this theoretical study is to determine whether the Heyrovsky reaction could occur in base. We found the Heyrovsky step is allowed in the second step reaction and in the first step of oxidation.

In base the Volmer reaction uses a water molecule as the proton source rather than a hydronium ion so that, in place of reactions (2.1) and (2.2), the Heyrovsky and Volmer steps are respectively written:

$$H(ads) + H_2O(l) + e^- \rightarrow H_2(g) + OH^-(aq) \qquad (2.4)$$

and

$$H_2O(l) + e^- \rightarrow H(ads) + OH^-(aq) \qquad (2.5)$$

The cause of the structure sensitivity observed for acid electrolyte in Ref. 76 for the apparent mechanisms for H_2 oxidation over platinum surfaces has not been determined, though it is known that on Pt(100) the Heyrovsky step is taking place with a high

coverage of under-potential-deposited (upd) hydrogen, H(ads). The available active sites for H_2 oxidation are believed to be widely scattered in low concentration on the surface.[76] Such sites are presumably too sterically restricted for H_2 adsorption and dissociation. Other surfaces may also have large amounts of upd hydrogen, but if the Tafel-Volmer oxidation mechanism is being followed, the reaction presumably occurs over sites that permit dissociative adsorption of H_2. It has been known for over thirty years that platinum surfaces in vacuum are active for hydrogen-deuterium exchange,[78-81] and platinum surfaces readily adsorb hydrogen dissociatively and desorb it. Adsorbed CO poisons the exchange reaction.[81] This reactivity is consistent with the Tafel reaction playing a role during H_2 oxidation on electrode surfaces at low upd H coverage. It could be that at high upd H coverage H(ads) poisons the (111) and (110) surfaces of platinum against the Heyrovsky oxidation step, but not the (100) surface.

2.2 Computational Details and the Theoretical Model used in HOR and HER Calculations

During the potential-dependent activation energy and transition state structure calculations, the hybrid density functional B3LYP theory in Gaussian 03[56] was used in this study. An effective core potential and the double-ξ valence orbital (LANL2DZ) basis set were used for Pt and the 6-31+G** basis set was used for O and H. The 6-31+G** basis set, with diffuse functions on O, specified by the +, and polarization functions on O and H, specified by the **, was chosen in accordance with previous work showing it yields good structures and electron affinities for neutral systems.[32] In the prior work, modeling these reactions in acid, diffuse functions, were not included in the basis

set because the electron affinities of the positively charged intermediates were accurate without them.

For eqs (2.4) and (2.5), the H_2O(aq) and OH^-(aq) were modeled with two hydration shells with the forms $H_2O \cdot\cdot(H_2O \cdot\cdot H_2O)_3$ for H_2O(aq) and $OH^- \cdot\cdot(H_2O \cdot\cdot H_2O)_3$ for OH^-(aq). The OH^-(aq) model was structurally optimized. In the subsequent calculations for the OH^-(aq) model and the H_2O model, the optimized OH^-(aq) model structure was used and two variables, the hydrogen bond distances, were optimized. The O-H bond lengths in both shells of water molecules and the angles about the hydrogen bonds were kept fixed but the orientations of the H_2O and OH^- were optimized. See the structure insert in Fig. 2.1.

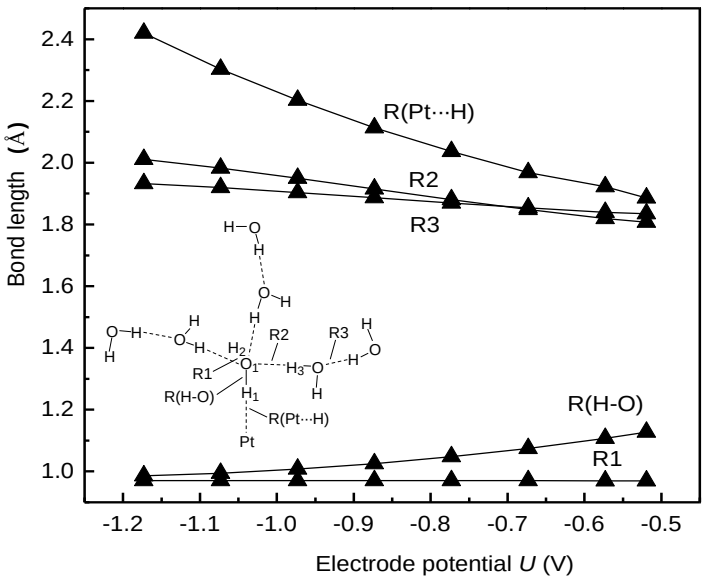

Figure 2.1 Structure model used in the calculations for forming and oxidizing Pt-H bonds in base and potential dependences of transition state parameter values. From Ref. 53.

The purpose of the constraints is two-fold: they reduce the number of parameters, which greatly speeds the determinations of electron transfer transition states, and they correspond to allowing a breathing mode for the solvation shells. This is a reasonable model given the absence of interactions with additional solvent water molecules. A Madelung potential term was added to the Hamiltonian, which corresponds to the sum of electrostatic potential contributions at the reaction center caused by a ~0.1 M mono-hydroxyl basic electrolyte, with the assumption that the hydroxyl ions and compensating cations are distributed in a regular array above the electrode surface. This is called the double layer model for base, and it is the same model used previously for determining reversible potentials for the onset of upd H(ads) and the onset of H_2O(ads) oxidation to OH(ads) on platinum.[32]

2.3 Electrode Potential-Dependent Activation Energies of Volmer step and Heyrovsky step

The reduction and oxidation activation energies were calculated as functions of the electrode potential. Beginning with the optimized reduction precursor, for which the electron transfer activation energy is zero, the electron transfer activation energies at higher potentials were determined using constrained variation theory.[48,82] Similarly, activation energies for the oxidation reaction were calculated for potentials negative of the oxidation precursor potential. The potential where these two curves cross is taken to be the reversible potential for the reaction on the platinum site.[30] This crossing point can also be predicted using the internal energy for the reduction precursor, E_{rp}, the internal

energy for the oxidation precursor, E_{op}, and the energy of the electron on the vacuum scale, -4.6 eV - eU^o:

$$U^o = (E_{rp} - E_{op})/e - 4.6\ V \qquad (2.6)$$

This formula is related to the linear relationship between reaction energies and reaction Gibbs free energies first noted in Ref. 30.

2.3.1 Activation energy of the Volmer reaction, H deposition and removal

The local reaction center model presented in the previous section was used, and adsorption on a Pt 1-fold atop site was modeled. The model was essentially a molecule cut from the electrode surface and electrolyte. Figure 2.1 shows the five internuclear distances that were varied and their values at transition states in the range -1.2 V to -0.5 V. Note that there are three hydrogen bonds of length R2 and three of length R3. The $H_1O_1H_2$ angle in the center water molecule and the $H_1O_1H_2H_3$ dihedral angle, both affecting tilt, were also varied.

The calculated electrode potential-dependent activation energies for the Volmer step may be seen in Fig. 2.2. The reduction precursor potential, U_{rp}, the oxidation precursor potential, U_{op}, and the reversible potential, U_{rev}, are, respectively, -0.154 V, 0.454 V, and 0.128 V vs. the standard hydrogen electrode (SHE). However, because there is a difference between the calculated Pt–H bond strength and the strength of the H adsorption bond to the surface that needs to be adjusted for, this is not the final result. The calculated Pt–H bond is 3.53 eV,[48] while the empirical values of H adsorption bond strength is reported to be 2.75 eV for low H coverage and 2.55 eV for high H coverage.[82]

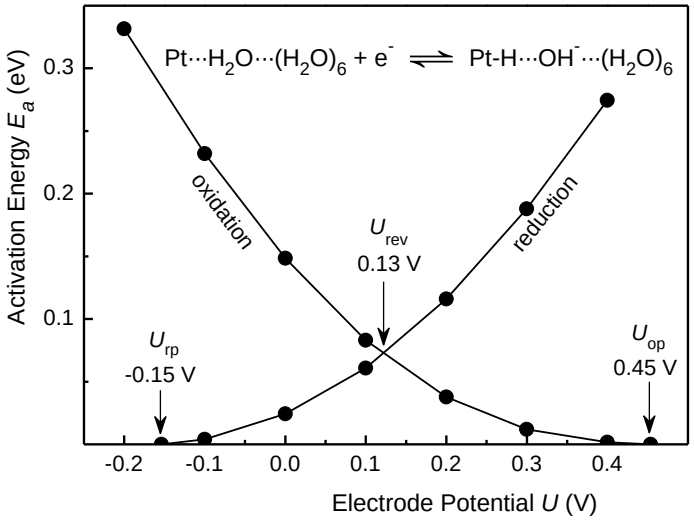

Figure 2.2 Activation energies calculated for the Volmer reaction in base, using the model in Fig. 2.1. Predicted reduction precursor, reversible, and oxidation precursor potentials are shown, corresponding to 0.1 M base on SHE scale. From Ref. 53.

By decreasing the stabilities of Pt–H bond strengths in the above reactions, and assuming the activation energy curves do not change shape, the curves in Fig. 2.2 may be shifted negative by 0.78 V for low H coverage and by 0.98 V for high H coverage to get the final predictions shown in Fig. 2.3.

The predicted reversible potentials are then -0.65 V for low H coverage and -0.85 V for high H coverage. The first result matches an earlier calculation for low coverage.[32] The high coverage value is close to the -0.77 V reversible potential for the hydrogen electrode in 0.1 M base. Voltammograms show the onset potential vs. the reversible hydrogen electrode (RHE) for upd H in 0.1 M base is ~0.35 V for Pt(111).[77] On the standard hydrogen electrode scale, this becomes -0.42 V and compared with the -0.65 V

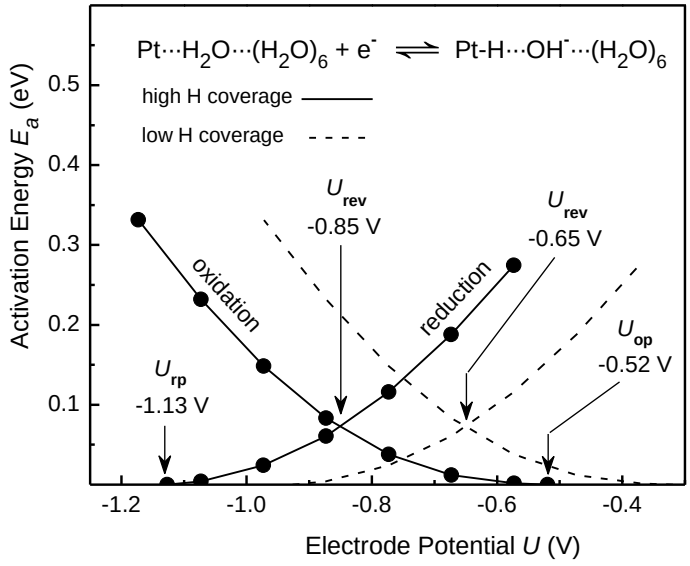

Figure 2.3 The results from Fig. 2.2 after correction for Pt-H bond strength at low and high H(ads) coverage. The SHE potential scale is used. From Ref. 53.

low H-coverage prediction, this is ~0.23 V high. This overestimate can be understood by comparing the base voltammograms with acid ones and applying what was learned in the acid studies to the base studies. A thermodynamic analysis by the Alicante group of carefully prepared and measured single crystal platinum electrodes in acid showed that lateral interaction (Frumkin behavior) accounted for about 0.20 eV of the decrease in upd H free energy of adsorption beginning at 0 V and maximum coverage.[83] The remaining component of the free energy change was shown to be due to the configurational component (Langmuir behavior), and in the low-coverage limit the total free energy change was about 0.4 eV on Pt(111), corresponding to the ~0.4 V onset potential for upd H in acid. The change in upd H adsorption enthalpy and energy were about 0.15 eV for

this surface, and those findings explain why the theoretical studies from this laboratory[47,49,50] that used adsorption bond strengths accounted for only about half of the potential ranges defined by the upd H peaks on Pt(111) in acid. For the Pt(100) and (110) surfaces, the Alicante group deduced much smaller Frumkin effects and evidence was found for overlap of water oxidation voltammetric peaks, forming OH(ads), with the upd H peaks so that onset potentials for upd H were not clearly defined. The voltammograms for 0.1 M base in Ref. 77 are similar: for Pt(111) the base voltammogram is nearly identical to the acid one in the upd H region, and for (100) and (111) surfaces there are similarities to the acid voltammogram that suggest complications from OH(ads) formation and the obscuring of upd H onset potentials.

The electrode potential-dependent structure parameters of the transition states of the Volmer step are in Fig. 2.1. It is seen that the distance between the platinum atom and the hydrogen atom decreases substantially as the potential is increased, that the internuclear distance R(HO) increases, and that the two hydrogen bond distances decrease. These changes all serve to increase the electron affinity of the OH part of the water molecule that becomes solvated OH^-.

The activation energy at the reversible potential, 0.075 V, is low compared to the (111) and (110) values of 0.48 and 0.24 eV from Ref. 77. Contributing factors to the disagreement could be inaccuracies in the theoretical model and also complexities involving surface coverage of H(ads) and H(ads) combination rates.

2.3.2 Activation energy of the Heyrovsky reaction, H_2 formation and oxidation

In base the Heyrovsky reaction is

$$Pt–H \cdot\cdot H_2O \cdot\cdot(H_2O \cdot\cdot H_2O)_3 + e^- \rightleftharpoons Pt \cdot\cdot H–H \cdot\cdot OH^- \cdot\cdot(H_2O \cdot\cdot H_2O)_3 \qquad (2.7)$$

The structure and six varied bond lengths are shown in Fig. 2.4 along with their transition state values for the -1.3 V to -0.5 V electrode potential range. The two tilt angles were also varied and the Pt–H ··H trimer was constrained to be linear.

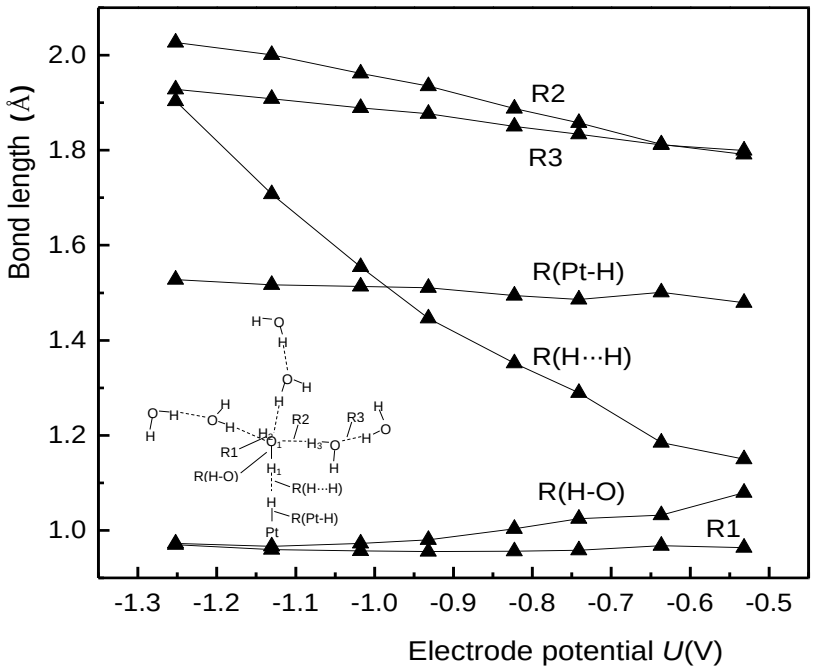

Figure 2.4 Structure model used in the calculations for the Heyrovsky reaction for H_2 formation and oxidation in base and potential dependence of transition state parameter values. From Ref. 53.

The electrode potential-dependent activation energies for the Heyrovsky step on the right hand side in Fig. 2.5 are already adjusted for high-coverage Pt–H bond strength, as

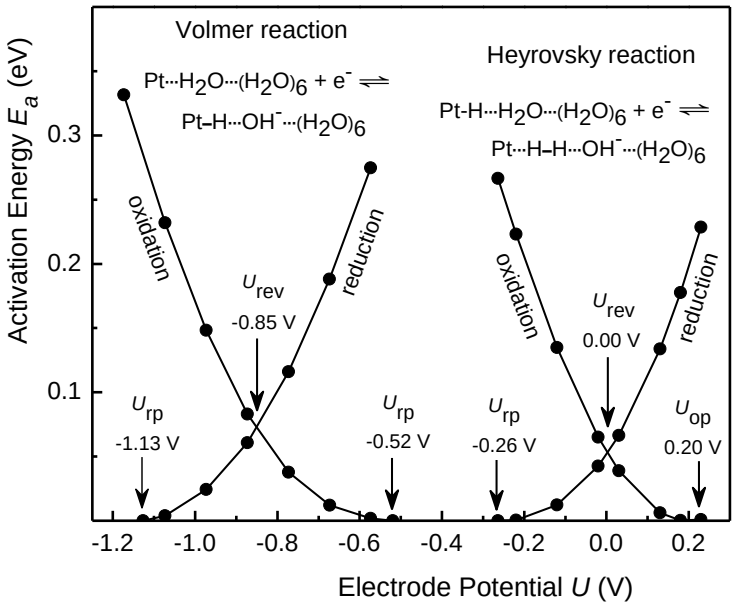

Figure 2.5 Electrode potential-dependent activation energies of Heyrovsky reaction compared with those for the Volmer reaction both for high H(ads) coverage. See caption to Fig. 2.3. From Ref. 53.

are the Volmer step results on the left-hand side. The reduction precursor potential, U_{rp}, the oxidation precursor potential U_{op}, and the reversible potential U_{rev} are, respectively, -0.26 V, 0.20 V, and 0.00 V. In Fig. 2.4 it is seen that R(H–H) shortens rapidly as the potential increases. This is because a H–H σ bond forms after reduction, and to increase the EA to match the Fermi level at high potential the half-filled σ bonding orbital must become more stable, which is accomplished by decreasing the H–H internuclear distance. However over this potential range R(Pt–H) remains ~1.5 Å, indicating a strong Pt-H interaction even in the oxidation precursor, and in the oxidation precursor R(H–H) is long, about 0.4 Å longer than the gas phase molecular value of 0.74 Å. These two observations

show that there is a strong combined interaction between H_2 and the platinum site and hydroxyl. The behavior in acid was similar.[49]

In Fig. 2.5, the reversible potential, U_{rev}, for the Heyrovsky reaction for high H coverage, 0.00 V, is significantly different from the -0.77 V reversible potential of the hydrogen electrode in 0.1 M base and the -0.85 V predicted reversible potential for the Volmer step at high H(ads) coverage. At 0.0V Pt surface will be nearly saturated with OH(ads), but at potentials less than about -0.2 V, for Pt(111) the activation energies apply because the double layer region begins there. For the (110) and (100) surfaces OH(ads) formation interferes with the analysis. The activation energy for the Heyrovsky step for H_2 oxidation at -0.85 V is about 1.2 eV based on the model of having an oxidation precursor on the clean surface at 0.20 V, a potential at which the surface should be blocked by OH(ads). However, the surface is nearly saturated by OH(ads), possibly including O(ads), at that potential, and a study of the oxidation step on a new surface model would be required before drawing any definite conclusion about the activation energy for this step at the reversible potential for the two-electron process. The activation energy for forming H_2 is, however, zero below 0.26 V, which means H_2 formation can follow the Volmer-Heyrovsky mechanism at potentials less than the reversible potential for the two-electron process. The high 0.00 V reversible potential for the Heyrovsky step is the result of the high stability of the Pt ··H ··H ··OH^- complex. The bond strength of H_2 to Pt + solvated OH^- is 1.97 eV, whereas in the acid case the bond strength was calculated to be significantly less, 0.44 eV.[49]

2.4 Conclusions on HER and HOR reactions

This study predicts the interesting result that in base only the Pt–H forming reaction has a reversible potential compatible with the reversible potential for the two-electron HER-HOR reactions and that at potentials less than this both the Tafel combination and the Heyrovsky step are possible for H_2 evolution. The theory predicts that on an idealized clean platinum surface HOR can proceed rapidly by the Heyrovsky-Volmer reaction at a potential 0.85 V greater than the reversible potential for the two-electron process and at intermediate potentials the activation energy for the Heyrovsky step becomes high, implying that only Tafel-Volmer oxidation is possible in this range. However, the actual (110) and (100) surfaces are nearly saturated with OH(ads) over most of this potential range. Thus the idealized model will have to be modified in the future for studying the Heyrovsky step during H_2 oxidation on those two surfaces. These conclusions differ from those presented in the theoretical study of hydrogen oxidation on Pt in acid.[50] In the acid study the Heyrovsky and Volmer steps were both predicted to have reversible potentials close to 0 V for high H(ads) coverage. Thus, the Heyrovsky-Volmer mechanism was predicted to take place for the (110) surface in the low overpotential region, based on comparing the predicted Tafel plot with experiment.[50] The (111) and (110) surfaces had different Tafel behaviors, interpreted as Tafel-Volmer for (100) but for (111) no assignment could be made.[76] The present theory results for base suggest the Tafel-Volmer mechanism for H_2 oxidation and a mixture of Volmer-Tafel and Volmer-Heyrovsky mechanisms for H_2 evolution on platinum surfaces.

Chapter 3

Oxygen Reduction Reaction

on Platinum Electrodes

in Basic Solution

* Based on publication in Ref. 54.

3.1 Background of Oxygen Reduction Reaction in Base

In this chapter we present results of a systematic theoretical study of the four one-electron reduction steps of O_2(ads) in basic electrolyte. Constrained variational theory is used to calculate electron transfer energies as functions of electrode potentials.[48] This is done within a local reaction center model containing the bonds involved in the chemical reaction that occurs upon electron transfer, and a representation of the environment. The procedure has been employed already to explore some of the reactions relevant to oxygen reduction in acid.[30,48,51,84] It will be shown that O_2^-(ads) is the first reduction product and that on an open unrestrained surface site it dissociates into O(ads) + O^-(ads), which are subsequently reduced to two water molecules and four OH^-(aq).

The electrochemical reduction of oxygen on platinum electrodes has been studied for about 40 years. It is the cathode reaction in fuel cells, and the four-electron reduction to water is the desired reaction and the two-electron reduction to hydrogen peroxide is to be avoided. The mechanistic details are not well known. As reviewed by Yeager,[85] two oxygen reduction mechanisms are considered to lead to the water product: the direct 4-electron pathway where the oxygen is reduced to water at the standard electrode potential U^o = 1.229 V,

$$O_2 + 4H^+ + 4e^- \rightarrow 2H_2O \qquad (3.1)$$

and a pathway where oxygen is first reduced to hydrogen peroxide (U^o = 0.695 V) by a 2-electron reduction, followed by a second two-electron reduction to form water (U^o = 1.763 V):

$$O_2 + 2H^+ + 2e^- \rightarrow H_2O_2 \quad (3.2)$$

$$H_2O_2 + 2H^+ + 2e^- \rightarrow 2H_2O \quad (3.3)$$

The figures displayed in this chapter are for 0.1 M base and potentials are reported using the standard hydrogen electrode, SHE, scale. The quoted experimentally measured potentials when referenced to the Ag/AgCl electrode or the standard calomel electrode (SCE) are converted to the SHE scale. When comparisons between theory and experiment are made, the theoretical values, which are our predictions for 0.1 M base, are converted by the Nernst equation to values corresponding to the pH of the experimental measurements and given on the SHE scale.

The release of H_2O_2 into the electrolyte is to be avoided in fuel cell applications because of its corrosive property and because more power is generated by the four-electron reduction. If H_2O_2 bonds strongly enough to the electrocatalyst, it will not be released, and the stability imparted to it by the adsorption bond will shift the potential for forming H_2O_2(ads) to a lower overpotential relative to the 1.229 V four-electron value.

It has been difficult to observe intermediates formed on electrocatalyst surfaces during O_2 reduction in both acid and base electrolytes. There is theoretical[34,51] and indirect experimental[84] evidence that on platinum electrodes in acid electrolyte the first reduction step forms adsorbed peroxyl molecule, OOH(ads). On a crowded adsorption site, usually assumed to be a site where only one oxygen atom can bond, the second reduction then forms H_2O_2, which desorbs. On a more open adsorption site, usually assumed to be a site

where both oxygen atoms can bond, OOH(ads) dissociates, and three electron and proton transfers reduce the O(ads) + OH(ads) to two water molecules.

There is experimental[86-94] and theoretical[95,96] evidence that on platinum electrodes in 0.1M to 1.0 M acid electrolyte OH(ads), a product of water oxidation and an intermediate in O_2 reduction, has a reduction onset potential at low coverage close to 0.6 V. On Pt skins on several platinum alloys containing electropositive transition metals the onset potential is about 50 mV higher. At higher coverage of OH(ads), the potential for reducing OH(ads) to water will increase because the OH(ads) becomes less stable at higher coverage. Theoretical calculations for the oxidation of H_2O(ads) at different potentials in acid electrolyte show that activation energies are low at electrode potentials of 0.6 V and higher, indicating that the reaction is fast at these potentials.[48] From theory, the OH(ads) reduction potential remains low up to the typical working potential of a fuel cell, 0.8 V. However, an additional factor is the decrease in the rate of the O_2 reduction reaction due to the increasing coverage by OH(ads), which will block more and more O_2 adsorption sites as the potential increases. Theory and experiment indicate that the activation energy for reducing O_2(ads) to OOH(ads) at potentials close to 0.8 V is approximately 0.2 eV.[51,84]

Evidence for OOH(ads) formation in acid electrolyte has been found for polycrystalline gold electrodes in the presence of Bi^{3+} by means of surface enhanced Raman vibrational spectroscopy(SERS).[97,98] This electrode had a very high overpotential and poor catalytic activity relative to platinum, which probably allowed the OOH(ads) intermediate to be trapped. With Bi^{3+} present, the reduction on the rotating disc electrode was by four electrons, though it was not determined whether H_2O_2 was an intermediate.

In contrast to reduction in acid electrolyte, where a hydronium ion is the source of the proton and water is a product of the reaction, in basic electrolyte a water molecule is the source of the proton and OH^-(aq) is a product of the reaction. There is evidence for reversible superoxide anion formation in 0.1 M basic electrolyte on a platinized platinum electrode coated with a hydrophobic film.[99,100] The superoxide anion, O_2^-, is the analog in basic electrolyte to the OOH that forms during the first reduction step in acid electrolyte. The pK_a for the peroxyl radical is 4.8,[101] so that in basic solutions it dissociates into H^+(aq) + O_2^-(aq) but in acidic solutions it remains OOH(aq). The standard reversible potential for reducing O_2(g) to OOH(aq) in acid is –0.046 V, and the standard reversible potential for reducing it to O_2^-(aq) in 1.0 M base is -1.159 V.[101] The 1.113 V more negative potential for O_2^-(aq) formation relative to OOH(aq) formation is related to the low adiabatic electron affinity of O_2 even when solvated. The electron affinity of O_2 in the presence of the hydronuim ion is higher, which leads to a higher potential.[30] In Ref. 99, an approximate reversible potential of -0.265 V(SCE) was measured and this is -0.023 V on the SHE scale. This potential is more positive than the -1.100 V potential for forming O_2^-(aq) in 0.1 M base. The different potential and the quasi-reversible character of the voltammograms indicate that the superoxide anion is interacting with the electrode. The reversible potential for the four-electron reduction to water for 0.1 M base is 0.459 V, and so the reversible potential for the O_2^-(ads) step represents an overpotential of 0.477 V relative to this.

The formation of O_2^-(ads) in basic pH = 11 electrolyte has also been observed on a platinum film by comparing cyclic voltammograms and measurements using surface-enhanced infrared reflection adsorption spectroscopy with attenuated total reflection

(ATR-SIERAS).[102] The absorption signal ranged from 1016 cm^{-1} at 0.2 V(Ag/AgCl) to 1005 cm^{-1} at -0.5 V(Ag/AgCl). Since the gas phase value for O_2^- is 1090 cm^{-1},[103] the small shift means the net interaction with the platinum surface and the electrolyte is weak. Calculations suggested the weak interaction correlates with a high (1/2 monolayer) coverage by the superoxide anions.[102] The voltammogram is even more irreversible than that in Ref. 99, so it is difficult to assign an accurate reversible potential for forming adsorbed superoxide ion, but from the data given in Ref. 102, we estimate a value of 0.0 V(Ag/AgCl), or 0.2 V (SHE). The reversible potential for the four-electron reduction to water at this pH is 0.578 V, so the overpotential relative to this is around 0.4 V, relatively low.

The Anderson group has previously used a linear Gibbs energy relationship to determine reversible potentials and therefore probable mechanisms for two-electron[38] and four-electron reduction[35,37,39,104] reactions over various electrocatalytic materials in the past using. In that work it was shown that on the ideal catalyst O_2 should adsorb weakly to the catalytic site to avoid heat and free energy loss, which will increase the overpotential, and the H_2O product should bond weakly to the site so as to not require a high temperature to remove it. On the ideal catalyst each intermediate step will have a reversible potential equal to the reversible potential for the overall four-electron reaction and a small activation energy. The formation potentials for under-potential-deposited (upd) H from water reduction and OH(ads) from water oxidation on platinum in base have been predicted with the same method.[32] The potential for forming OH(ads) at pH = 11 is about 0.2 V negative of the O_2^-(ads) formation potential in Ref. 102, so some surface blocking by OH(ads) in those experiments is likely, just as in the case of acid

electrolyte. The potential for forming upd H in 0.1 M base is 0.5 V negative of the O_2^- (ads) formation potential, so surface blocking by H is unlikely, just as is the case for acid electrolyte.

3.2 Method and Model used in Oxygen Reduction Reaction Calculations

The hybrid density functional B3LYP theory in Gaussian 03[56] was employed for structure and energy calculations. The double-ξ valence orbital (LANL2DZ) basis set and an effective core potential were used for Pt; and for O and H the 6-31+G** basis set was used. The 6-31+G** basis set, with diffuse functions on O and polarization functions on O and H was found to yield good structures and electron affinities for neutral systems in previous work.[32] Both H_2O(aq) and OH^-(aq) were modeled with two hydration shells, the inner one making three hydrogen bonds to the O atom: $H_2O \cdot\cdot(H_2O \cdot\cdot H_2O)_3$ for H_2O(aq) and $OH^- \cdot\cdot(H_2O \cdot\cdot H_2O)_3$ for OH^-(aq). The $OH^- \cdot\cdot(H_2O \cdot\cdot H_2O)_3$ was structurally optimized, with the hydrogen bonds to the O atom given the same value and the ones between the water molecules also made the same but optimized independently of the other three. The structure parameters thus determined were used in subsequent calculations and only the two sets of hydrogen bond distances were reoptimized. To account for the counter ions and the electrolyte field at the reaction center, a Madelung potential term[56] corresponding to a ~0.1 M mono-hydroxyl basic electrolyte, with hydroxyl ions and cations in a regular array above the electrode surface, was added to the Hamiltonian. We call this as the double layer model for base, and it is the same model used previously for determining reversible potentials for the onset of under-potential-deposited (upd) H(ads) and the onset of H_2O(ads) oxidation to OH(ads) on platinum.[32] This is the same model used to calculate reversible potentials and

electrode potential-dependent electron transfer activation energies for the hydrogen oxidation and evolution reactions on platinum in chapter 2 and Ref 53.

3.3 Electrode Potential-Dependent Activation Energies of Oxygen Reduction Reactions on Platinum in Base

For determining the mechanisms of the overall oxygen reduction reaction in basic solution, the local reaction center model included a dual platinum site as was used in previous studies of the reduction steps in acid.[51] The potential-dependent activation energies for each of the four electron transfer steps were calculated using 6-31+G** B3LYP with point charge included. The potentials of the crossing points of the reduction and oxidation activation energy curves are the equilibrium points and are defined to be the reversible potentials.

3.3.1 O_2^-(ads) Formation and its Dissociation

The reduction precursor for the first electron transfer step is shown in Fig. 3.1, where the O_2 is shown bridging the two Pt atoms, spaced 2.775 Å apart as on an unreconstructed surface of bulk platinum, and with a water molecule hydrogen bonded to the left-hand O. The electron transfer forms superoxide, O_2^-(ads):

$$Pt_2O_2 \cdot\cdot H_2O \cdot\cdot (H_2O \cdot\cdot H_2O)_3 + e^- \rightleftharpoons Pt_2O_2^- \cdot\cdot H_2O \cdot\cdot (H_2O \cdot\cdot H_2O)_3 \qquad (3.4)$$

The transition state structure parameters for the potential range studied -0.70 V to 0.02 V, that is, from slightly less than U_{rp} to slightly greater than U_{op}, are shown in Fig. 3.2.

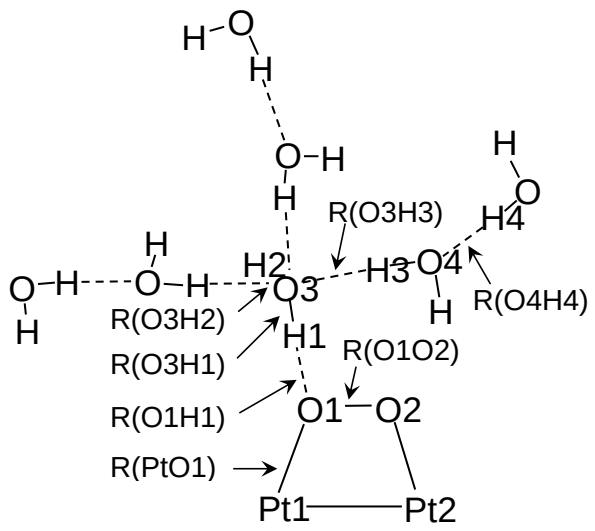

Figure 3.1 Structure model used in the calculations for the O_2^- formation step in base. Internuclear distances optimized in the calculations are defined. From Ref. 54.

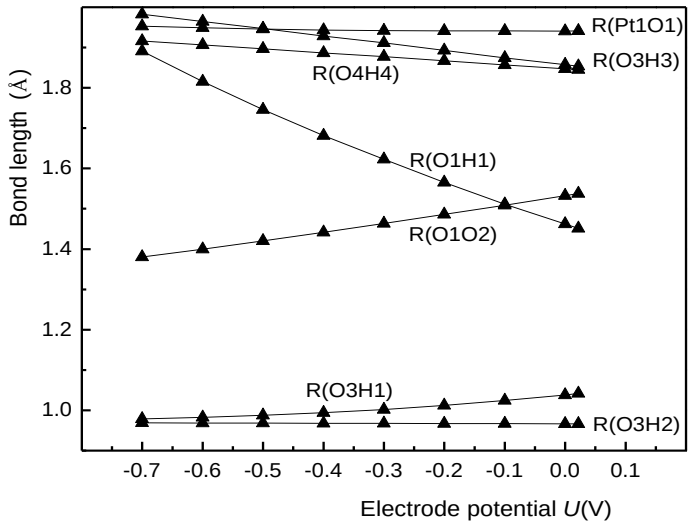

Figure 3.2 Optimized parameters defined in Fig. 3.1 for the electron transfer transition states for forming and oxidizing O_2^-(ads) in base over the potential range ~ -0.7 V to ~ 0.0 V (SHE). From Ref. 54.

The hydrogen atom H1 in the center water molecule was kept in the Pt1-Pt2-O2-O1 plane. A non-planar model might lower the calculated activation energies as shown in the early study for acid solution, but because of the weak interaction in this case, the lowering should be relatively small.[51] The H2-O3-O1-O2 dihedral angle was optimized for the oxidation precursor and this value was used for all subsequent calculations because of difficulties in optimizing this angle when determining electron transfer transition states.

The calculated activation energy curves are in Fig. 3.3. As may be seen in the figure, U_{rp} = -0.60 V, U_{op} = 0.02 V, and U_{rev} is -0.23 V, almost midway between the precursor

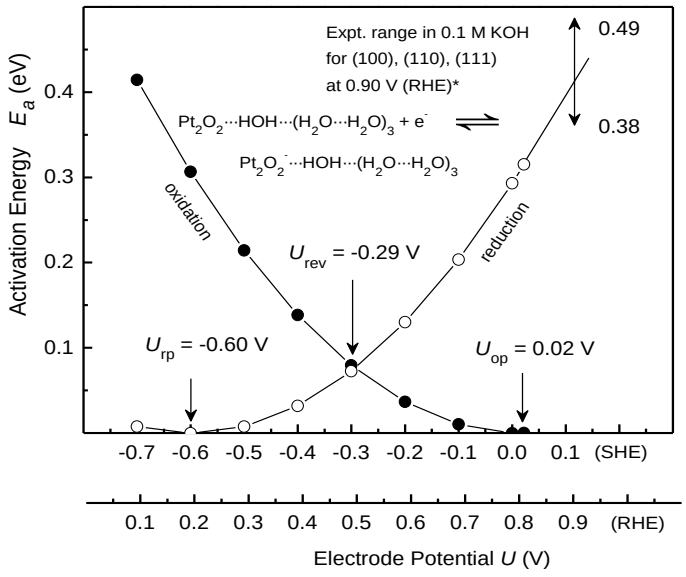

Figure 3.3 Potential dependencies of activation energies calculated for forming and oxidizing O_2^-(ads) in base. From Ref. 54. Structure and structure parameters are shown in Figs. 3.1 and 3.2. Solid dots are calculated results and open circles are derived results (see text). The experimental activation energies from Ref. 105 were reported on the reversible hydrogen electrode (RHE) scale for 0.1 M base and this scale is shown for comparison with the SHE scale.

values. Reversible potentials at the crossing points are in accordance with equation (2.6). The activation energy at the reversible potential is 0.08 eV, a small value. It is noted that the reduction curve, based on open circles in Fig. 3.3, was derived using the transition state structures that were calculated for the values shown as closed circles on the oxidation curve. The circles are "derived points". Derived oxidation activation energies, $E_a^{ox\prime}(U)$, can be determined from calculated reduction activation energies, $E_a^{re}(U)$, the total energies of the reduction and oxidation precursors, E_{rp} and E_{op}, the electron affinity, $EA(U)$, of the system in the transition state structure charged positively by removing an electron from it, and the reduction activation energy, $E_a^{re}(U)$, using the formula:

$$E_a^{ox\prime}(U) = -EA(U) + E_a^{re}(U) + E_{rp} - E_{op} \qquad (3.5)$$

Derived activation energies for reduction are given similarly by the formula:

$$E_a^{re\prime}(U) = IP(U) + E_a^{ox}(U) + E_{op} - E_{rp} \qquad (3.6)$$

The derived points also provide a check of the calculated points that are sometimes erroneous because of convergence difficulties. Computational convergence could not be achieved in the constrained variation calculations for reduction. Results for the subsequent electron transfer steps, for which convergence for the reduction and oxidation calculations did not present a problem, will be given in the following, where the level of agreement between calculated and derived oxidation and reduction curves is within a few hundredths of an electron volt.

That $Pt_2O_2^- \cdot\cdot H_2O \cdot\cdot (H_2O \cdot\cdot H_2O)_3$ is of the form O_2^-(ads) is established from the structure and charge distribution. As Fig. 3.2 shows, over the potential range of the calculations the O-O internuclear distance, R(O1O2) in Fig. 3.2, increases from a bit less than 1.4 Å to a bit more than 1.5 Å. For the reduction precursor it is 1.401 Å, which is close to the low-coverage slab-band density functional result, 1.39 Å quoted for O_2^-(ads) in the absence of any solvation interactions in Ref. 102. For the oxidation precursor the O-O bond length is ~0.15 Å greater than the calculated gas phase O_2^- value of 1.35 Å, which is the same as the 1.35 Å measured value.[103] It may also be seen in Fig. 3.2 that the oxidation precursor has a close hydrogen bonded water molecule, R(O1H1) ~1.45 Å, whereas in the neutral reduction precursor this distance is longer at about 1.8 Å, indicating a weaker electrostatic attraction. This means the added electron charge distribution seems associated with the O_2 part of the reaction center. This is confirmed by the data in Table 3.1 which show that in the oxidation precursor the net O_2 charge minus the net Pt charge is -0.91 e.

Table 3.1 Mulliken charges on the atoms for the first reduction precursor. Atoms defined in Fig. 3.1. From Ref. 54.

Atom	O1	O2	H1	O3	H2	Pt1	Pt2
Charge (e)[a]	-0.582	-0.570	0.555	-1.005	0.398	0.130	0.113

a. *e* stands for the charge of an electron, -1.602×10^{-19} coulombs.

For O_2 reduction in acid it is believed that the first step determines the effective activation energy for the overall four-electron process, and at ~0.30 V overpotential in

0.1 M acid the effective Arrhenius activation energy is about 0.3 eV.[84] Schmidt et al. made Arrhenius measurements of the activation energy of ORR on Pt(111), Pt(100) and Pt(110) at 0.35 V overpotential in 0.1 M base and obtained 0.49 eV, 0.44 eV and 0.38 eV.[105] The reduction curve in Fig. 3.3 shows the activation energy is 0.42 eV at 0.35 V overpotential or 0.88 V on the reversible hydrogen electrode (RHE) scale. This value lies within the experimental range of activation energies for the three surfaces. The theoretical model is quite accurate in this case. In the acid studies, based on the assumption that the first step determines the measured effective activation energy, the theory underestimated the measured value at this overpotential.[51,84]

Unlike in the case of acid, where OOH(ads) was predicted to be the first reduction intermediate, O_2^-(ads) is predicted to be the first reduction intermediate in base. The OOH(ads) intermediate in acid was calculated in previous work to dissociate with a ~0.06 eV activation energy[106] and the resulting O(ads) will be reduced to OH(ads) and OH(ads) is reduced to H_2O. A very similar result is calculated here for base: O_2^-(ads) dissociates with a 0.10 eV activation energy, forming O^-(ads) and O(ads) which are subsequently reduced. The activation energy for breaking the O-O bond in O_2^-(ads) was determined by optimizing the oxidation precursor structure for a series of increasing O_2^- bond length values from 1.64 Å to 2.44 Å and the transition state came at about 1.9 Å.

3.3.2 Proton transfer reaction from H_2O to O^-(ads), forming OH(ads) + OH^-(aq)

The reduction of O^-(ads) was modeled with the two O(ads) on adjacent 1-fold sites on the two Pt atoms, the whole reaction center bearing a -1 charge. The protonation of O^-(ads) involves charge rearrangement, with a proton in H_2O(aq) transferring to the O^-(ads):

$$O^-(ads) \cdot\cdot HOH(aq) \rightarrow OH(ads) + OH^-(aq) \qquad (3.7)$$

To determine the transition state, the OH bond length in the water molecule providing the proton, R(O3H1), was stepped through a sequence of values and the remaining parameters were variationally optimized. The OH was constrained to be in a plane containing the two Pt atoms in order to keep the water molecules in the solvation shell from interacting with the Pt atoms, something that would be blocked by other adsorbed molecules on a surface. The PtOH angle varied from 169.6 ° at the initial hydrogen bonded structure to 139.6 ° at the transition state and at the same time the O1H1 internuclear distance decreased from a hydrogen bond distance of 1.45 Å to 1.04 Å, which is a value approaching the OH equilibrium distance of ~ 0.98 Å. During this, the OH bond in the water molecule increased from 1.04 Å in the initial structure to 2.10 Å in the transition state. The resulting energy barrier was about 0.3 eV, which is less than the activation energies discussed in the previous section.

3.3.3 Reduction of O(ads) to OH(ads)

The single oxygen atom is more stable on the bridging site and this site was used for calculating activation energies for reduction to OH(ads):

$$Pt_2O \cdot\cdot H_2O \cdot\cdot (H_2O \cdot\cdot H_2O)_3 + e^- \rightleftharpoons Pt_2OH \cdot\cdot OH^- \cdot\cdot (H_2O \cdot\cdot H_2O)_3 \qquad (3.8)$$

The reaction center model for this reaction is shown in Fig. 3.4 and transition state values for the six varied internuclear distances determined over the potential range -0.46 V to

0.24 V are in Fig. 3.5. In this model O1, H1, and O2 are constrained to a line that is perpendicular to the platinum axis in recognition that steric interactions with coadsorbed molecules should prevent this angle from becoming very small. It is known from density functional slab-band calculations using the Vienna Ab-initio Simulation Package (VASP) that OH(ads) may be slightly more stable on a 1-fold site of Pt(111) surfaces and that the OH tilts over on the surface, forming a 110.6 ° angle to it,[33] whereas the present model corresponds to 180 ° or no tilt. The H1O2H2H3 dihedral angle was 99.2 ° and the H1O2H2 angle in the center water molecule was 106.5 ° for the reduction precursor, and for the oxidation precursor these angles became 84.3 ° and 106.6 °.

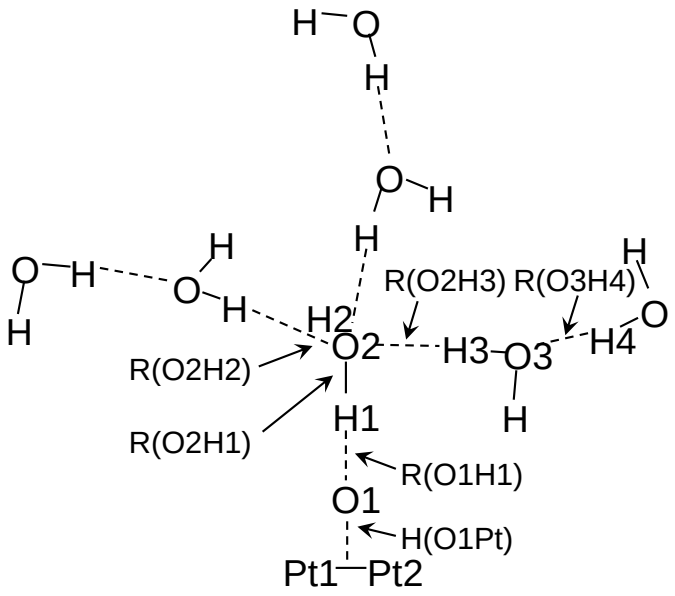

Figure 3.4 Structure model used in the calculations for the reduction of O(ads) on a 2-fold site to OH(ads) in base. Internuclear distances optimized in the calculations are defined. Angle constraints were imposed as discussed in the text. From Ref. 54.

For the transition state determinations the dihedral angle was given a constant value and the average value 91.7 ° was used. In the transition states the H1O2H2 angle hardly changed and went through a maximum of 106.7 ° at the reversible potential.

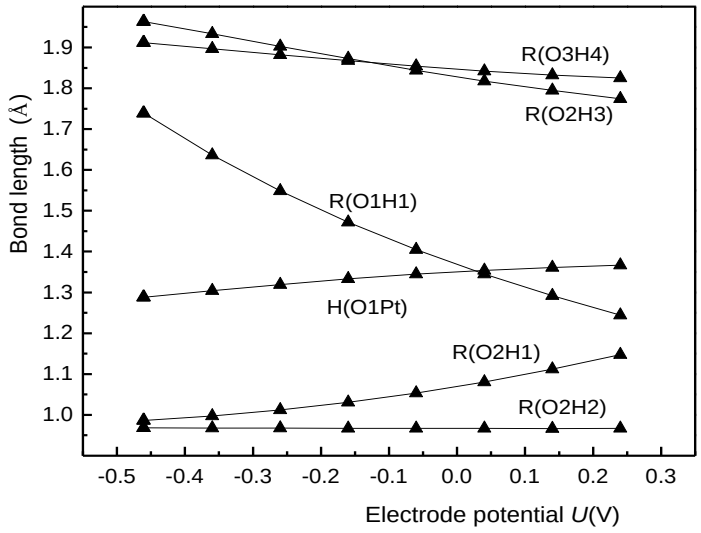

Figure 3.5 Optimized parameters defined in Fig. 3.4 for the electron transfer transition states for forming and oxidizing OH(ads) on a two-fold site in base over the potential range ~ -0.5 V to ~ 0.2 V (SHE). From Ref. 54.

To determine the effect of the constraint to linearity in the structure, calculations were made with the XO1H1 angle as a variable, where X is in the center of the PtPt axis, and with the dihedral angle at 91.7 °, and the water angle at 106.5 °. The result was small stabilizations, 0.01 eV for the reduction precursor and 0.13 eV for the oxidation precursor. The angle decreased slightly to 174.4 ° for the reduction precursor and for the oxidation precursor, there was large change to 119.6 °. However, these small changes energy mean that constraining the XO1H1 to 180 ° did not affect the activation energies significantly.

At the transition states R(O1H1) shortens rapidly as the potential increases, as shown in Fig. 3.5, which is consistent with the formation of OH(ads). At the same time, the distance between OH(ads) and Pt and the hydrogen bond distance to the newly forming OH^-(aq) both increase.

The calculated electrode potential-dependent activation energies for the OH(ads) formation step are in Fig. 3.6, where it may be seen that U_{rp}, U_{op}, and U_{rev} are -0.46 V, 0.04 V and -0.24 V. The activation energy at the reversible potential is 0.06 eV. The activation energy at 0.35 V overpotential is 0.36 eV, which similar to the activation energy that was calculated for forming OO^-(ads) in the first reduction step.

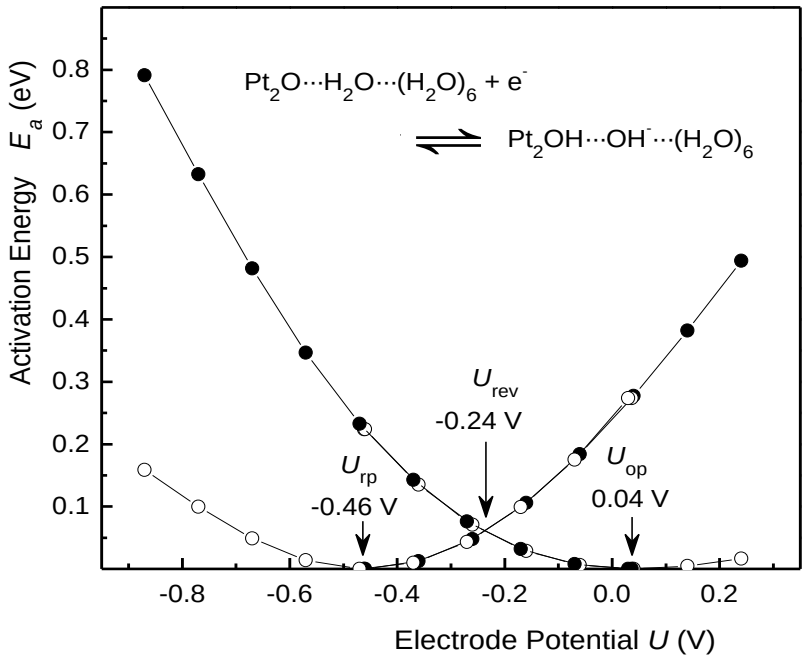

Figure 3.6 Potential dependencies of activation energies calculated for forming and oxidizing OH(ads) on a bridge site in base. Structure and structure parameters are shown in Figs. 3.4 and 3.5. Solid dots are calculated results and open circles are derived results (see text). From Ref. 54.

3.3.4 Reduction of OH(ads) to H_2O(ads)

The protonation of O^-(ads) and the reduction of O(ads) each yielded OH(ads). The reduction of OH(ads) to H_2O(ads) was modeled by

$$Pt_2OH \cdot\cdot H_2O \cdot\cdot (H_2O \cdot\cdot H_2O)_3 + e^- \rightleftharpoons Pt_2OH_2 \cdot\cdot OH^- \cdot\cdot (H_2O \cdot\cdot H_2O)_3 \qquad (3.9)$$

The OH species favors 1-fold sites on platinum and the structure model is shown from two perspectives in Figs. 3.7 and 3.8. The H5O1Pt1Pt2 dihedral angle was fixed at 105.91 °, a value taken from previous calculations in Ref. 32.

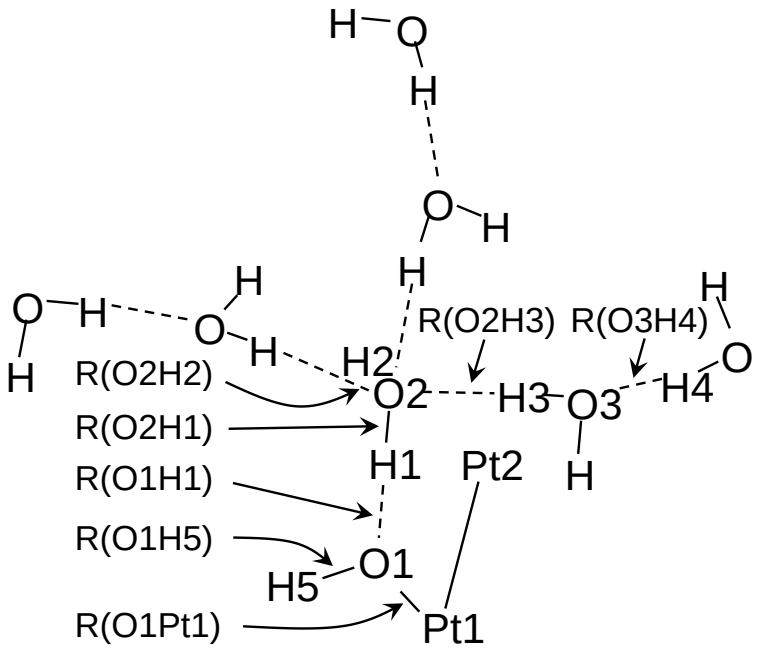

Figure 3.7 Structure model used in the calculations for the reduction of OH(ads) on 1-fold site to OH(ads) in base. Internuclear distances optimized in the calculations are defined. Angle constraints were imposed as discussed in the text. For a second view clarifying the structure, see Fig. 3.8. From Ref. 54.

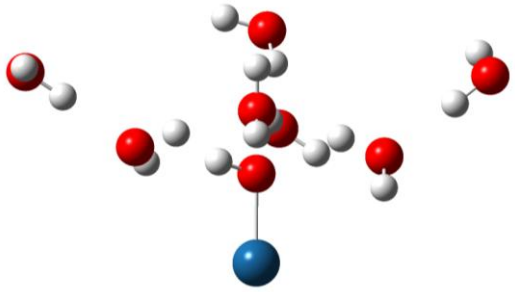

Figure 3.8 Ball and stick view of Fig. 3.7 looking down the PtPt axis. From Ref. 54.

The seven varied bond lengths are shown in Fig. 3.9 along with their values over the electrode potential range -0.49 V to 0.92 V. The H1O1Pt1 angle and H5O1Pt1 angle were also varied, taking respective values in the case of 121.5 ° and 105.4 ° for the reduction precursor; and 123.6 ° and 110.0 ° for the oxidation precursor. Figure 3.9 shows how the bond lengths change from the PtOH ··H-OH reduction precursor to the $PtOH_2$ ··OH^- oxidation precursor.

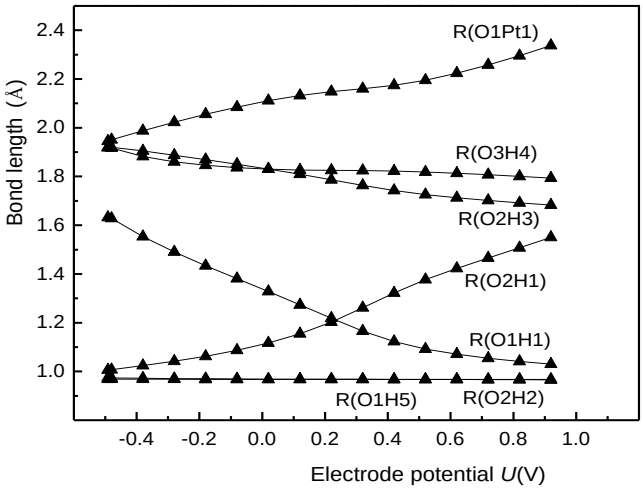

Figure 3.9 Optimized parameters defined in Fig. 3.7 for the electron transfer transition states for forming and oxidizing H_2O(ads) on a one-fold site in base over the potential range ~ -0.5 V to ~ 0.9 V (SHE). From Ref. 54.

The calculated electrode potential-dependent activation energies for the OH reduction step are in Fig. 3.10. The reduction precursor potential U_{rp}, the oxidation precursor potential U_{op}, and the reversible potential U_{rev} are respectively -0.49 V, 0.67 V and -0.26 V. The activation energy at the reversible potential is 0.09 eV, and the activation energy is 0.42 eV at 0.35 V overpotential (0.88 V on the RHE scale), also similar to the activation energy of the first step.

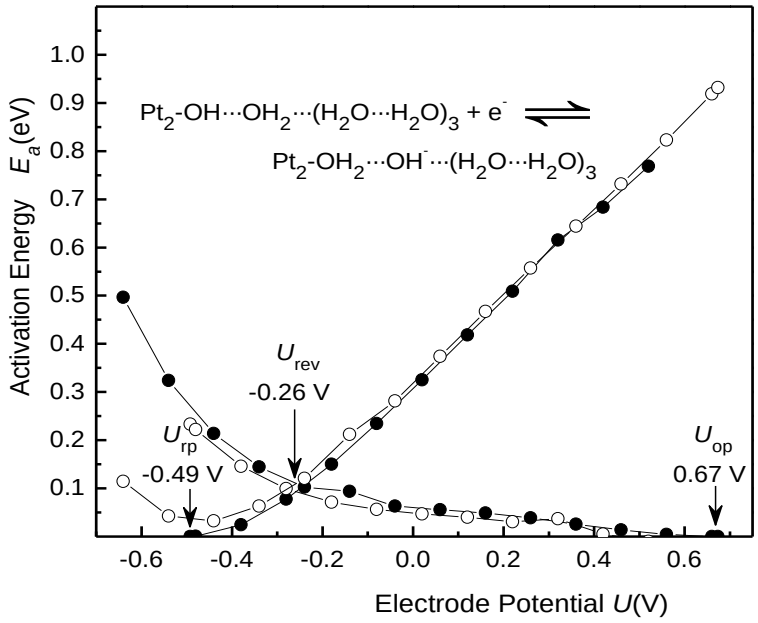

Figure 3.10 Potential dependencies of activation energies calculated for forming and oxidizing H_2O(ads) on a one-fold site in base. Structure and structure parameters are shown in Figs. 3.7 and 3.9. Solid dots are calculated results and open circles are derived results (see text). From Ref. 54.

3.4 Conclusions on Oxygen Reduction Reactions on Platinum in Base

All of the three types of electron transfer steps are predicted to have similar properties. The predicted reversible potentials for 0.1 M base are: -0.29 V for O_2(ads) reduction to

O_2^-(ads), -0.24 V for O(ads) reduction to OH(ads), and -0.26 V for OH(ads) reduction to H_2O(ads). All three of the electron transfer steps have low activation energies at these potentials, ranging from 0.06 eV to 0.09 eV. The calculated reversible potential for forming O_2^-(ads) is 0.27 V negative of result reported in Ref. 99 and it becomes -0.17 V at *pH* = 11, which is 0.4 V negative of our estimate from the results reported in Ref. 102. We consider this to be reasonable agreement considering the simplicity of the reaction center model and the uncertainties in the experimental estimates of the reversible potentials. The calculated activation energies at 0.35 V overpotential (0.88 V on the RHE scale) are all about the same: 0.42 eV for forming O_2^-(ads) from O_2(ads), 0.36 eV for forming OH(ads) from O(ads) and 0.42 eV for forming H_2O(ads) from OH(ads). The reversible potential for reduction of O_2 to O_2^-(aq) is -0.284 V,[101] which is nearly the same as the value predicted here for forming O_2^-(ads). The less negative values on the platinum electrodes suggest that O_2^- bonds ~0.3 eV more strongly to the catalytic site than O_2. All of the activation energy values lie close to or within the 0.38 eV to 0.49 eV range reported experimentally in Ref. 105 for three single crystal surfaces at this potential. Thus, based on the present model study, it is not possible to say that one of the steps dominates and it is probable that the rate of the four-electron reduction is a function of rate constants for more than one electron transfer step. Based on adsorption bond strengths calculated for this model of the catalytic site,[51] once the reduction is complete, the two water molecules can be displaced by an O_2 molecule, so the cycle can repeat.

Chapter 4

Oxygen Reduction Reaction

on Platinum in Acid

4.1 Background of Oxygen Reduction Reaction in Acid

On a working cathode, the overpotential for the four-electron reduction of oxygen is about 0.4 V and since the standard reversible potential in acid is 1.229 V, the cathode potential is approximately 0.8 V. As the potential is increased from the double layer potential range to above 0.6 V – 0.7 V, a platinum electrode surface begins to become blocked by OH(ads) formed from either water oxidation or as an intermediate in the oxygen reduction reaction. It is believed that as the potential is increased up to ~0.8 V the surface becomes sufficiently blocked that the adjacent dual platinum sites that are needed for the four-electron reduction to take place are no longer available. At potentials less than approximately 0.695 V, which is the standard reversible potential for oxygen reduction to hydrogen peroxide in acid, reduction can proceed by a two-electron pathway. In fact, the four-electron process dominates as the potential decreases to approximately 0.3 V, where ring-disk experiments show hydrogen peroxide generation begins in 0.1 M acid.[107] Evidently, under-potential-deposited hydrogen is blocking sites at potentials from 0.3 V to 0.0 V, leaving isolated platinum adsorption sites on which oxygen can only be reduced by two electrons to hydrogen peroxide, which desorbs. In this study both four-electron and two-electron reductions were considered. The four one-electron transfers that take place during oxygen reduction to water on platinum in 0.1 M acid are investigated in this section to develop a mechanism for comparison with the earlier 0.1 M base study of Chapter 3, also in Ref. 54.

4.2 Mechanisms of Oxygen Reduction Reactions on Platinum electrodes in Acid Solution

For modeling the bridging of the two O atoms in O_2, in what is generally believed to be the first step in its four-electron reduction to water, at least two Pt atoms are needed. In the calculations they are fixed at the bulk spacing, 2.775 Å. MP2 calculations would not converge properly to electronic ground states for this system, so a switch to B3LYP was made. For the first reduction step, forming OOH(ads), the calculated U_{rp} and activation energies were in close enough agreement with experimental determinations and this supported the suggestion that the first reduction step in the four-electron process limits the current at electrode potentials of ~0.8 V and less.[51,84] The present study includes an exploration of all four one-electron transfer steps that take place during oxygen reduction to water in acid. The B3LYP hybrid density functional method was used with the 6-31+G** basis set, with the point charge added to the Hamiltonian to model the sum of electrostatic contribution of ions in the 0.1 M electrolyte to the potential at the reaction center.

In Anderson's lab, the theoretical studies of oxygen reduction reactions have also been done previously using MP2/6-31G** calculations[29,31] and B3LYP/6-31G** calculations.[38,51]

4.2.1 Four-electron Reduction on the Dual Platinum Site in Acid

The O_2 molecule bonds to the Pt_2 model with a stability of 0.94 eV and a dissociation activation energy of 0.74 eV, according to B3LYP calculations without the diffuse function.[106] Density functional band calculations yielded a molecular adsorption bond strength of ~0.7 eV on the extended (111) surface.[34] The present calculations with the diffuse functions gave an adsorption bond strength of 0.85 eV. The energy loss upon oxygen adsorption generates heat and insures there will be an overpotential for platinum

cathodes, a concept introduced recently in a study of copper laccase cathodes.[35,36] Based on the calculated activation energy, O_2(ads) should be stable toward dissociation. Consequently, the first reduction step might be expected to form OOH on Pt_2 according to

$$Pt_2O_2\cdots H^+OH_2\cdots(OH_2)_2 + e^- \rightarrow Pt_2OOH\cdots OH_2\cdots(OH_2)_2 \qquad (4.1)$$

The structure of the reduction precursor for this step, with O_2 di-σ bonded to the two Pt atoms, is shown in Fig. 4.1. The Pt-Pt distance is assigned the bulk value of 2.775 Å. Considering the surface crowding that would be present on an actual electrode, Pt1, Pt2, O1, O2, and H1 were constrained to be in the same plane and the O2H1O3 angle was kept linear. The hydronium ion was rotated so that the local reaction center model had C_{2v} symmetry. For transition state calculations, the bond angles and dihedral angles were fixed at the values of the optimized oxidation precursor structure, as was done for OH reduction in the previous section.

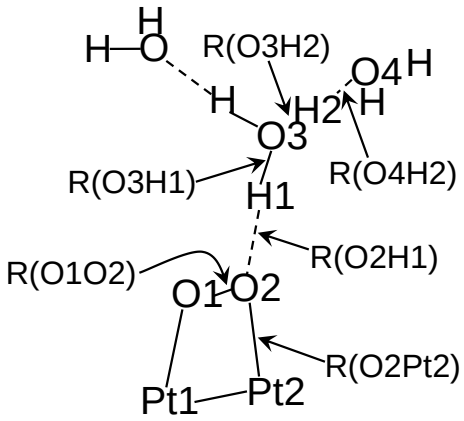

Figure 4.1 Structure model used for Pt_2O_2 reduction and Pt_2OOH oxidation calculations in acid. Internuclear distances optimized in the calculations are defined. Angle constraints were imposed as discussed in the text.

The potential-dependent transition state structure parameters are shown in Fig. 4.2. The O-H^+ bond stretched and O2···H internuclear distance decreased to increase the electron affinity of the positive local reaction center model as the electrode potential was increased. For the oxidation of Pt_2OOH, the shortening of the O3H1 bond in the neutral structure served to decrease the ionization potential of the structure to match the reduced electrode work function caused by the potential decrease.

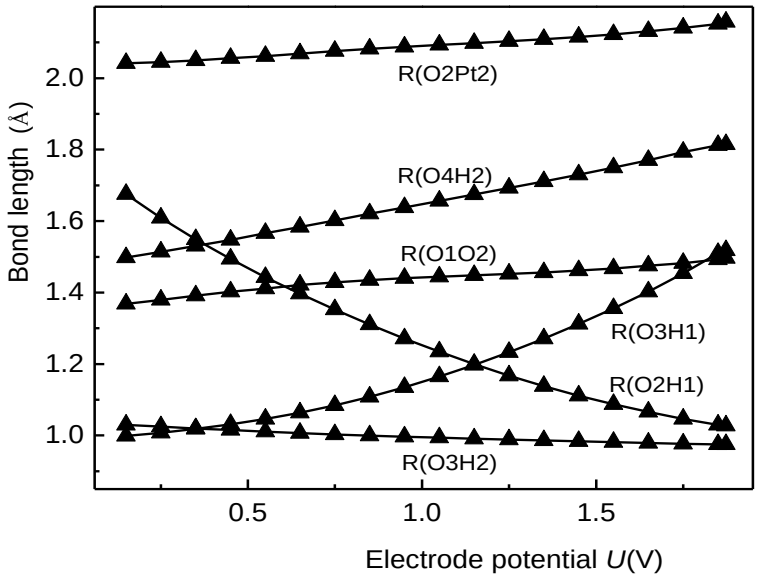

Figure 4.2 Potential dependencies of transition state parameters (Fig. 4.1) for Pt_2O_2 reduction and Pt_2OOH oxidation in acid calculated using B3LYP 6-31+G** with the point charge in the Hamiltonian.

The activation energy curves are shown in Fig. 4.3. The reduction precursor potential, oxidation precursor potential, and the reversible potential are, respectively, 0.33 V, 1.87 V and 1.08 V. The reduction precursor potential is in the 0.2 V to 0.4 V range that was deduced from extrapolations of Tafel-plots by Damjanovic, Conway and Sepa.[108-111] A

value of 0.39 V was obtained for the reduction precursor potential in an earlier calculation using the 6-31G** basis set for oxygen atoms.[51] The activation energy at the calculated reversible potential in Fig. 4.3 is 0.24 eV. In the earlier study the reversible potential was ~0.73 V with an activation energy of ~0.14 eV. The differences show that these two parameters are sensitive to the presence of the diffuse function.

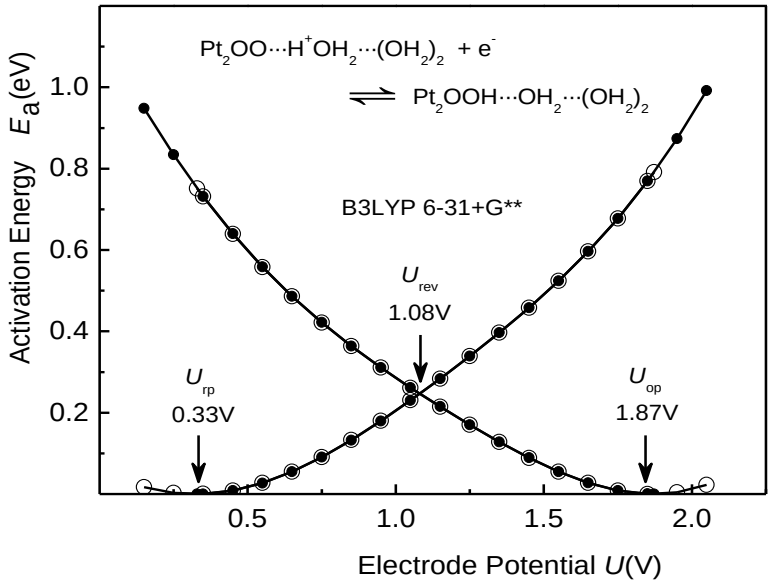

Figure 4.3 Potential dependencies of activation energies for Pt_2O_2 reduction and Pt_2OOH oxidation in acid calculated using B3LYP 6-31+G** with the point charge in the Hamiltonian. Dots are calculated points and circles are derived points.

A small 0.05 eV activation barrier was calculated for breaking the O-O bond in Pt_2OOH. This is nearly the same as the 0.06 eV barrier determined in the absence of the diffuse functions in Ref. 106. The dissociation barrier for the O-O bond in the oxidation precursor was also small, and so dissociation to O and OH on the catalyst will be rapid. Consequently, we will study next the reductions of Pt_2O to Pt_2OH and Pt_2OH to Pt_2OH_2.

An oxygen atom favors the bridging site on the Pt_2 model, so we carried out its reduction to OH(ads) on this site:

$$Pt_2O\cdots H^+OH_2\cdots(OH_2)_2 + e^- \rightarrow Pt_2OH\cdots OH_2\cdots(OH_2)_2 \qquad (4.2)$$

The local reaction center model is shown in Fig. 4.4. In this model, atoms O1, H1 and O2 were constrained to be linear and perpendicular to the Pt1-Pt2 bond because the adsorbed $O\cdots H_3O^+(aq)$ group would otherwise get too close to other Pt atoms in an extended surface. As usual, the angles were fixed to the values in the oxidation precursor.

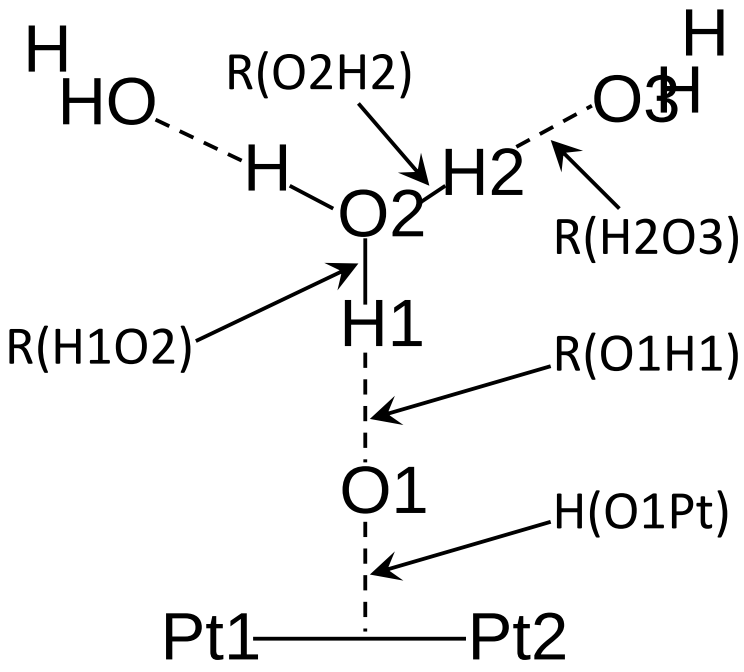

Figure 4.4 Structure model used in the calculations for bridging Pt_2O reduction and bridging Pt_2OH oxidation in acid using B3LYP 6-31+G**. Internuclear distances optimized in the calculations are defined. Angle constraints were imposed as discussed in the text.

The potential-dependent structure parameters are in Fig. 4.5, where there is evidence for convergence problems around 1.4 V to 1.5 V. This is associated with the gap in the calculated activation energies shown in Fig. 4.6, but the gap was filled in by fitting the data with a 3rd order polynomial. The reduction and oxidation precursor potentials, are respectively, 0.54 V and 1.97 V and the reversible potential is 1.11 V, which is close to the experimental onset potential of ~1.0 V.[87] The activation energy at the reversible potential is 0.19 eV.

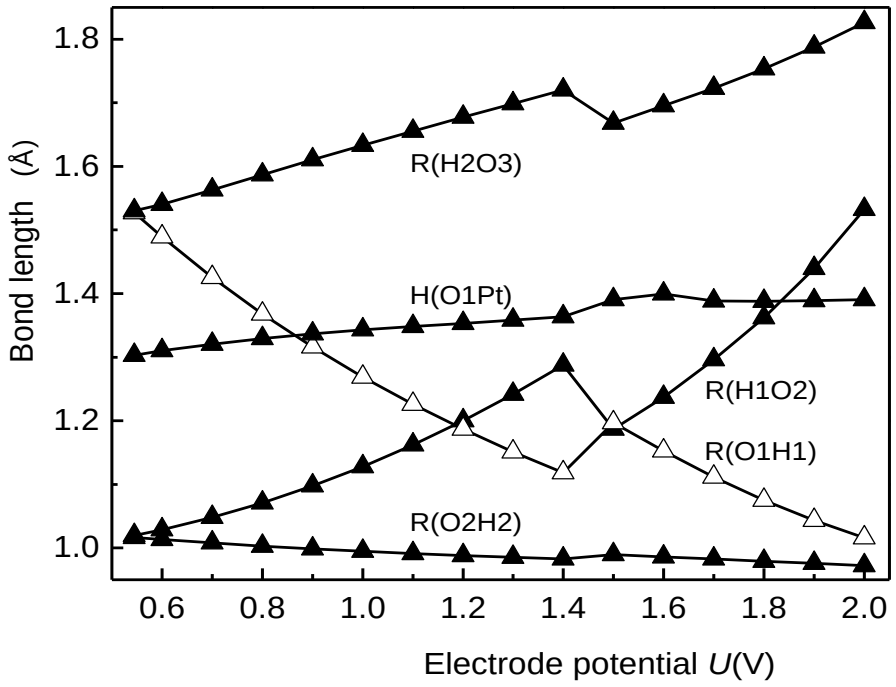

Figure 4.5 Potential dependencies of transition state parameters (Fig. 4.4) for bridging Pt_2O reduction and bridging Pt_2OH oxidation in acid calculated using B3LYP 6-31+G** and the point charge in the Hamiltonian.

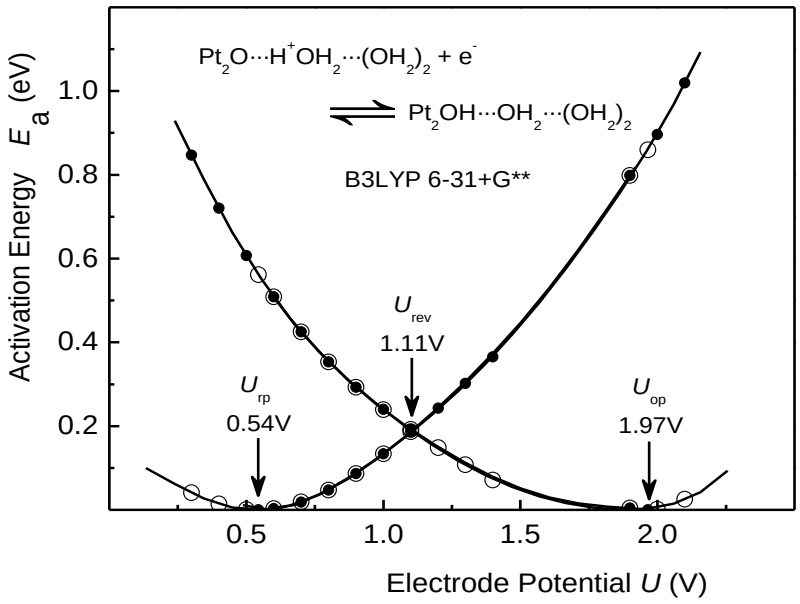

Figure 4.6 Potential dependencies of activation energies for bridging Pt_2O reduction and bridging Pt_2OH oxidation in acid calculated using B3LYP and 6-31+G** with the point charge in the Hamiltonian. Dots are calculated points and circles are derived points.

The OH bonds strongest on the 1-fold site of Pt_2, and its reduction to H_2O on the 1-fold site was carried out in the same manner as for the single Pt atom in section 3:

$$Pt_2OH\cdots H^+OH_2\cdots(OH_2)_2 + e^- \rightarrow Pt_2OH_2\cdots OH_2\cdots(OH_2)_2 \qquad (4.3)$$

As usual, the bond angles and dihedral angles were fixed at the values of the optimized neutral oxidation precursor structure. This structure is shown in Fig. 4.7, the potential-dependent parameters are in Fig. 4.8, and the activation energies are in Fig. 4.9.

The reduction precursor, oxidation precursor, and the reversible potentials are, respectively, 0.50 V, 1.92 V, and 1.24 V. This reversible potential is 0.08 V less than

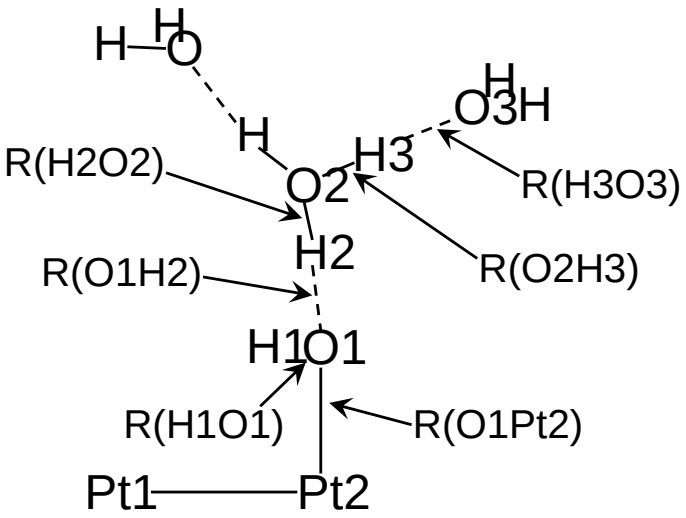

Figure 4.7 Structure model used for 1-fold Pt_2OH reduction and 1-fold Pt_2OH_2 oxidation in acid. Internuclear distances optimized in the calculations are defined. Angle constraints were imposed as discussed in the text.

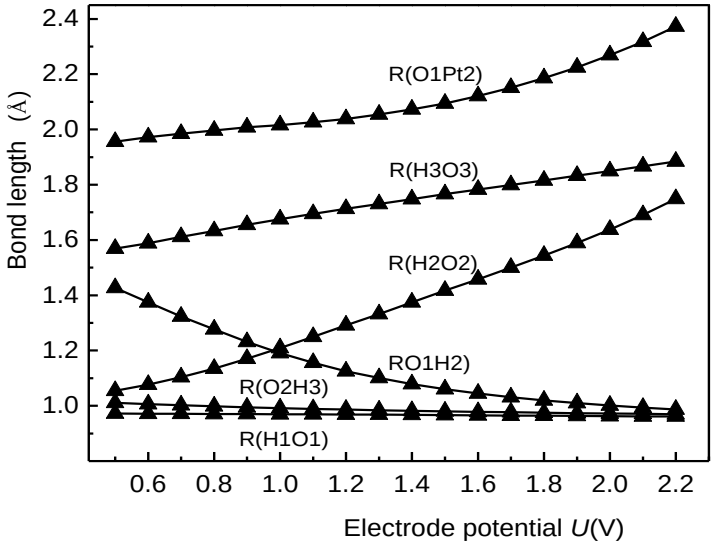

Figure 4.8 Potential dependencies of transition state parameters (Fig. 4.7) for 1-fold Pt_2OH reduction and 1-fold Pt_2OH_2 oxidation in acid calculated using B3LYP 6-31+G** and the point charge in the Hamiltonian.

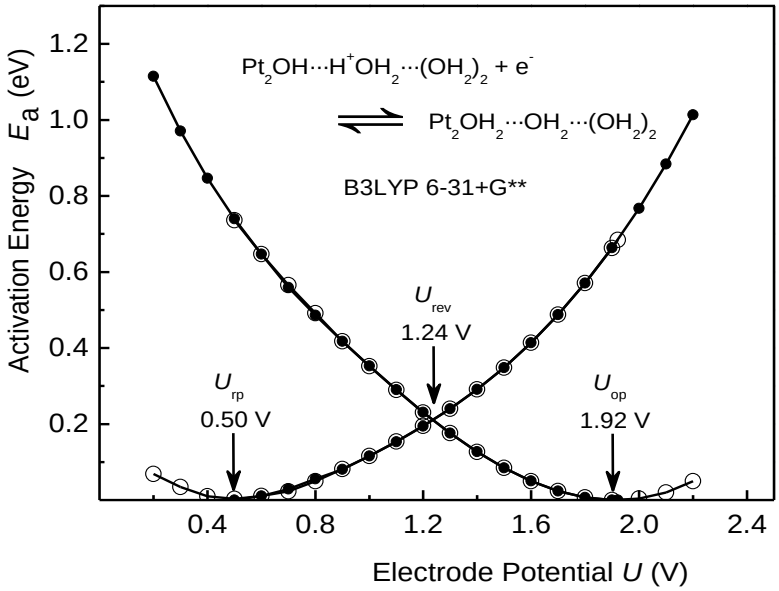

Figure 4.9 Potential dependencies of activation energies for 1-fold Pt_2OH reduction and 1-fold Pt_2OH_2 oxidation in acid calculated using B3LYP 6-31+G** with the point charge in the Hamiltonian. Dots are calculated points and circles are derived points.

that obtained using a single Pt atom, but it is still larger than the ~0.7 V experimental value. The activation energy at the reversible potential is ~0.21 eV which is 0.09 eV larger than for the single Pt atom. These comparisons show sensitivity to the local reaction center model chosen, but the small value for the activation energy is still consistent with thermodynamic control for this reaction step.

Using experimental bulk solution potentials given in Table 4.1 and calculated bond strengths in Table 4.2, the linear Gibbs energy relationship yields the standard reversible potentials shown in Table 4.3. Included in Table 4.3 are reversible potentials from the above local reaction center calculations adjusted to *pH* = 0. In the Table, the OH reduction potential was calculated to be greater than the O reduction potential when both

the local reaction center model and the linear Gibbs energy relationship model were used. These results are in disagreement with the experimental results in Refs. 87 and 112. The stability that OH(ads) experiences in the presence of H_2O(ads) causes the O(ads) reduction potential to increase and the OH(ads) reduction potential to decrease, with the net result that the OH reduction potential will be less than the O reduction potential.[69,70] The Pt_2-OH_2 and Pt_2-OH bond strengths are 0.375 eV and 2.545 eV, respectively. These are close enough to the low coverage experimental values that for these reactions no bond strength corrections are needed for the reversible potential predictions.

Table 4.1 Standard reversible potentials, U^o, for reactions in acid.[a]

Reaction	U^o (V)
$O_2(g) + H^+(aq) + e^- \rightleftharpoons OOH(aq)$	-0.046
$OOH(aq) + H^+(aq) + e^- \rightleftharpoons HOOH(aq)$	1.440
$OOH(aq) + H^+(aq) + e^- \rightleftharpoons O + H_2O(aq)$	0.107
$HOOH(aq) + H^+(aq) + e^- \rightleftharpoons OH(g) + H_2O(l)$	0.714
$OH(g) + H^+(aq) + e^- \rightleftharpoons H_2O(l)$	~2.813[b]
$O_2(g) + H^+(aq) + e^- \rightleftharpoons O(aq) + OH(g)$	-2.757
$O(aq) + H^+(aq) + e^- \rightleftharpoons OH(g)$	2.047

a. Ref. 101

b. This is expected to be close to the value for OH(aq) but a reliable experimental determination is available only for the OH(g).

Table 4.2 Calculated bond strengths (eV) to Pt and Pt_2 using B3LYP 6-31+G**.

molecule	Pt_1	Pt_2		Experimental range
		1-fold	2-fold	
O	3.811	3.089	3.886	4.1 - 3.5[a,b]
OH	2.767	2.454	2.510	2.5 - 1.5[b,c]
H_2O	0.332	0.375	-	-
O_2	0.779	-	0.853	-
OOH	1.667	-	1.355	-
H_2O_2	0.232	-	-	-

a. Yeo, Y. Y.; Vattuone, L.; King, D. A. *J. Chem. Phys.* 1997, 106, 392-401.

b. Ref. 87

c. Mooney, C. E.; Anderson, L. C.; Lunsford, J. H. *J. Phys. Chem.* 1993, 97, 2505-2506.

Table 4.3 Predicted standard reversible potentials, U^o (V), from the local reaction center (LRC) model are in the first column. Values in the second column were determined using bulk solution potentials and calculated adsorption bond strengths in a linear Gibbs energy relationship (LGER).[a] Values in the third column are activation energies at the predicted reversible potentials from the LRC calculations. Base results in the fourth column are from LRC calculations.[b]

	Predicted U^o (pH = 0)				Predicted U^o (pH = 14)	
	Reaction	LRC	LGER	$E_a(U^o)$	LRC	
On Pt_2	O_2(2-fold ads) + H^+ + e^- → OOH(2-fold ads)	1.14	1.21	0.24	O_2(ads) + e^- → O_2^-(ads)	-0.35
	O(2-fold ads) + H^+ + e^- → OH(2-fold ads)	1.17	0.67	0.19	O(ads) + H_2O + e^- → OH(ads) + OH^-	-0.30
	OH(1-fold ads) + H^+ + e^- → H_2O(1-fold ads)	1.30	0.73	0.21	OH(ads) + H_2O + e^- → H_2O(ads) + OH^-	-0.32
On Pt	O_2(ads) + H^+ + e^- → OOH(ads)	1.85	1.17	0.31	-	-
	HOO(ads) + H^+ + e^- → HOOH(ads)	1.53	0.01	0.17	-	-
	HOO(ads) + H^+ + e^- → O(ads) + H_2O(l)	2.82	2.25	0.69	-	-
	HOOH(ads) + H^+ + e^- → OH(ads) + H_2O	3.12	3.25	0.06	-	-
	O(ads) + H^+ + e^- → OH(ads)	2.16	1.00	0.39	-	-
	OH(ads) + H^+ + e^- → H_2O(ads)	1.38	0.38	0.12	-	-

a. Ref. 35

b. Ref. 54

Comparing the local reaction center model results in acid, adjusted for *pH* = 0, with the local reaction center model results in base, taken from Ref. 54 and adjusted for *pH* = 14, it can be seen in Table 4.3 that the calculated reversible potential for the O_2(ads) reduction step is 1.37 V higher in acid, the reversible potential for O(ads) reduction on the 2-fold site is 1.35 V higher in acid, and the reversible potential for OH(ads) reduction on the 1-fold site is 1.50 V higher in acid. It was argued in Ref. 54 that the reversible potentials in base should be close to the experimental values. On the reversible electrode scale, the voltammograms showing water oxidation and O_2 reduction are similar for acid and base electrolytes.[107] Thus, on the standard hydrogen electrode scale the onset potential for water oxidation in base is about 0.83 V less than in acid. This suggests that the present model for OH(ads) reduction in acid is yielding reversible potentials around 0.6 V positive of the correct value. The reversible potentials for the other two reactions are probably similarly overestimated. As discussed above, one can consider shifting the potential scales of the activation energy curves into alignment with the expected reversible potentials.

4.2.2 Two-electron Reduction on Single Platinum Site in Acid

In cases of site blocking, particularly by under-potential-deposited hydrogen, O_2 may be restricted to bond to a single Pt atom site on the catalyst surface. In this case, the local reaction center model has O_2 bonding strongest in the end-on orientation, as shown in Fig. 4.10. The reduction yields end-on bonded OOH according to the equation

$$PtO_2\cdots H^+OH_2\cdots(OH_2)_2 + e^- \rightarrow PtOOH\cdots OH_2\cdots(OH_2)_2 \qquad (4.4)$$

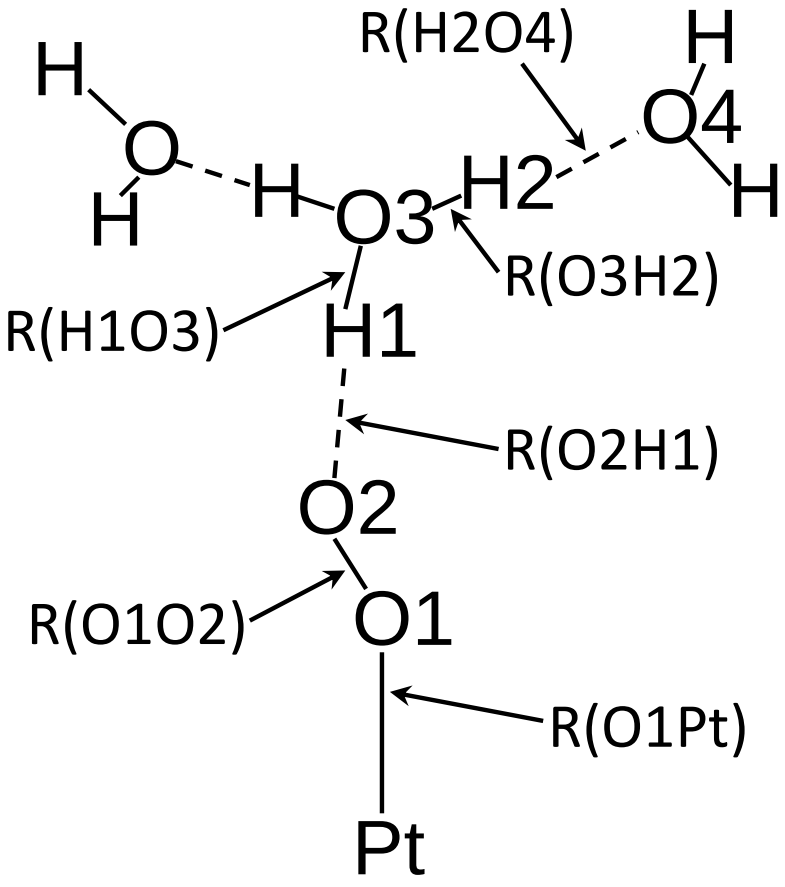

Figure 4.10 Structure model used in the calculations for PtO_2 reduction and PtOOH oxidation calculations in acid. Internuclear distances optimized in the calculations are defined. Angle constraints were imposed as discussed in the text.

Transition state parameters in Fig. 4.11 show the expected behavior for proton and electron transfer reactions and the activation energies in Fig. 4.12 show a rather high 1.79 V reversible potential with a relatively high 0.31 eV activation energy. These results and other calculated potentials and activation energies in the section are in Table 4.3. The bond angles and dihedral angles were fixed at the values of the optimized neutral oxidation precursor structure.

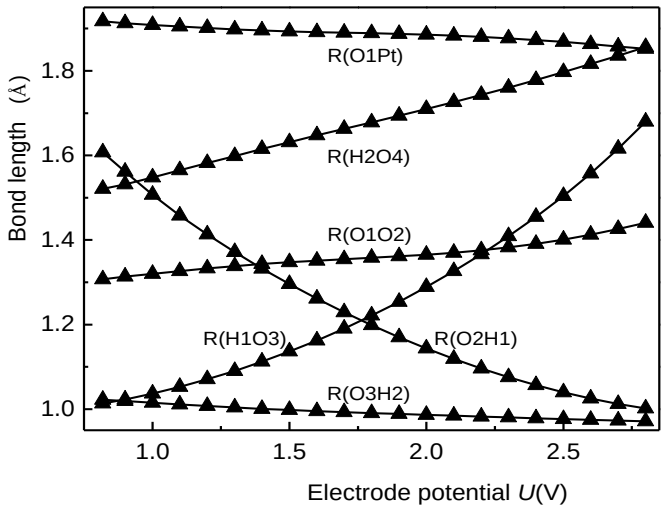

Figure 4.11 Potential dependencies of transition state parameters (Fig. 4.10) for PtO_2 reduction and PtOOH oxidation in acid calculated using B3LYP 6-31+G** and the point charge in the Hamiltonian.

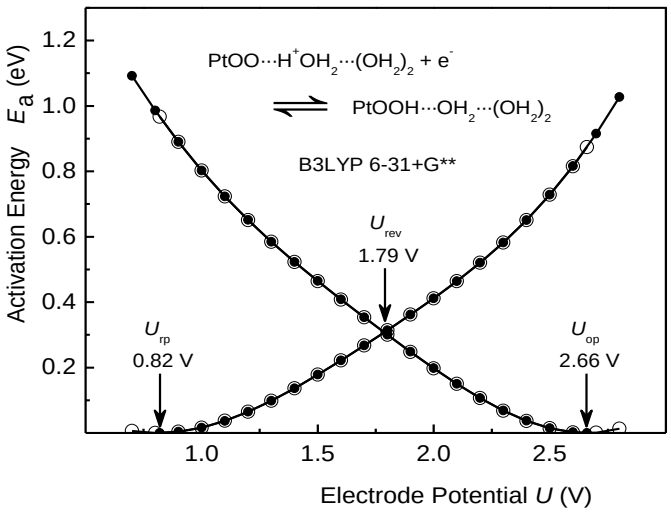

Figure 4.12 Potential dependencies of activation energies for PtO_2 reduction and PtOOH oxidation in acid calculated using B3LYP and 6-31+G** with the point charge in the Hamiltonian. Dots are calculated points and circles are derived points.

Next, the reduction of PtOOH to PtHOOH according to the reaction

$$PtOOH\cdots H^{+}OH_2\cdots(OH_2)_2 + e^{-} \rightarrow PtHOOH\cdots OH_2\cdots(OH_2)_2 \qquad (4.5)$$

was calculated. The structure is shown in Fig. 4.13 and the potential-dependent structure parameters and activation energies are given in Fig. 4.14 and Fig. 4.15. The reversible potential is 1.47 V with a smaller 0.17 eV activation energy. The hydrogen peroxide molecule is calculated to bond to the site by only 0.23 eV, so it should be released into the solution.

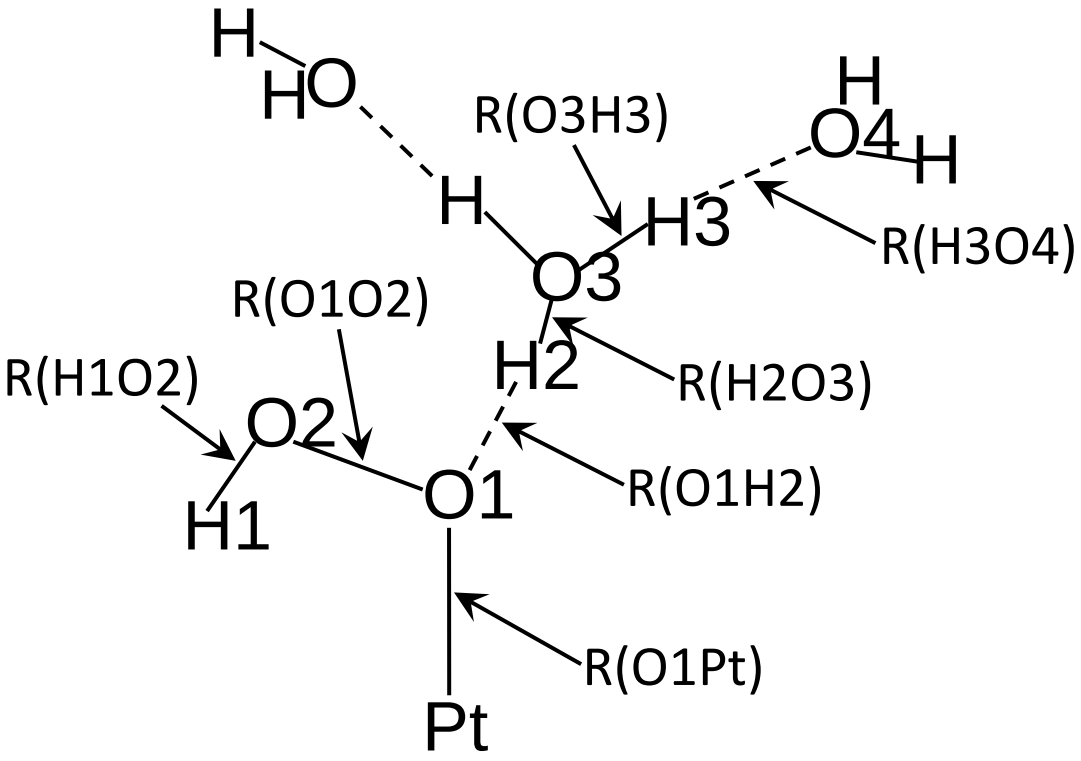

Figure 4.13 Structure model used in the calculations for PtOOH reduction and PtHOOH oxidation in acid. Internuclear distances optimized in the calculations are defined. Angle constraints were imposed as discussed in the text.

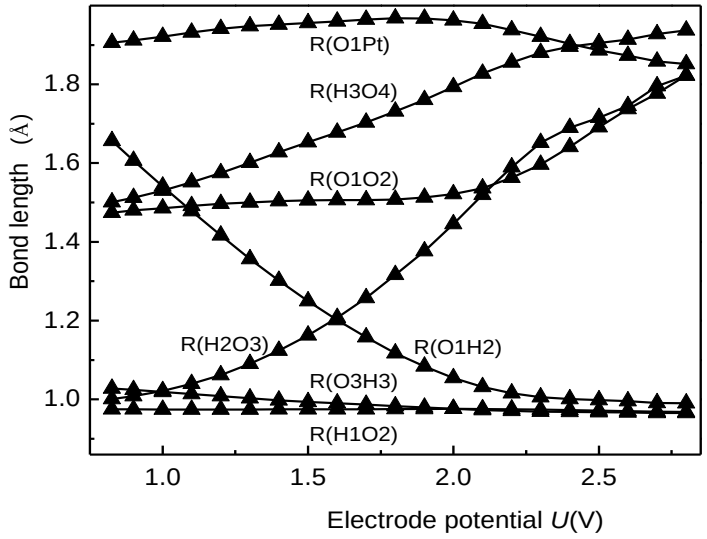

Figure 4.14 Potential dependencies of transition state parameters (Fig. 4.13) for PtOOH reduction and PtHOOH oxidation in acid calculated using B3LYP 6-31+G** and the point charge in the Hamiltonian.

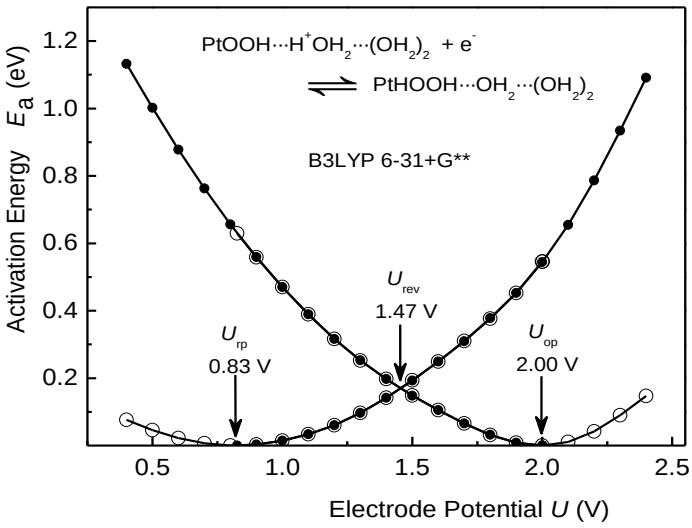

Figure 4.15 Potential dependencies of activation energies for PtOOH reduction and PtHOOH oxidation in acid calculated using B3LYP and 6-31+G** with the point charge in the Hamiltonian. Dots are calculated points and circles are derived points.

Another possibility for PtOOH reduction is the formation of PtO + H_2O instead of PtHOOH, according to the reaction

$$PtOOH\cdots H^{+}OH_2\cdots(OH_2)_2 + e^{-} \rightarrow PtO + HOH\cdots OH_2\cdots(OH_2)_2 \qquad (4.6)$$

The structure used in this step is shown in Fig. 4.16. For minimizing the number of variables, the H1O2H2 angle was given a constant value 105.8 °, favoring the product structure. Since the positive reduction precursor structure has an O-O bond and the product, O(ads) + H_2O(l), does not, all other bond angles and dihedral angles were fixed at the optimized reduction precursor values. The transition state calculations for the reduction reaction were performed and the oxidation activation energies were derived from the reduction results. Given the above structure constraints, there was no stable oxidation precursor up to an O-O distance of 11 Å and to achieve a stable state would require allowing the water to rotate to form a hydrogen bond to PtO, but this complication was not pursued. The potential-dependent parameters and activation energies are given in Figs. 4.17, 4.18, and 4.19. For a clearer view, Fig. 4.17 shows the parameters without the O-O distance included and Fig. 4.18 includes the O-O distance, based on the reduction activation energy calculations, and shows a rapid increase in O-O distance at higher potentials, increasing to 5.798 Å at the derived oxidation precursor potential. As may be seen in Fig. 4.19, the reduction and oxidation precursor potentials are widely separated, having values -0.42 V and 4.00 V. The reversible potential, 2.76 V, is 1.29 V higher than the reversible potential for forming HOOH(ads). As Figs. through 4.17 to 4.19 show, the transition states are poorly defined for this reaction, apparently the

result of numerical difficulties in the transition state seeking program. The 0.69 eV calculated activation energy at the calculated reversible potential is relatively uncertain.

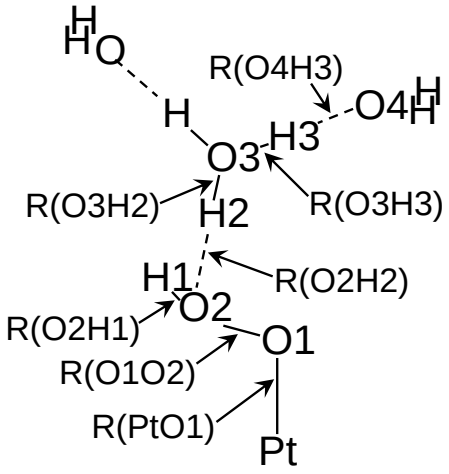

Figure 4.16 Structure model used for PtOOH reduction to PtO + H_2O and PtO + H_2O oxidation calculation to PtOOH in acid. Internuclear distances optimized in the calculations are defined. Angle constraints were imposed as discussed in the text.

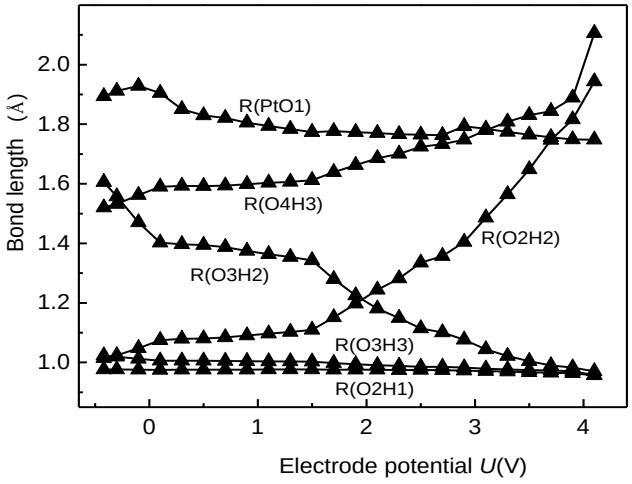

Figure 4.17 Potential dependencies of transition state parameters (Fig. 4.16) for PtOOH reduction to PtO + H_2O and PtO + H_2O oxidation to PtOOH in acid calculated using B3LYP 6-31+G** and the point charge in the Hamiltonian. The O-O distance is shown in Fig. 4.18.

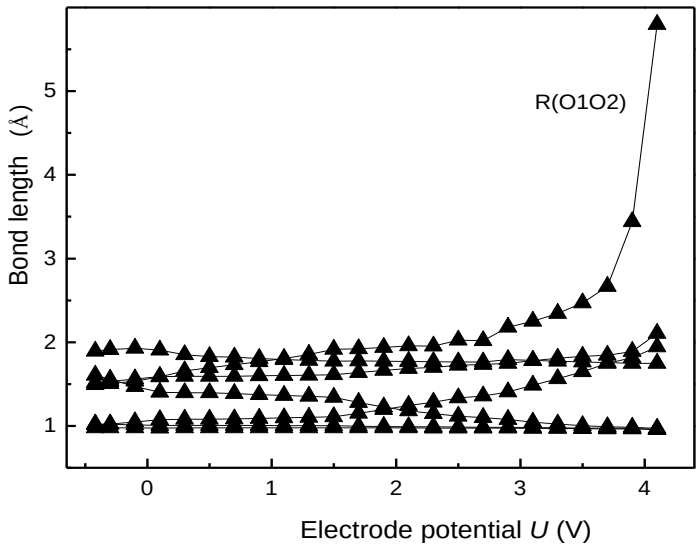

Figure 4.18 A second view of data in Fig. 4.17, this figure including R(O1O2).

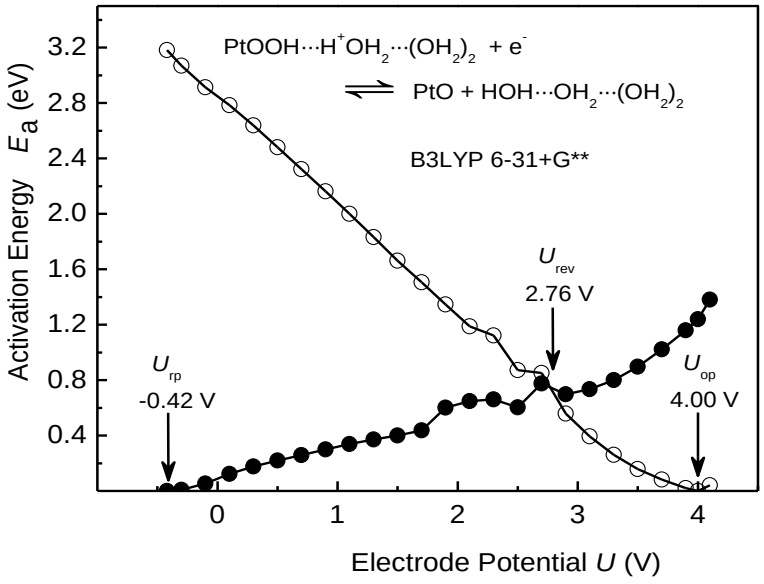

Figure 4.19 Potential dependencies of activation energies for PtOOH reduction to PtO + H_2O and PtO + H_2O oxidation to PtOOH in acid calculated using B3LYP 6-31+G** with the point charge in the Hamiltonian. Dots are calculated points and circles are derived points.

If the PtHOOH lingers, could it undergo further reduction? We examined the reaction

$$PtHOOH\cdots H^{+}OH_2\cdots(OH_2)_2 + e^{-} \rightarrow PtOH\cdots OH_2\cdots OH_2\cdots(OH_2)_2 \qquad (4.7)$$

using the structure in Fig. 4.20. The potential-dependent parameters and activation energies are in Figs. 4.21 and 4.22. In this case, the 3.06 V reversible potential is high, but the activation energy is very small at 0.06 eV. These results mean that the four-electron reduction should proceed in parallel with the two-electron reduction over one-fold sites.

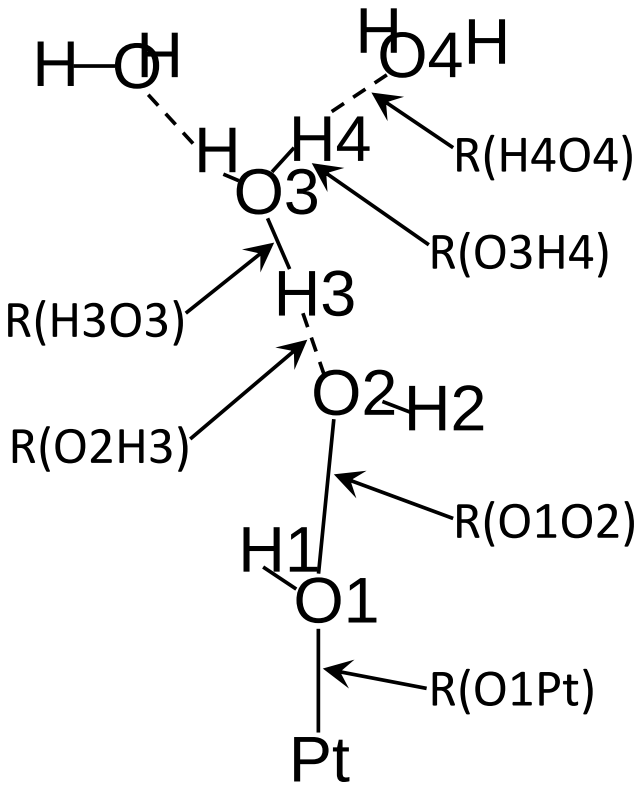

Figure 4.20 Structure model used in the calculations for PtHOOH reduction to PtOH + H_2O and PtOH + H_2O oxidation to PtHOOH in acid. Internuclear distances optimized in the calculations are defined. Angle constraints were imposed as discussed in the text.

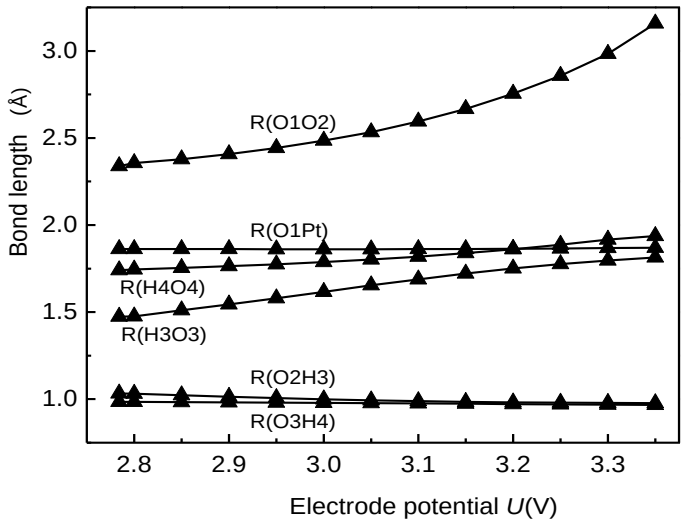

Figure 4.21 Potential dependencies of transition state parameters (Fig. 4.20) for PtHOOH reduction to PtOH + H_2O and PtOH + H_2O oxidation to PtHOOH calculations in acid using B3LYP 6-31+G** and the point charge in the Hamiltonian.

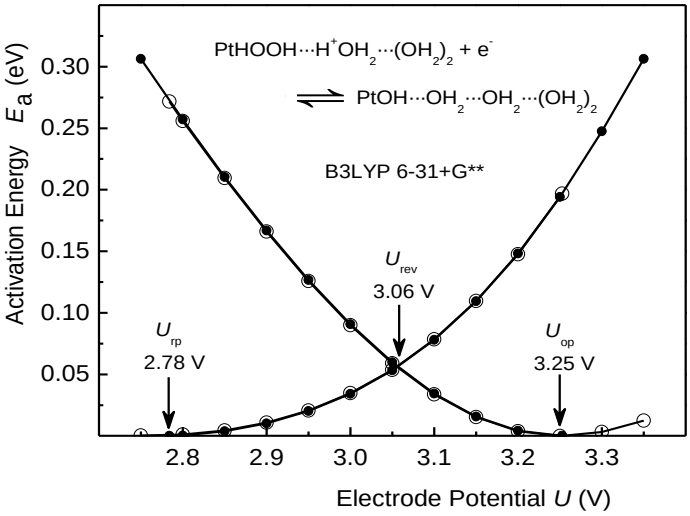

Figure 4.22 Potential dependencies of activation energies for PtHOOH reduction to PtOH + H_2O and PtOH + H_2O oxidation to PtHOOH in acid calculated using B3LYP and 6-31+G** with the point charge in the Hamiltonian. Dots are calculated points and circles are derived points.

Interestingly, PtHOOH was calculated to undergo the rearrangement

$$PtHOOH \rightarrow PtO\cdots H_2O \qquad (4.8)$$

with an activation energy of 0.22 eV. Consequently, it was necessary to study the reduction of PtO to PtOH:

$$PtO\cdots H^+OH_2\cdots(OH_2)_2 + e^- \rightarrow PtOH\cdots OH_2\cdots(OH_2)_2 \qquad (4.9)$$

using the structure in Fig. 4.23. Transition structures parameters are shown in Fig. 4.24. The activation energy curves given in Fig. 4.25 show a high reversible potential of 2.10 V with 0.39 eV activation energy, a high value.

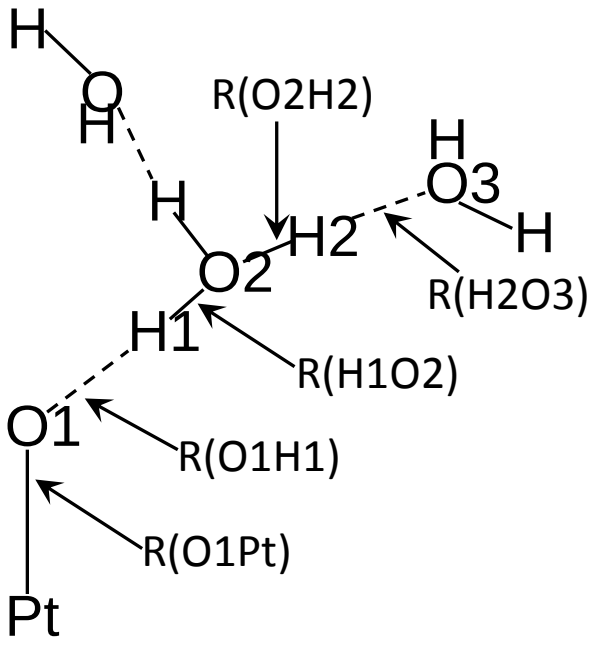

Figure 4.23 Structure model used in the calculations for PtO reduction and PtOH oxidation in acid calculated. Internuclear distances optimized in the calculations are defined.

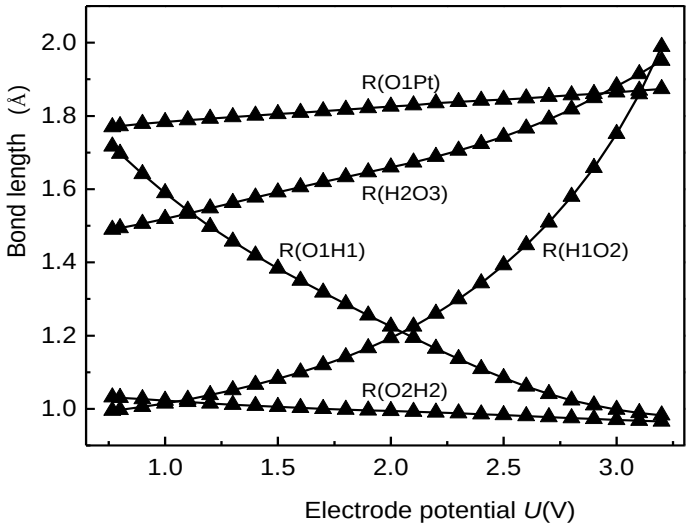

Figure 4.24 Potential dependencies of transition state parameters (Fig. 4.23) for PtO reduction and PtOH oxidation calculations in acid using B3LYP 6-31+G** and the point charge in the Hamiltonian.

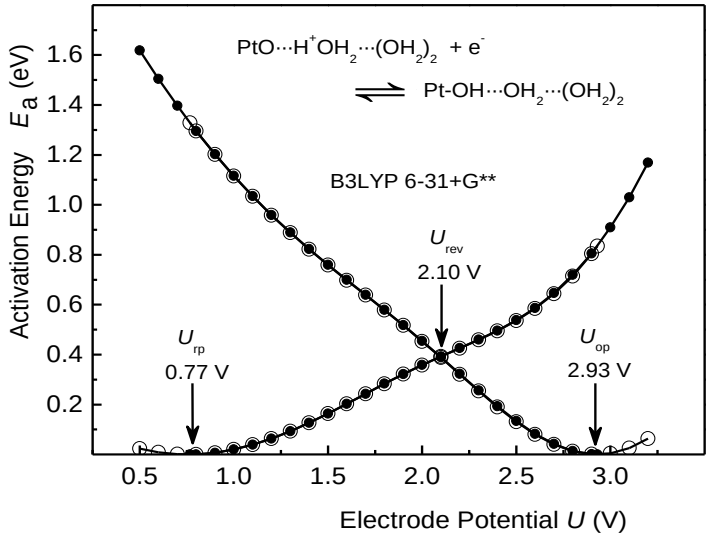

Figure 4.25 Potential dependencies of activation energies for PtO reduction and PtOH oxidation in acid calculated using B3LYP 6-31+G** with the point charge in the Hamiltonian. Dots are calculated points and circles are derived points.

Following the reduction of O(ads) to OH(ads), the OH(ads) is then reduced to H_2O(ads):

$$PtOH\cdots H^+OH_2\cdots(OH_2)_2 + e^- \rightarrow PtOH_2\cdots OH_2\cdots(OH_2)_2 \qquad (4.10)$$

using the structure in Fig. 4.26. Transition structures parameters are shown in Fig. 4.27. The activation energy curves given in Fig. 4.28 show a reversible potential of 1.32V with activation energy of 0.12 eV.

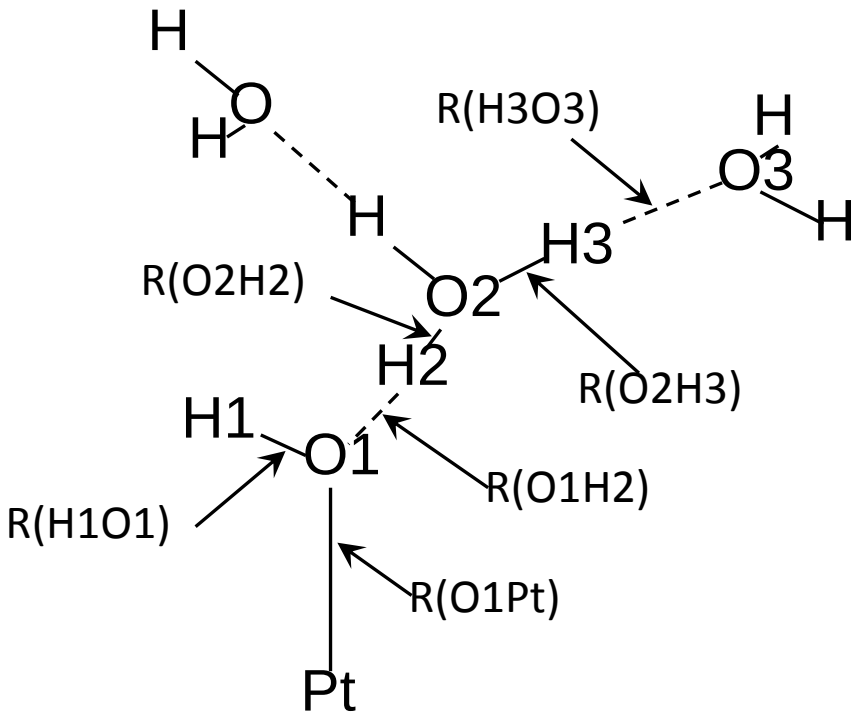

Figure 4.26 Structure model used in the calculations for PtOH reduction and $PtOH_2$ oxidation in acid calculated. Internuclear distances optimized in the calculations are defined.

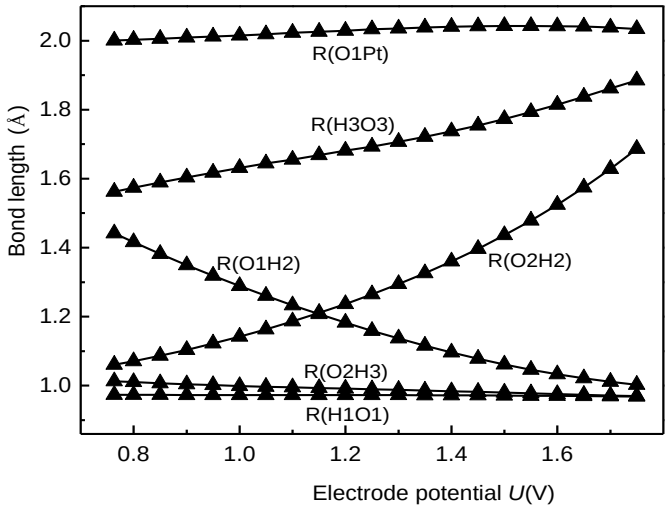

Figure 4.27 Potential dependencies of transition state parameters (Fig. 4.23) for PtOH reduction and $PtOH_2$ oxidation calculations in acid using B3LYP 6-31+G** and the point charge in the Hamiltonian.

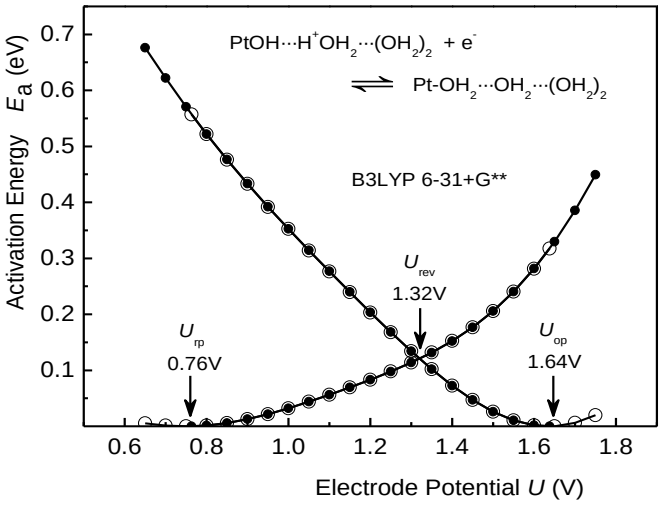

Figure 4.28 Potential dependencies of activation energies for PtOH reduction and $PtOH_2$ oxidation in acid calculated using B3LYP 6-31+G** with the point charge in the Hamiltonian. Dots are calculated points and circles are derived points.

4.2.3 Tallying up Gibbs Energies in the Linear Gibbs Energy Relationship Approach

The linear Gibbs energy approach for predicting standard reversible potentials for reacting intermediates on the electrode surface is dependent on the bond strengths of the intermediates to the surface and there is no ambiguity concerning of point charge term in the Hamiltonian or the solvation models as in their determination from activation energy curves in the local reaction center methods. This method was already applied to O(ads) and OH(ads) reduction in the Pt_2 section above, and here predictions for the other 1-electron transfer reactions on Pt_1 are given. All results are in Table 4.3. In this section the O_2 reduction is examined using reversible potentials from the linear Gibbs energy approach.

Each step of an ideal oxygen reduction catalyst will have 1.229 V reversible potential. Then ΔG^o for the overall four-electron reduction will be -4×1.229 eV = -4.916 eV. In fact, ΔG^o for the overall catalytic process always sums to -4.916 eV, even when some steps have reversible potentials that are at high overpotentials relative to 1.229 V, i.e. the sum is -4.916 eV even for a poor catalyst.

When reversible potentials are calculated using the linear Gibbs energy relationship, the experimental reversible potentials for reactions in bulk solution are modified using the calculated bond strengths of reaction intermediates to the electrocatalyst. The necessary bulk solution potentials are listed in Table 4.1.

Consider the reduction sequence $Pt_2OH_2 + O_2 \rightarrow Pt_2O_2 + H_2O \rightarrow Pt_2OOH + H_2O \rightarrow Pt_2O + Pt_2OH + H_2O \rightarrow Pt_2O + 2\ H_2O \rightarrow Pt_2OH + 2\ H_2O \rightarrow Pt_2OH_2 + 2\ H_2O$. Using the linear Gibbs energy relationship results for Pt_2 that are given in Table 4.3, the sum of free

energies for this reaction sequence is only 3.289 eV. The 1.206 V potential for the first reduction step, forming OOH on the 2-fold site, is based on the model assumption that the O_2 adsorption energy, 0.853 eV, is reduced by twice the 0.375 eV water adsorption energy. What has happened to the missing 1.627 eV Gibbs energy? The calculations yield 1.355 eV for desorbing OOH from the bridging site, 2.961 eV for dissociating OOH into O + OH, -3.886 eV for bonding O to a bridging site, and -2.454 eV for bonding OH to 1-fold site. The net result is that 2.024 eV internal energy is lost, essentially as heat. This energy is not equal to the 1.627 eV missing Gibbs energy and the 0.397 eV difference is due to the $P\Delta V - T\Delta S$ contributions that are omitted in the internal energy calculations. The lost internal energy dominates the 0.56 V and 0.50 V overpotentials, relative to 1.23 V, for the O(ads) and the two OH(ads) reduction steps, respectively, based on Table 4.3.

In another pathway over the Pt_2 2-fold site, where the first reduction step leads directly to O(ads) + OH(ads), the reversible potential is calculated to be high at 2.730 V. This is due the strong bonding of the O to the bridging site and OH to the 1-fold site. The heat loss for this mechanism is manifested in the high overpotentials for O(ads) and OH(ads) reduction as discussed above.

Now focusing on the linear Gibbs energy relationship results in Table 4.3 for the reduction sequence $PtOH_2 + O_2 \rightarrow PtO_2 + H_2O \rightarrow PtOOH + H_2O \rightarrow PtHOOH + H_2O \rightarrow PtOH + 2\ H_2O \rightarrow PtOH_2 + 2H_2O$ over the single Pt 1-fold site, the sum of free energies is only 4.806 eV. The 1.174 V potential for the first reduction step to form OOH(ads) on the single Pt 1-fold site is based on the model assumption that the O_2 adsorption energy, 0.779 eV, is decreased by the water adsorption energy, 0.332 eV. The 0.11 eV difference

in Gibbs energy is due to the $P\Delta V - T\Delta S$ contributions that are missing in the internal energy calculations. In this case, there are two large overpotentials, relative to 1.23V, 1.22 V overpotential for OOH(ads) reduction and 0.85 V overpotential for OH(ads) reduction. These can be traced to the heat loss associated with the 2.02 V underpotential, relative to 1.23 V, for the HOOH(ads) reduction to OH(ads) + H_2O(l). This heat loss is due to the weakness of the Pt-HOOH bond, 0.232 eV, and the high strength of the Pt-OH bond, 2.767 eV. The OOH → HOOH step has a reversible potential of 0.01 V, but in the presence of under-potential-deposited hydrogen, the Pt-OOH bond would be expected to weaken, which would be expected to shift this potential positive into the experimentally observed potential range, ~0.3 V.[107]

A second pathway over the single Pt 1-fold site is Pt-OH_2 + O_2 → PtO_2 + H_2O → PtOOH + H_2O → PtO + $2H_2O$ → PtOH + $2H_2O$ →$PtOH_2$ + $2H_2O$. The reversible potential for the PtOOH to PtO + H_2O step is calculated to be 2.251 V. The Gibbs energy sum is again 4.806 eV because the internal rather than Gibbs energies were calculated. For this pathway the OH(ads) reduction step has the highest overpotential relative to 1.229 V.

4.3 Conclusions of Calculations of Oxygen Reduction Reactions on Platinum Electrodes in Acid Solution

The O_2 reduction studies involving the Pt_2 model and the local reaction center approach yielded comparable results in acid and base for the first reduction step and subsequent reductions, but with a potential off-set of 0.6 V for the O(ads) and OH(ads) reduction steps beyond that due to the difference in *pH*. Because the base potential

results appeared to be in agreement with experimental values, the implication is that the acid results were 0.6 V too positive, but one could shift the curves to put the reversible potentials at the expected positions. With these shifts, local reaction center model predictions are close to the predictions with the linear Gibbs energy relation for O(ads) and OH(ads) reduction in acid. The reversible potentials for the first electron transfer steps do not follow this trend because different intermediates are formed, OOH(ads) in acid and superoxide, O_2^-(ads) in base. It has been shown that the qualitative error in reversible potential predictions, namely the predicted reversible potential for O(ads) reduction being lower than the reversible potential for OH(ads) reduction in these calculations will be corrected by the stabilization of OH(ads) by adjacent OH_2(ads).

Calculation of O_2 reduction properties performed using the single-adsorption-site model show greater differences between results obtained using the local reaction center model and results from the linear Gibbs energy relationship for the O_2(ads), OOH(ads), and HOOH(ads) reduction steps. For the former, differences range from 1.5 V to -0.2 V and for the latter they are both about 1 V. Why the two methods treat reductions of molecules with O-O bonds so differently is not yet known.

Chapter 5

Advancements in the Local Reaction Center Model for Electrocatalysis

5.1 Comprehensive Methodological Study of Local Reaction Center Model Theory

The local reaction center theory employs local reaction center models for calculating the electrode potential dependencies of electron transfer activation energies for adsorbed species. Comparisons of results of many studies using this method showed results were dependent on the calculation approach used, the choice of basis set, and the choice of point charge model used to represent the contribution to the potential at the reaction center by the electrolyte at the interface. This chapter presents a comprehensive study of these dependencies.

A single reaction was chosen for this study, reduction of Pt-OH to Pt-OH_2 at pH = 1.0.[48] For testing the effect of computational method, results from B3LYP hybrid density functional and MP2 calculations were compared; for testing the effect of a diffuse function on oxygen, results from calculations using the 6-31G** standard basis set with polarization functions and the 6-31+G** standard basis set with polarization functions and a diffuse function on each oxygen atom were compared; and for testing the effect of changing the point charge model, results of calculations with and without the point charge were compared.

Gaussian 03[56] was employed. OH and H_2O were bonded to a single platinum atom. The point charge contribution to the Hamiltonian was varied. Since the charge and its position have been chosen ad hoc, it will be examined below whether the charge can simply be viewed as an adjustable parameter for aligning the reduction precursor, oxidation precursor, and reversible potentials. A modified version of the linear extrapolation approach in the constrained variational theory of Ref. 48 was used

throughout. The modification includes second order Hessian matrix elements in the extrapolations to speed convergence to transition state structures.[82]

5.2 Results for $OH + H^+ + e^- \rightarrow H_2O$ and the reverse reaction on platinum: dependence on methodology

To predict the reversible potentials using the linear Gibbs energy model, the structures of Pt-OH and Pt-OH_2 were optimized using the four procedures and the bond strengths determined for making predictions of the reversible potential for the reaction

$$OH(ads) + H^+(aq) + e^- \rightleftharpoons H_2O(ads) \qquad (5.1)$$

As may be seen in Table 5.1, in the case of water, the HOH angle ranges between 105.9 ° and 107.5 °, the PtOH angle ranges between 102.4 ° and 106.0 °, the Pt-O distance ranges

Table 5.1 Calculated structure parameters and adsorption energies for a water molecule bonded to a Pt atom. In all four cases the ground states have singlet spin multiplicity.

Method	basis set	R(PtO)/Å	R(OH)/Å	Θ(HOH)/°	Θ(PtOH)/°	Bond strength/eV
B3LYP	6-31G**	2.062	0.973	106.5	102.4	0.628
	6-31+G**	2.067	0.972	107.5	104.4	0.332
MP2	6-31G**	2.058	0.971	105.9	103.8	0.567
	6-31+G**	2.062	0.970	107.0	106.0	0.362

between 2.058 Å and 2.067 Å, and the O-H distance ranges between 0.970 Å and 0.973 Å. As also may be seen in Table 5.1, the platinum water bond has a strength of about 0.60 eV for the 6-31G** basis set, and it is about 0.35 eV when the diffuse function is added to the oxygen.

Table 5.2 gives the data for PtOH, where it may be seen that the range of calculated Pt-OH bond strengths is 2.77 eV to 3.00 eV. These results characterize the sensitivity of the structure parameters and the bond strengths to the above changes in method and basis set. Based on the approximate standard reversible potential of 2.81 V for reduction of aqueous OH,[101] the linear Gibbs energy relationship yields standard reversible potentials for forming PtOH of 0.52 V and 0.38 V for B3LYP without and with diffuse functions, respectively. For the MP2 approach, the corresponding values are 0.40 V and 0.20 V.

Table 5.2 Calculated structure parameters and adsorption energies for OH adsorbed on a Pt atom. In all four cases the ground states have doublet multiplicity.

Method	basis set	R(PtO)/Å	R(OH)/Å	Θ(PtOH)/°	Bond strength /eV
B3LYP	6-31G**	1.872	0.976	106.6	2.923
	6-31+G**	1.878	0.975	107.8	2.767
MP2	6-31G**	1.865	0.976	105.6	2.985
	6-31+G**	1.877	0.976	107.1	2.978

Using more accurate low-coverage platinum surface OH adsorption and water adsorption bond strengths from density functional slab-band calculations, the linear Gibbs energy

relationship yields 0.7 V,[34] which is close to the experimental value of ~0.6 V[87,112] for *pH* = 1. Recent band calculations show that when OH is adsorbed on Pt(111), it is stabilized when an adjacent adsorbed water molecule is present. This stabilization is significant due to the negative charge on OH(ads) which results in stronger hydrogen bonding of water to it than when in the bulk solution phase.[69,70] This stabilization will contribute to decreasing the 0.7 V prediction to a lower value.

For the constrained variation calculations in acid, hydronium ions are the source of the protons consumed in each of the one-electron reduction steps. As in our past theoretical work, the hydronium ion has two hydrogen bonded water molecules, affording solvation stabilization,[30,31] and the third hydrogen is coordinated by hydrogen bonding to the oxygen-containing species being reduced as in Fig. 5.1. The $H_3O^+\cdots(OH_2)_2$ part was

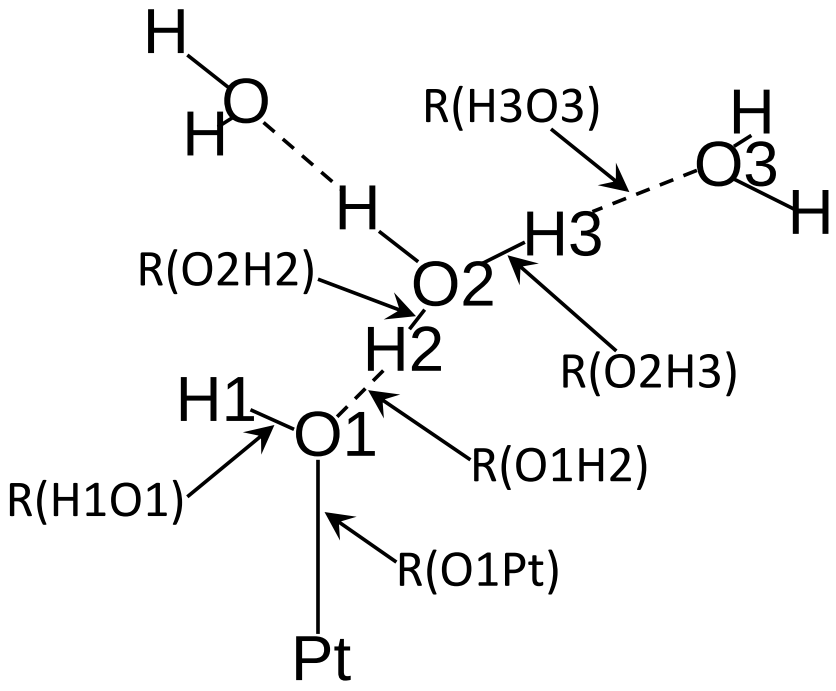

Figure 5.1 Structure model used for the Pt-OH reduction and Pt-OH_2 oxidation calculations in acid. Internuclear distances optimized in the calculations are defined.

fully optimized for each of the four types of calculations. The structures are all the same as or close to the MP2 results in Ref. 30. Oxidation and reduction precursor structures were calculated with the two water molecules constrained to not change their structure and orientation while the hydrogen bond lengths and OH bond lengths in the H_3O^+ parts were optimized. These constraints reduced the number of parameters, which is important for minimizing the possibility of failure in the constrained variation calculations due to the complexity of the energy surfaces and the electron affinity or ionization potential surfaces. One wants to use parameters on which these surfaces have strong dependencies. When determining the reduction precursor energy and the activation energies, the PtOH and H1O1H2 angles were constrained to the values calculated for the oxidation precursors. The PtOH angles were set equal. These constraints served to further reduce the number of variables; this approach was generally used in the past.[31,41-54]

For the oxidation precursor, the B3LYP calculations without diffuse functions yielded respective increases of 0.8 ° and 1.9 ° for the HOH and PtOH angles compared with the Pt-OH_2 structures in Table 5.1. When diffuse functions were added, the respective changes were 0.6 ° and 2.4 °. Trial calculations showed that angle variations of this magnitude changed the total energy by about 0.01 eV, which is a small value that justifies the model for use in determining transition states.

Transition states were calculated with the point charge potential added to the Hamiltonian. First, the oxidation and reduction precursor structures were reoptimized with the point charge present by varying the six internuclear distances in Fig. 5.1. Only the three hydrogen bond distances and the OH^+ distance in the hydronium ion change more than 0.01 Å and the net effect of the point charge was to reduce the distortion in the

solvated hydronium ion that was caused by its hydrogen bonding to the OH on platinum. Potential-dependent transition states were calculated and their activation energies determined with reference to the precursor energies. As functions of potential, the six variables had the same behavior for the four methods; the B3LYP 6-31+G** results in Fig. 5.2 are representative. There it may be seen that, as the potential increases, the

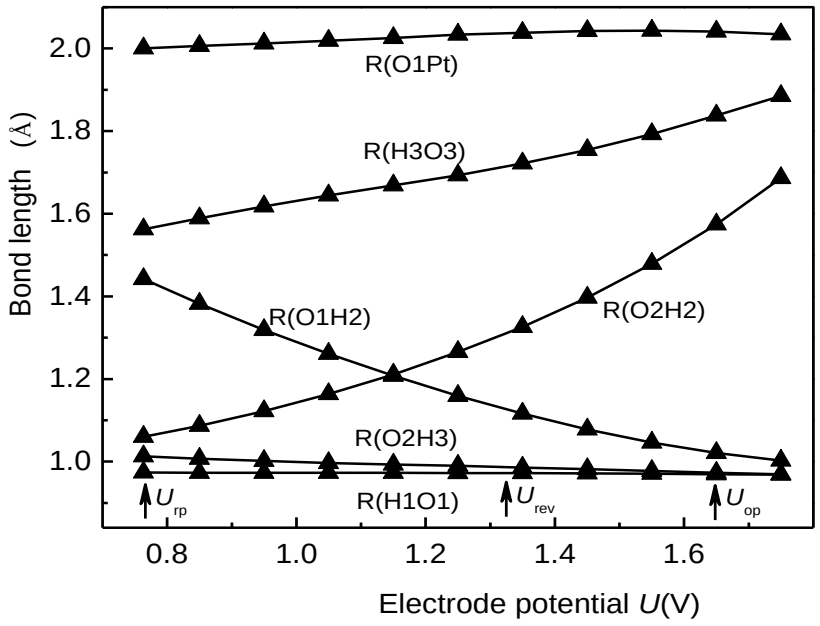

Figure 5.2 Potential dependencies of transition state structure parameters (Fig. 5.1) for Pt-OH reduction and Pt-OH_2 oxidation in acid calculated using B3LYP 6-31+G** and the point charge in the Hamiltonian. The left arrow marks the reduction precursor potential and the right arrow marks the oxidation precursor potential. The central arrow marks the structure of the reversible potential.

proton rapidly pulls away from the oxygen of the hydronium ion and at the same time it rapidly approaches the oxygen of PtOH. The two solvating water molecules

simultaneously pull away from the hydronium ion. These changes are associated with the need to increase the electron affinity of the local reaction center as the electrode potential is increased. U_{rp}, U_{op}, and U_{rev} are marked in Fig. 5.2 to show that the proton is not midway between the O atoms at the reversible potential defined in Fig. 5.3. Figures 5.4-5.6 have those results for the other calculations.

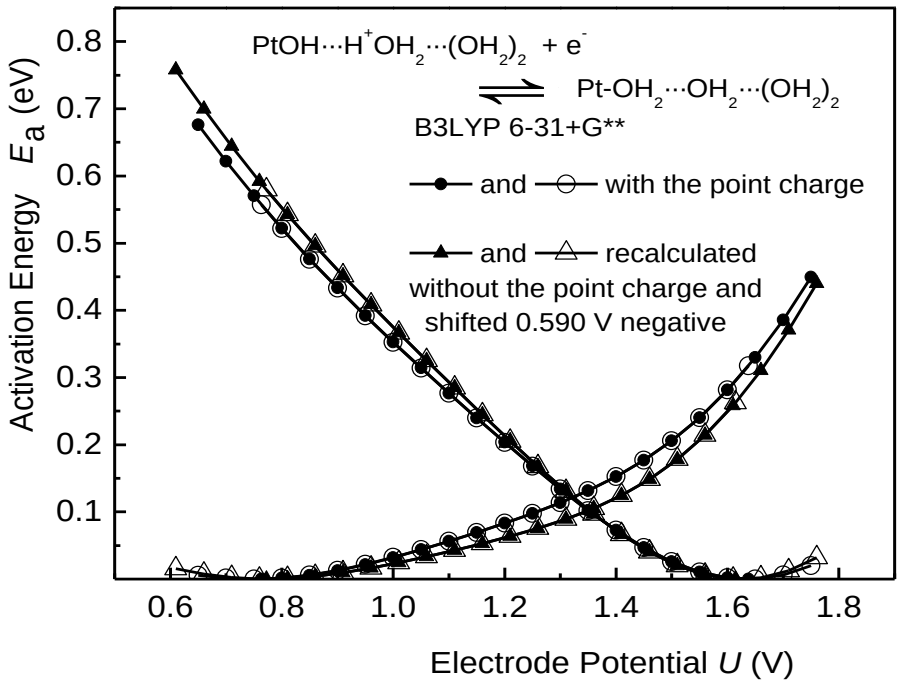

Figure 5.3 Potential dependencies of activation energies for Pt-OH reduction and Pt-OH_2 oxidation in acid calculated using B3LYP 6-31+G** with the point charge in the Hamiltonian and with the point charge omitted. Solid symbols are calculated points and open symbols are derived points as discussed in the text.

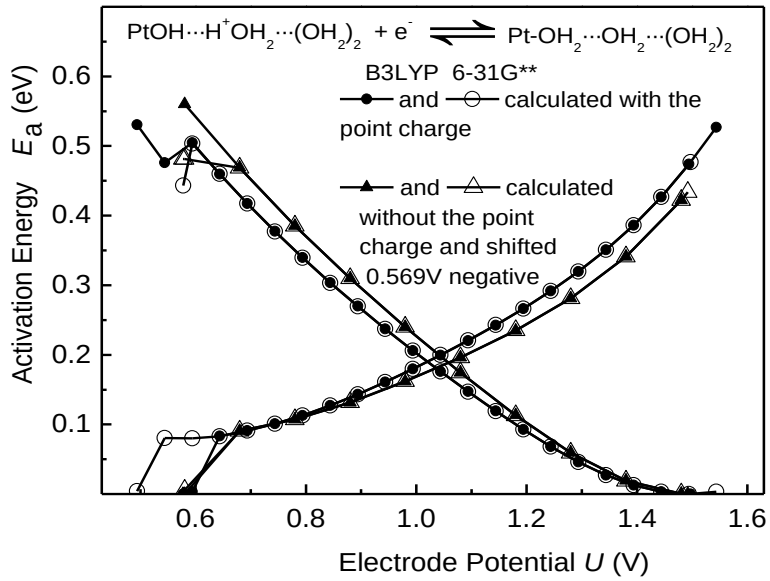

Figure 5.4 As in Fig. 5.3 but for the 6-31G** basis set.

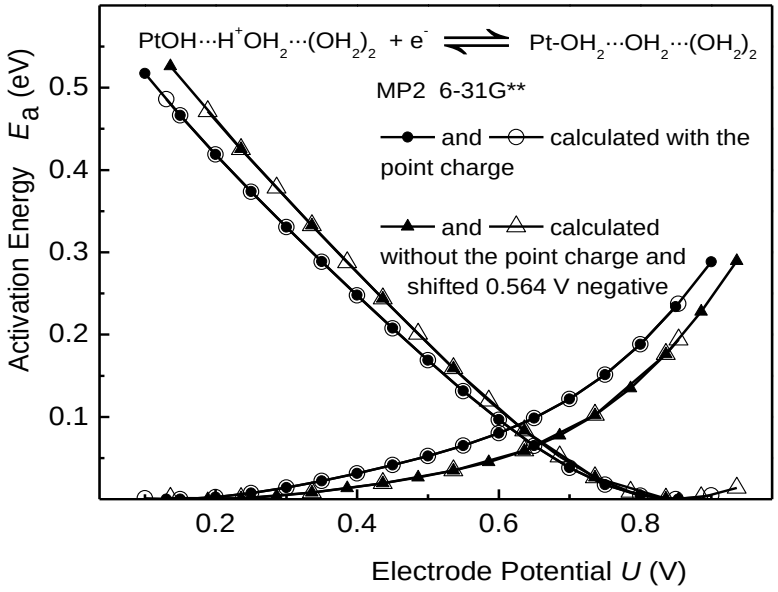

Figure 5.5 As in Fig. 5.3 but for MP2 6-31G**.

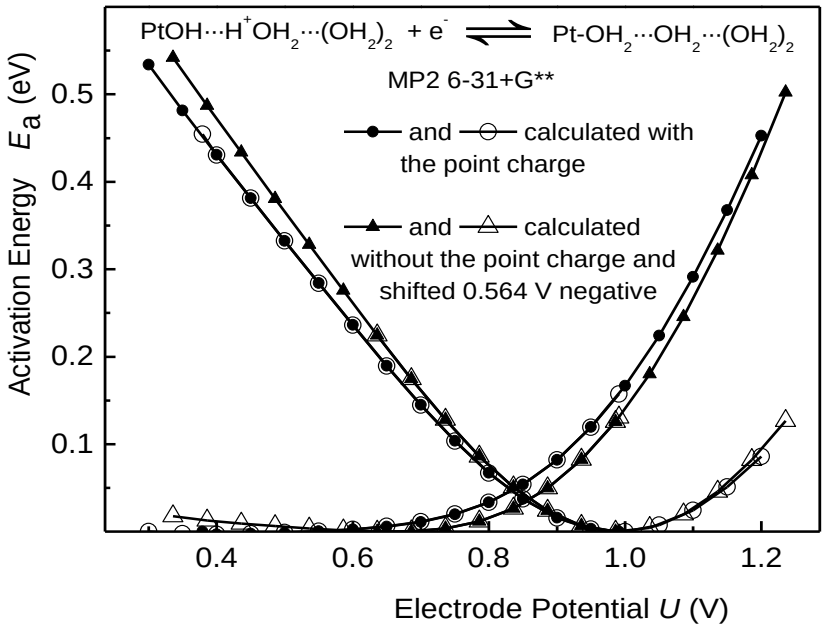

Figure 5.6 As in Fig 5.3 but for MP2 6-31+G**.

The precursor potentials, reversible potentials, and the activation energies at the reversible potentials from calculations with and without the point charge are given in Table 5.3. We note from the results in Table 5.3 that the MP2 method gives a reversible potential for OH(ads) reduction in this model that is 0.5 V less than the B3LYP result and quite close to the experimental onset potential, but the agreement is fortuitous because the stabilization of OH(ads) by H_2O(ads) was not included. For all four methods, the effect of adding the point charge is to decrease all of these potentials by about 0.6 V, with one exception being the reduction potential using MP2. The addition of the diffuse function shifts the potentials positive by 0.14 V to 0.31 V with one exception involving the reduction precursor in the absence of the point charge, for which the shift is 0.45 V.

Table 5.3 Calculated reduction precursor potentials, U_{rp} (V), reaction reversible potentials, U_{rev} (V), oxidation precursor potentials, U_{op} (V), and activation energies E_a (eV) at the reaction reversible potentials for Pt-OH reduction to Pt-OH_2 using the local reaction center approach with and without the point charge.

		with point charge					without point charge				
Method	Basis set	Fig.	U_{rp}	U_{rev}	U_{op}	E_a	Fig.	U_{rp}	U_{rev}	U_{op}	E_a
B3LYP	6-31G**	5.4	0.56	1.01	1.49	0.19	5.4	1.15	1.63	2.06	0.19
	6-31+G**	5.3	0.76	1.32	1.64	0.12	5.3	1.36	1.94	2.20	0.10
MP2	6-31G**	5.5	0.13	0.62	0.85	0.09	5.5	0.75	1.22	1.42	0.07
	6-31+G**	5.6	0.38	0.83	0.99	0.05	5.6	1.20	1.42	1.56	0.04

The apparent discrepancies are the result of the difficulty in finding reduction precursor potentials. The difficulty arises because for the reduction precursors the electron affinity is more sensitive to structure variation than is the total energy. The activation energies at the reversible potentials shown in Table 5.3 are less than 0.2 eV for the B3LYP calculations and less than 0.1 eV for the MP2 calculations. Such low activation energies suggest that at room temperature H_2O(ads) oxidation and OH(ads) reduction will be under thermodynamic control and not kinetic control. Adding diffuse functions decreases the activation energies by about 40% to 60%.

Superimposed on Figs. 5.3-5.6 are the calculated results in the absence of the point charge (open and closed triangles) shifted so that the oxidation precursor potentials match. In each case, the curves have similar shapes. Reversible potentials at the crossing points are in accordance with equation (2.6). The circles and open triangles are "derived points".

In all the figures the curves are well-defined by both calculated and derived points. The constrained variation program being used for this study is not designed to yield reduction activation energies negative of U_{rp} or oxidation energies positive of U_{op}.[82] These forbidden ranges correspond to the Marcus inverted regions for which activation energies are positive only on semiconductor electrodes.[27] However they can be calculated as derived points, as shown in figures. Although the precursor potentials and reversible potential in Table 5.3 seem well-behaved for B3LYP without diffuse functions and the activation energies at the reversible potentials are in Fig. 5.4 are nearly the same for all methods of calculation, a convergence problem in the lower potential range are evident.

5.3 Conclusions of the Methodology Study

We conclude this section with a general observation that, by changing the point charge, one can shift the precursor potentials and activation energy curves either left or right on the potential scale. This suggests the possibility of shifting a set of calculated curves to match a known experimental datum such as the reversible potential or the precursor potential and then making predictions of activation energies at other potentials. The MP2 6-31G** result is already very close to the experimental value of ~0.6 V and all the others could be brought into alignment by increasing the point charge or simply shifting the curves. Other issues that would have to be considered in a detailed analysis would include corrections to the Pt-OH bond strength relative to its strength when adsorbed on an extended Pt surface and hydrogen bonding stabilization of OH(ads) by neighboring OH(ads) or H_2O(ads).

Chapter 6

Electrode Potential-Dependent Structure of OH Reduction on the Acid Electrolyte-Pt Surface Interface:A Combination of Density Functional Theory and Modified Poisson -Boltzmann Theory

6.1 Introduction of This New Method: A Combination of Density Functional Theory and Modified Poisson-Boltzmann Theory

The density functional theory has been making quantitative predictions for understanding the properties of the electrochemical reactions at the liquid-solid interfaces in fuel cells. However, it is still challenging to accurately seek the Gibbs free energy of the reaction center because of the difficulty in properly describing both of the potential-dependent bond strengths between the adsorbates and the electrode surfaces and the interaction between the adsorbates and the electrolyte. The potential-dependency requires charging the electrode surface which needs counter charges neutralizing the system. The best procedure for this is DFT slab-band calculations with the counter charge distribution determined self-consistently by a modified Poisson-Boltzmann (MPB) approach.[113-117] Such a program using DFT and MPB and a dielectric continuum solvation model was written by Jinnouchi in this lab recently.[69,70] The investigation in this chapter employed this newly-developed computational code, called Interface 1.0, to study the potential-dependent structure of the OH reduction step studied in Chap. 5.

6.2 Computational Details and Model used in the OH Reduction Step on Platinum Surface in Acid Solution

The calculations were carried out using Interface 1.0 in the two-dimensional periodic boundary condition option. The revised Perdew-Burke-Ernzerhof functional (RPBE) was used.[118] The Pt(111) surface was modeled by one layer of Pt slab with the theoretically predicted lattice constant of 4.03 Å from a bulk crystal calculation. The experimental value for Pt crystal is reported to be 3.93 Å.[89] The translation cell had 18 atoms, which

makes the calculations slow. Using multiple Pt layers must await parallelization of Interface 1.0. The structure of 1/6 monolayer coverage solvated OH(ads) was modeled by a OH adsorbed on a two-dimensional platinum slab in a $\sqrt{3} \times 3$ unit cell and the OH group is connected with a hydronium ion by a hydrogen bond as shown in Fig. 6.1. This is the same model as in local reaction center model study in Chapter 5. The hydronium ion is stabilized by two solvation water hydrogen bonding to it as in the previous acid studies. The six Pt atoms in the slab are fixed and the other atoms are free to relax.

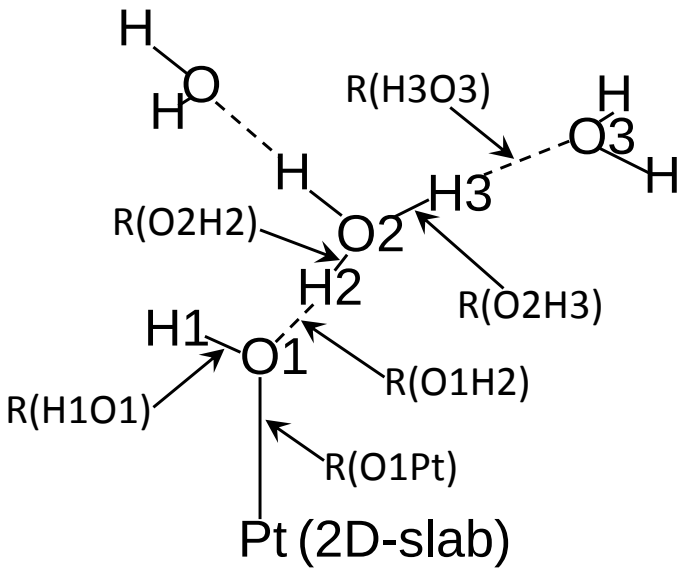

Figure 6.1 Structure of model used for OH(ads) on Pt(111) surface

6.3 Results of OH(ads) on Pt(111) Surface in Acid Solution

For tuning the electrode potential, a series of optimizations, each with a different net charge in the unit cell, were carried out. The electrode potential on the standard hydrogen electrode, SHE, scale is calculated from the Fermi energy of the band calculation by the formula

$$U = -(\varepsilon_F - \phi_{SHE})/e \quad (6.1)$$

where ε_F is the Fermi energy level, e is the charge of an electron, and ϕ_{SHE} is the thermodynamic work function of SHE, which is calculated to be -4.43 eV using RPBE. This value is in the range of experimental values from -4.80 eV to -4.28 eV.[26,119] Net charges in the unit cell were -0.2*e*, 0.0*e*, 0.4*e*, 0.5*e*, 0.6*e*, and +1.0*e* and the resulting Fermi levels and electrode potentials are shown in Fig. 6.2. The Fermi energy level

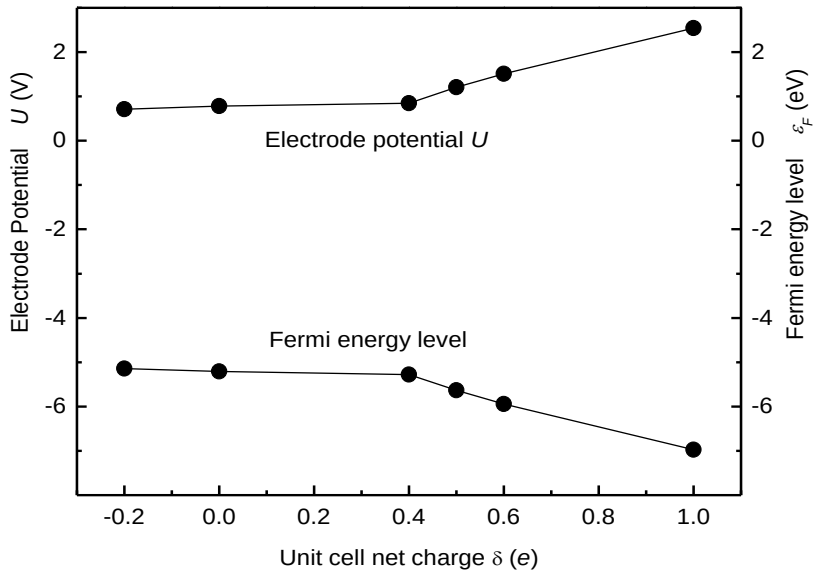

Figure 6.2 Dependencies of Fermi energy level and electrode potential on the net charge of the unit cell for Pt_6-OH ··HOH_2 ··$(H_2O)_2^{\delta}$. δ is the net charge.

increases from -6.972 eV to -5.143 eV as the net charge decreases from +1.0*e* to -0.2*e* which means adding electrons to the structure raises its Fermi energy level. The

corresponding electrode potential decreases from 2.542 V to 0.713 V according to equation (6.1).

Four views of the reduction precursor are shown in Figs. 6.3-6.6 and Figs. 6.7-6.10 are for the oxidation precursor. Figures 6.3 – 6.6 show that the unit cell with +1.0*e* charge has a apparent OH(ads) + hydronium ion structure, while the neutral unit cell apparently has a H_2O(ads) + H_2O(aq) structure. At this coverage steric interaction are absent but coulombic interactions between the positively charged reduction precursors will be present. The calculated potential-dependent structure parameters are shown in Fig. 6.11. In Figure 6.1, the two internuclear distances R(O1H2) and R(O2H2) define the position of proton in the hydronium ion between the OH(ads) and the oxygen atom in the hydronium ion. May be seen in Fig. 6.11, R(O1H2) and R(O2H2) change suddenly at the electrode potential ~0.8 V which is approximately the OH(ads) reduction potential and the working Pt cathode electrode potential in fuel cells. As the electrode potential decreases, R(O1H2) decreases and R(O2H2) increases showing the proton in the hydronium ion is approaching the OH(ads) and leaving the water of the hydronium ion. Above 0.8 V, R(O2H2) stretches from 1.00 Å to 1.05 Å which are normal lengths of O-H bond, and R(O1H2) shortens from 1.76 Å to 1.52 Å which are hydrogen bond lengths. In this electrode potential region, the structure is a OH(ads) hydrogen bonding to a hydronium ion. Below 0.8 V, R(O1H2) drops quickly to 0.99 Å; R(O2H2) increases quickly to 1.90 Å. In the electrode potential region lower than 0.8 V, the structure apparently changes into a H_2O(ads) hydrogen bonding to a H_2O(aq). As the structure changes to water like, the adsorbed water moves away from the platinum surface where the R(O1Pt) quickly significantly from ~2.0 Å to 2.33 Å – 2.69 Å. The changing of

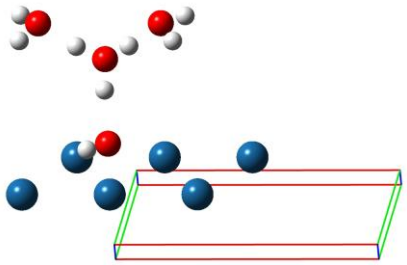

Figure 6.3 One unit cell for Pt_6-OH ··HOH_2 ··$(H_2O)_2^{+1}$

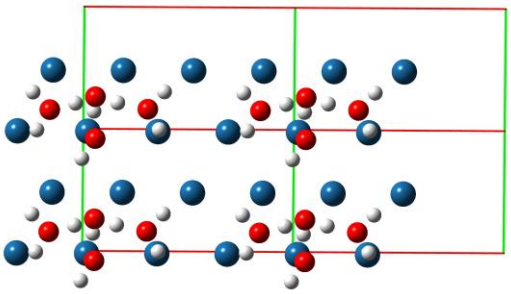

Figure 6.4 Top view of four unit cells for Pt_6-OH ··HOH_2 ··$(H_2O)_2^{+1}$

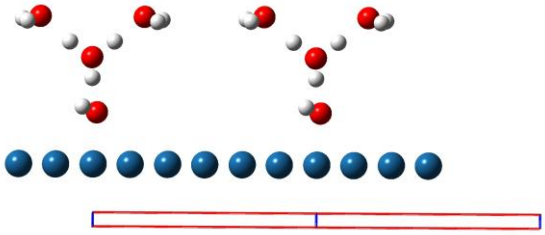

Figure 6.5 Front view of four unit cells for Pt_6-OH ··HOH_2 ··$(H_2O)_2^{+1}$

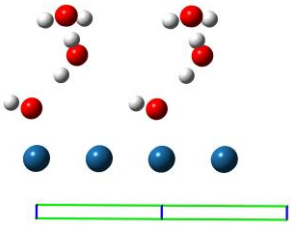

Figure 6.6 Side view of four unit cells for Pt_6-OH ··HOH_2 ··$(H_2O)_2^{+1}$

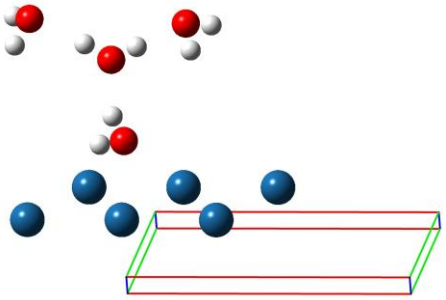

Figure 6.7 One unit cell for Pt_6-OH ··HOH_2 ··$(H_2O)_2$

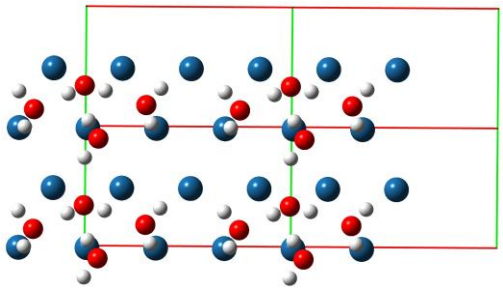

Figure 6.8 Top view of four unit cells for Pt_6-OH ··HOH_2 ··$(H_2O)_2$

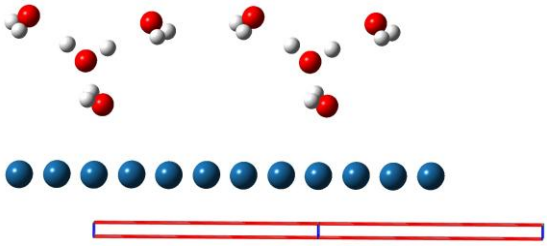

Figure 6.9 Front view of four unit cells for Pt_6-OH ··HOH_2 ··$(H_2O)_2$

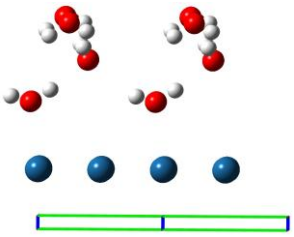

Figure 6.10 Side view of four unit cells for Pt_6-OH ··HOH_2 ··$(H_2O)_2$

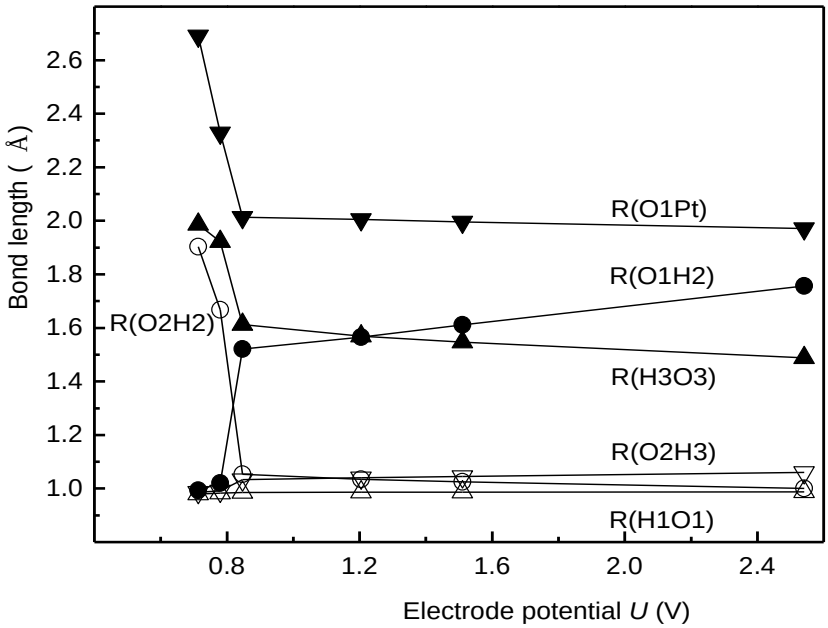

Figure 6.11 Calculated electrode potential-dependent structure parameters for Pt_6-OH ··HOH_2 ··$(H_2O)_2$

R(H3O3) shows that as the hydronium ion is reduced to water, the hydrogen bonding to the solvation water molecules weakens and the solvating water molecules move away a little. This structure change at ~0.8 V corresponds to the OH(ads) reduction reaction on platinum electrodes. It is higher than the experimental value of 0.68 V at 1/4 ML but if co-adsorbed water were present it would stabilize OH(ads) and decrease the calculated potential.[69,70]

The potential-dependent total energy of the unit cell is shown in Fig. 6.12. To make the total energies of the unit cell with different charges comparative one another, the total mass of the unit cell needs to be conserved. The mass of the neutral unit cell is made to be the reference. So the positive unit cell is added a certain fraction electron to make the total mass the same as the neutral unit cell, and, on the other hand, the negative unit cell

is taken a certain fraction electron away to make the total mass equal. To keep the equilibrium, the added or taken away fraction electron is assumed to be at the corresponding electrode potential or at the Fermi level. The mass conservation term is

$$E_{\mathrm{mc}} = \varepsilon_F \delta \tag{6.2}$$

where δ is the net charge of the unit cell. The comparative total energy is

$$E_{\mathrm{tot}} = E_{\mathrm{unit\ cell}} + E_{\mathrm{mc}} \tag{6.3}$$

where $E_{\mathrm{unit\ cell}}$ is the calculated energy of the unit cell. The total energy curve in Fig. 6.12

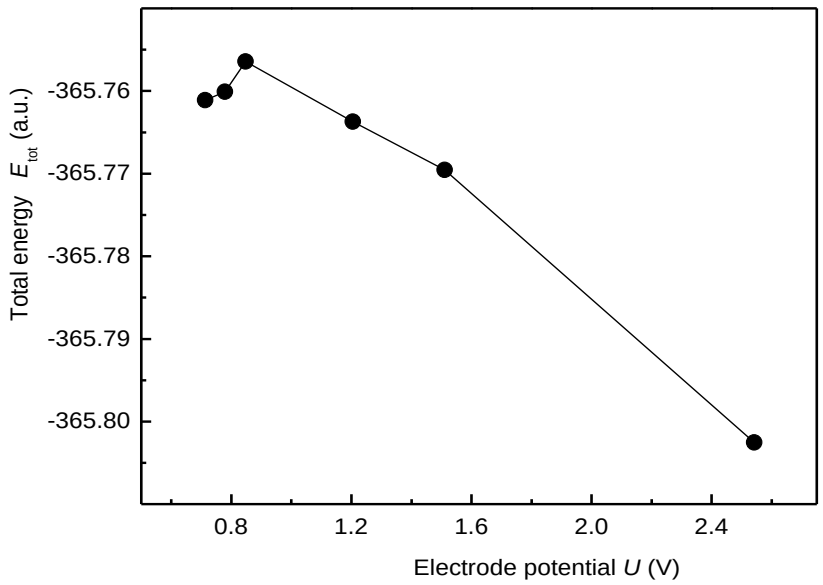

Figure 6.12 Electrode potential-dependent total energy of the unit cell for Pt_6-OH ··HOH_2 ··$(H_2O)_2$

shows that the energy has a peak at ~0.8 V which is the structure changing potential. At this potential the H2-O1 bonds are about half-formed. Above this value, as the potential increases, there are more empty bands in the platinum for the p electron donation from OH(ads). The stronger bonding lowers the total energy. Below 0.8 V, H2O1 bond becomes complete, lowering the energy some, but as the potential decreases the H_2O lone-pair donation bond to the surface becomes weaker so the total energy levels out. If the H_2O were allowed to reorient and form hydrogen bonds to the surface, the total energy would decrease.

6.4 Conclusions on the Electrode Potential-Dependent Structure of OH(ads) on Pt(111) Surface.

This study used the newly-developed combined DFT and MPB method to explore the potential-dependent adsorption structure of OH on platinum in acid solution. The surface charging was performed to realize tuning the electrode potential during structure optimization. The interesting results show that the structure change from OH(ads) to H_2O(ads) happens at ~0.8 V is close to the OH(ads) reduction potential at low coverage on platinum electrodes and also close to the working potential of oxygen cathodes in fuel cells. This new method improves the local reaction center model describing the structure and the adsorption bond strength at the adsorbate-solid electrochemical interface by self-consistently treating all features of the system.

Chapter 7

Miscellaneous Computations:

Conductivity in Boron-Doped Diamond

***** Based on Publication in Ref. 120.

7.1 Computations on Defect Diamond Clusters

A theoretical study on the origin of shallow n-type conductivity in boron-doped diamond with H or S co-doping has been done using density functional theory. This work was started by T. V. Albu and continued by L. N. Kostadinov and Y. Cai in Anderson's lab.[120-122] My contribution was to complete this theoretical study. The ionization potentials and the electron affinities of doped diamond were calculated using B3LYP hybrid density functional theory and nanocrystalline cluster models, while taking into account the quantum confinement of the charge carriers. In many cases donor and acceptor levels were created in the middle of the gap between the conduction and valence bands. The following is a brief summary of the main results and how they relate to observations of conductivity in doped diamond.

7.2 Cluster Models for the Defect Diamond

The cluster and geometry variables used in Ref. 121 were also used in this study, and they are illustrated in Fig. 7.1. For the structure optimizations and total energy calculations, the quantum chemical package Gaussian 03 was used. It has been demonstrated by Albu et al. that ionization potentials, IP, and electron affinities, EA, calculated by the B3LYP hybrid density functional method with a 6-31G basis for cluster models of point defects can be used to obtain accurate excitation energy predictions for defects in bulk diamond. In cases where the electron or hole added to the cluster model is free, the quantum confinement energy, which is the kinetic energy, for an electron or hole in a three-dimensional box approximately the size of the cluster model is determined. For the C44H42 cluster used, the quantum confinement energy is 2.07 eV,[121] and this

value is added to the electron affinity of the cluster and subtracted from the ionization potential of the cluster.

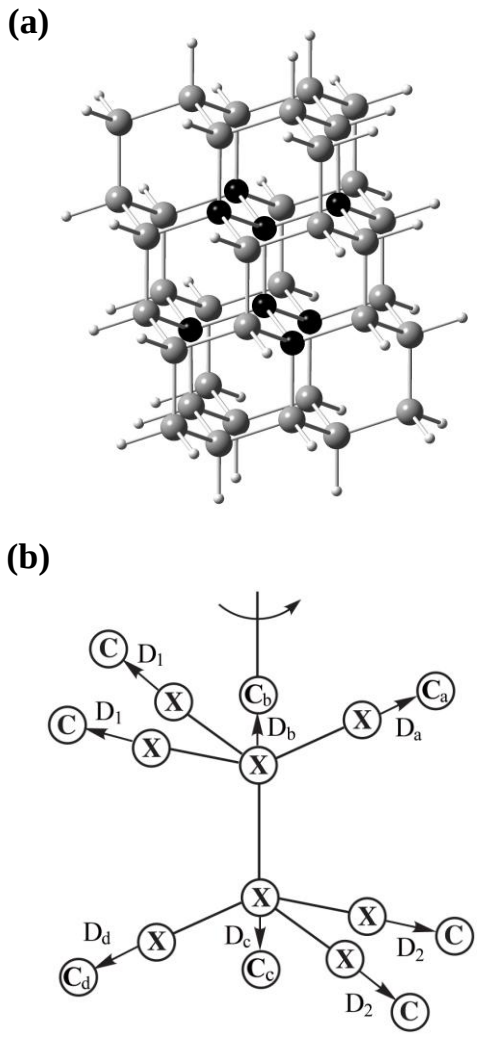

Figure 7.1 Cluster model used in this study with defect site atoms in black and structure variable optimized by motions along the [111] directions. The X's indicate positions of dummy atoms used to define the directions of relaxations during structure optimizations. Sp^3 hybridization of surface carbon atoms is maintained by bonding hydrogen atoms (small spheres) to them.

7.3 Results of Calculations for BB, SVS, and (B,S) co-doped complexes and BH_n, B_nH_m and vacancy complexes co-doped with H

The electronic structure results for the defects involving substitutional B and S are shown in Fig. 7.2. The calculated -IP and -EA for several of the BH_n defects and for other species are shown in Fig. 7.3. Optical results are without structure relaxation in the ions and thermal results include structure relaxation.

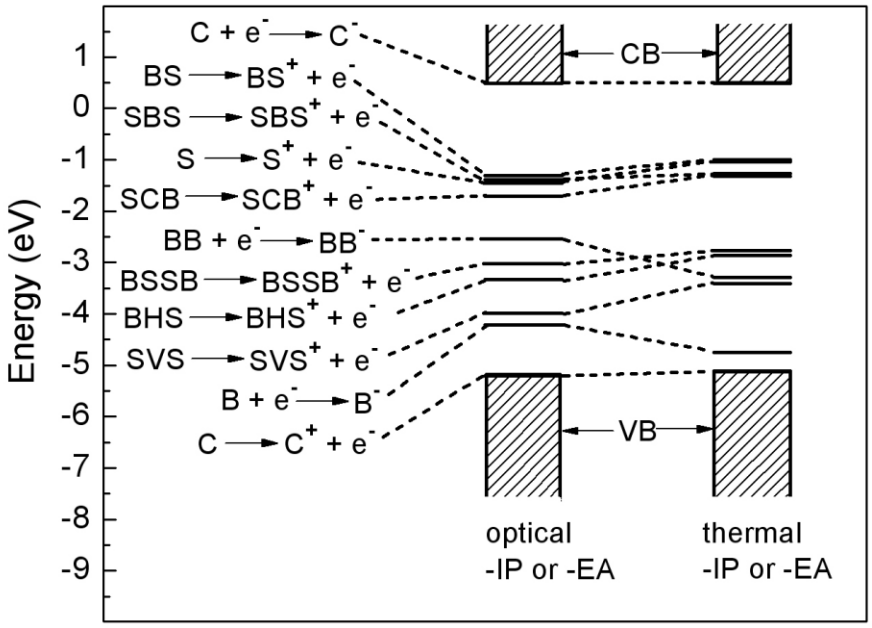

Figure 7.2 Calculated optical and thermal –IP and -EA for various diamond clusters with both boron and sulfur dopants. The ionization products are shown on the left. CB is the conduction band and VB is the valence band of bulk diamond.

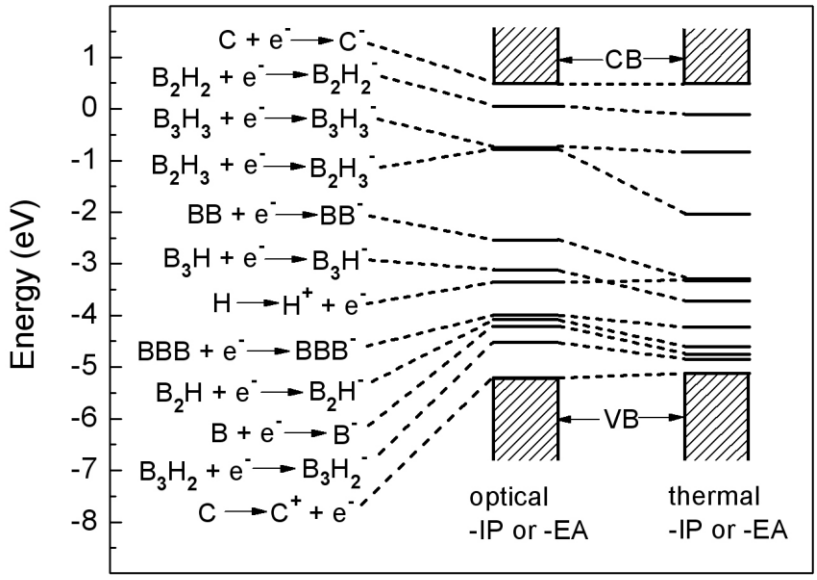

Figure 7.3 Calculated optical and thermal –IP/-EA for various diamond clusters with both boron and hydrogen dopants. The ionization products are shown on the left. CB is the conduction band and VB is the valence band of bulk diamond.

7.4 Conclusions on Calculations of Defect Diamond

The shallow n-type conductivity if diamond co-doped with boron and sulfur[123] can be explained in terms of specific defects and donor and acceptor states in the band gap as calculated here. For the SVS donor, the thermal excitation energy to the BB acceptor is small, 0.12 eV and in good agreement with measured activation energies in Ref. 123. The Fermi level lies 1.58 eV above the Fermi level for p-type boron-doped diamond, in satisfactory agreement with the 1.2 eV difference determined from a Mott-Schottky analysis.[123] Thus it appears that the SVS donor BB acceptor system may account for the

n-type conductivity observed in the co-doped diamond films. This conductivity is due to states in the band gap and net electron excitations to the diamond bulk conduction band.

The observed change in boron-doped diamond from p-type conductivity to n-type upon D (H) plasma treatment[124,125] can also be attributed to states in the band gap where interstitial H is the mid band gap donor and a B_nH_m complex serves as the mid band gap acceptor. Of the boron based defects tried, BB would be an excellent acceptor candidate, except it is expected to be passivated by the plasma treatment, just like B. BBHB has nearly the right acceptor property, and if it is present in the original boron-doped diamond or formed from BBB by the plasma treatment it might, within the errors of the calculations, be a shallow acceptor relative to H donors, allowing high electron mobility by the SIBG mechanism. However, BBHB can bond H too and become passivated. As pointed out in Ref. 124, annealing the n-type samples converts them to non-conducting and finally p-type as H diffuses out. Since one or two H_i are calculated to bond to BB and BBB more strongly the H_i bonds to B it would seem that, once hydrogenated, the BB and BBB defects would be robust toward annealing. This suggests the need for further theoretical studies of new cluster defects and at the same time suggests interesting experiments such as exposing the boron + sulfur-doped n-type diamond to D (H) plasma to see if it eliminates conductivity by passivating BB acceptors and increased exposure of boron-doped systems to the D (H) plasma to see if the proposed BBHB acceptors are passivated.

Additional calculations showed that any vacancies that form during low pressure diamond growth will not survive and will be saturated with H. Such defects will be deep donors.

Summary and Prospects of this Study

The mechanisms of the fundamental reactions of hydrogen evolution and oxidation and of oxygen reduction on platinum have been explored using theory in this thesis work. The potential dependencies of activation internal energy curves for electron transfer reactions were calculated using constrained variation theory in local reaction center model. The local reaction center model presented the properties of the bonds broken and formed in chemical reactions. Solvation medium was included as the potential contributed to the reaction center by summing over assumed ion distribution in the electrolyte. Using this theoretical method, the calculated potential-dependent activation energy curves should be useful to assistant making predictions and explanations of electrocatalytic mechanisms. Applications of the linear Gibbs energy relationship for predicting reversible potentials were not as accurate as past work using band theory because the small surface models generally did not give bond strengths equal to the adsorption bond strengths.

While having advantages, the current local reaction center model calculations have defects at the same time. The results of reversible potentials, precursor potentials, and activation energies are based on the total energies instead of the Gibbs free energies of the reaction center models. The contribution of $P\Delta V - T\Delta S$ in the Gibbs free energy is omitted. Secondly, coarse approximation is made by the Madelung term, which is a point charge placed in the local reaction center model to simulate the effect of the electric field of the electrolyte. Thirdly, the local reaction center model has a limited number of atoms being calculated because the computational cost of big cluster model cannot be afforded.

Those three parts introduce the main uncertainty to this theoretical method for electron transfer reactions. On the other hand, applications using the linear Gibbs energy relationship are less problematical and in some cases predictions are improved by including coadsorbed molecules.

The newly-developed program using the combined DFT and MPB, Interface 1.0, is a promising theoretical tool in the investigation of the interface and catalyzing electrochemistry.[69,70] In this thesis, the potential-dependent adsorption structure calculations of OH(ads) on Pt(111) surface in acid solution gave an interesting match between the potential region when the OH(ads) + hydronium ion change into H_2O(ads) + H_2O(aq) with the cathode electrode working potential of oxygen reduction in fuel cell. More studies like this are needed, such as O_2(ads) reduction to OOH(ads) to see how general and accurate this approach to reversible potential is.

Applications of the local reaction center model and the combined DFT and MPB method will be exiting to explore the electrochemical reactions catalyzed by different kinds of catalysts and to assist improving and finding new better catalyst materials.

Appendix

Quantum chemistry applies quantum mechanics to address issues and problems of chemical reactions. In quantum chemistry, the system is described by a wavefunction which can be found by solving the Schrödinger equation. This equation relates the stationary states of the system and their energies to the Hamiltonian operator, which can be viewed as the recipe for obtaining the energy associated with a wavefunction describing the positions of the nuclei and electrons in the system:

$$H\Psi = E\Psi \tag{1}$$

where H is the Hamiltonian operator, Ψ is the wavefunction to describe the state of the system, and E is the eigenenergy corresponding to the state of the system. Associated with each measurable parameter in a physical system is a quantum mechanical operator. The Hamiltonian operator contains the operations associated with the kinetic and potential energies:

$$H = T + V$$

$$= -\left(\frac{h^2}{8\pi^2}\right)\sum_i \frac{1}{m_i}\left(\frac{\partial^2}{\partial x_i^2} + \frac{\partial^2}{\partial y_i^2} + \frac{\partial^2}{\partial z_i^2}\right) + \sum_{i<j}\left(\frac{e_i e_j}{r_{ij}}\right) + V_{ne} \tag{2}$$

where T is the kinetic operator and V is the potential operator which includes electron-electron repulsion, nucleus-nucleus repulsion and electron-nucleus attraction. The

Schrödinger equation can be solved analytically for H, H_2^+ and analogues, but not for many-electron atoms and molecules. To study many-electron systems we have to rely on combinations variation and perturbation theory to obtain approximate wavefunctions and energies.

1. Methods Based on Wave Functions

1.1 Hartree-Fock Equation

One widely used approximation method is the Hartree-Fock method.[126,127] It is a single-determinant one-electron method when every electron moves in the potential field created by the nucleus plus the average potential of all the other electrons. This assumption leads to the independent-particle model, which essentially reduces the many-electron problem to the problem of solving a number of coupled single-electron equations. For a system with *n* electrons, the part in Hamiltonian for electrons is:

$$H^{\text{elec}} = T^{\text{elec}} + V^{\text{elec}}$$

$$= -\frac{\hbar^2}{2m}\sum_{i=1}^{n}\nabla_i^2 + \sum_{\text{i=1}}^{\text{n}}\sum_{\text{j}>i}\frac{\text{e}^2}{\text{r}_{\text{ij}}} - \sum_{i=1}^{n}\sum_{s}^{nuclei}\frac{Z_s e^2}{r_{is}} \qquad (3)$$

and the whole Hamiltonian for the system is:

$$H = H^{\text{elec}} + V^{\text{nucl}}$$

$$= -\frac{\hbar^2}{2m}\sum_{i=1}^{n}\nabla_i^2 + \sum_{i=1}^{n}\sum_{j>i}\frac{e^2}{r_{ij}} - \sum_{i=1}^{n}\sum_{s}^{nuclei}\frac{Z_s e^2}{r_{is}} + \sum_{s}^{nuclei}\sum_{t>s}^{nuclei}\frac{Z_s Z_t e^2}{R_{st}} \quad (4)$$

Trial wavefunctions are used and their parameters determinate variationally to obtain wavefunctions and energies for a system. For molecules, a linear combination of atomic orbitals, Φ_i, is used:

$$\Psi_{MO} = \sum_{i=1}^{n} C_i \Phi_i \quad (5)$$

where C_i are linear parameters. According to variation theory, the expectation value of the Hamiltonian H of any trail wavefunction Ψ_{trial} is greater than the true energy E_0 of the ground state wavefunction Ψ_0.

$$\langle \Psi_{trial}^{*} | H | \Psi_{trial} \rangle \geq E_0 \quad (6)$$

For the optimized variational wavefunction, the first derivative of energy respect to C_i is zero.

$$\frac{\partial E}{\partial C_i} = 0 \quad (7)$$

The set of atomic orbitals, Φ_i, combined to form the wave function is called the basis set. Considering the computational cost, the smaller basis set with the desired computational precision is preferred.

1.2 Slater Type Orbitals and Gaussian Type Orbitals

In the early molecular orbital calculations, Slater type atomic orbitals were widely used. There are functions that decrease exponentially with distance from the nuclei.[128]

$$\varphi(r,\theta,\Phi;\ \zeta,n,l,m) = (2\zeta)^n \sqrt{\frac{2\zeta}{(2n)!}} r^{n-1} e^{-\zeta r} \Psi_l^m(\theta,\Phi) \qquad (8)$$

where n = 1,2,..., r is the distance of the electron from the atomic nucleus, and ζ is a non-linear parameter and $\Psi_l^m(\theta,\Phi)$ are spherical harmonic functions. For minimal basis sets n and s and ζ are historically related to principle quantum number and effective nuclear charge. Atomic *s*, *p*, *d* etc. orbital shapes are given by linear combinations of the spherical harmonics. Later, it was realized by Frank Boys that Slater-type orbitals could be approximated as linear combinations of Gaussian orbitals.[129]

$$\Phi(x,y,z;\ \alpha,i,j,k) = \left(\frac{2\alpha}{\pi}\right)^{3/4} \left[\frac{(8\alpha)^{i+j+l} i!j!k!}{(2i)!(2j)!(2k)!}\right]^{1/2} x^i y^j z^k e^{-\alpha(x^2+y^2+z^2)} \qquad (9)$$

where *x*, *y*, and *z* are the Cartesian coordinates, α is an exponent which defines the orbital size, and *i*, *j*, *k* are non-negative integers corresponding to the shape of the orbital. When $i = j = k = 0$, Φ is 1*s*-type Gaussian orbital. For $i = 1$, $j = k = 0$, Φ is $2p_x$-type Gaussian orbital, and for $j = 1$, $i = k = 0$, Φ is $2p_y$-type Gaussian orbital. While $k = 1$, $i = j = 0$, Φ is a $2p_z$-type Gaussian orbital:

$$\Phi_{1s} = \left(\frac{2\alpha}{\pi}\right)^{3/4} e^{-\alpha(x^2+y^2+z^2)}$$

$$\Phi_{2p_x} = \left(\frac{128a^5}{\pi^3}\right)^{1/4} xe^{-\alpha(x^2+y^2+z^2)}$$

$$\Phi_{2p_y} = \left(\frac{128a^5}{\pi^3}\right)^{1/4} ye^{-\alpha(x^2+y^2+z^2)}$$

$$\Phi_{2p_z} = \left(\frac{128a^5}{\pi^3}\right)^{1/4} ze^{-\alpha(x^2+y^2+z^2)} \quad (10)$$

When $i + j + k = 2$, Φ is a *d*-type Gaussian orbital, and $i + j + k = 3$gives out an *f*-type Gaussian orbital. Because it is easier to calculate overlap and other integrals with Gaussian basis functions, this led to huge computational savings while maintaining accuracy, particularly when using contracted Gaussian functions which are linear combinations of the primitive Gaussian functions with different values of α to approximate the radial part of Slater-type orbitals:

$$\varphi(x, y, z; \{\alpha\}, i, j, k) = \sum_{m=1}^{M} C_m \Phi(x, y, z; \alpha_a, i, j, k) \quad (11)$$

where *M* is the number of primitive Gaussian functions used in the combination to make the contracted Gaussian functions.

During most molecular bonding, it is the valence electrons which principally take part in the bonding. In recognition of this fact, it is common to represent valence orbitals by more than one basis function, each of which can be composed of a linear combination of primitive Gaussian functions. Basis sets in which there are multiple basis functions

corresponding to each valence atomic orbital, are called valence double, triple, or quadruple-zeta basis sets. Since the different orbitals have different spatial extents, the combination allows the electron density to adjust its spatial extent appropriate to the particular molecular environment. Minimum basis sets are fixed and are unable to adjust to different molecular environments. The so-called Split-Valence basis sets are always needed for satisfactory results. In a Split-Valence basis set, the each core atomic orbital comprises one contracted Gaussian function which is a linear combination of primitive Gaussian functions, and each of the valence orbitals is split into multiple contracted Gaussian functions. The Split-Valence basis sets are denoted typically as X-YZg by Pople.[130] In this case, X represents the number of primitive Gaussians comprising each core atomic orbital basis function. The Y and Z indicate that each of the valence orbitals is composed of two basis functions, the first one composed of a linear combination of Y primitive Gaussian functions, the other composed of a linear combination of Z primitive Gaussian functions. The presence of two numbers after the hyphens implies that this basis set is a Split-Valence double-zeta basis set. Split-Valence triple- and quadruple-zeta basis sets are also used, denoted as X-YZWg, X-YZWVg, etc.

The most common addition to minimal basis sets is the polarization functions, denoted (in the names of basis sets developed by Pople[130]) by an asterisk, *. Double asterisks, **, indicate that polarization functions are also added to light atoms (hydrogen and helium). These auxiliary functions have one additional node. For example, the only basis function located on a hydrogen atom in a minimal basis set is a function for the 1*s* atomic orbital. When polarization is added to this basis set, a *p*-type function is added to the basis set. This adds some additional needed flexibility within the basis set, effectively making the

molecular orbitals involving the hydrogen atoms to be more asymmetric about the hydrogen nucleus. This gives a more accurate description, because the bonding between atoms makes the electron cloud around hydrogen atoms spherically asymmetric. Similarly, *d*-type functions can be added to a basis set with *p*-type orbitals, and f-functions to a basis set with *d*-type orbitals, and so on.

Another common addition to basis sets is the addition of diffuse functions to the heavy atoms which is denoted by a plus sign, +. Double plus signs, ++, indicate that diffuse functions are also added to light atoms (hydrogen and helium). These functions more accurately represent the outer portion of the atomic orbitals, which are distant from the atomic nuclei. These additional basis functions are particularly needed to produce more accurate electron affinities for large molecular systems and anions.

1.3 Perturbation Theory

Perturbation theory is a set of approximation schemes directly related to mathematical perturbation for describing a complicated quantum system in terms of a simpler one. The idea is to start with a simple system and gradually turn on an additional "perturbing" Hamiltonian representing a weak disturbance to the system. If the disturbance is not too large, the various physical quantities associated with the perturbed system will be continuously generated from those of the simple system. An unperturbed Hamiltonian H_0, which is also assumed to have no time dependence. It has known energy levels and eigenstates, arising from the time-independent Schrödinger equation:

$$H_0\left|n^{(0)}\right\rangle = E_n^{(0)}\left|n^{(0)}\right\rangle, \quad n = 1, 2, 3, \cdots \tag{12}$$

where n is the eigenfunction. The (0) superscripts denote that these quantities are associated with the unperturbed system. Now a perturbation is introduced to the Hamiltonian. Let V be a Hamiltonian representing a disturbance and λ be a dimensionless parameter that can take on values ranging continuously from 0 (no perturbation) to 1 (the full perturbation). The perturbed Hamiltonian is

$$H = H_0 + \lambda V \tag{13}$$

The perturbation term λV is added to the Hamiltonian for the ground state.

$$(H_0 + \lambda V)|n\rangle = E_n|n\rangle \tag{14}$$

The wave function and energy for the ground state can both be written as power series in λ:

$$|n\rangle = \left|n^{(0)}\right\rangle + \lambda\left|n^{(1)}\right\rangle + \frac{1}{2!}\lambda^2\left|n^{(2)}\right\rangle + \cdots \tag{15}$$

$$E_n = E_n^{(0)} + \lambda E_n^{(1)} + \frac{1}{2!}\lambda^2 E_n^{(2)} + \cdots \tag{16}$$

Substituting the power series of eq (15) and eq (16) into eq (14) get

$$(H_0 + \lambda V)\left(\left|n^{(0)}\right\rangle + \lambda\left|n^{(1)}\right\rangle + \cdots\right)$$

$$= \left(E_n^{(0)} + \lambda E_n^{(1)} + \frac{1}{2!}\lambda^2 E_n^{(2)} + \cdots\right)\left(\left|n^{(0)}\right\rangle + \lambda\left|n^{(1)}\right\rangle + \cdots\right) \quad (17)$$

Expanding this equation and comparing coefficients of each power of λ results in an infinite series of simultaneous equations. The equations for second order Møller-Plesset perturbation theory (MP2)[131] are obtained:

$$H_0\left|n^{(1)}\right\rangle + V\left|n^{(0)}\right\rangle = E_n^{(0)}\left|n^{(1)}\right\rangle + E_n^{(1)}\left|n^{(0)}\right\rangle \quad (18)$$

$$H_0\left|n^{(2)}\right\rangle + V\left|n^{(1)}\right\rangle = E_n^{(0)}\left|n^{(2)}\right\rangle + E_n^{(1)}\left|n^{(1)}\right\rangle + E_n^{(2)}\left|n^{(0)}\right\rangle \quad (19)$$

The correction of energy shifts are:

$$E_n^{(1)} = \left\langle n^{(0)}\middle|V\middle|n^{(0)}\right\rangle \quad (20)$$

$$E_n^{(2)} = \sum_{k\neq n} \frac{\left|\langle k^{(0)}|V|n^{(0)}\rangle\right|^2}{E_n^{(0)} - E_k^{(0)}} \left\langle n^{(0)}\middle|V\middle|n^{(0)}\right\rangle \quad (21)$$

2. Density Functional Theory

Density functional theory tries to solve the complicated many-body problem using the charge density of the system. Unlike the experimentally unavailable wave function of a system with N electrons which depends on 4N variables, three spatial and one spin variable for each of the N electrons, density functional theory uses the experimentally

observable and measurable electron density which is simply a function of the three spatial coordinates x, y and z.

2.1 The Thomas-Fermi Model

The first attempts to use the electron density rather than the wave function for obtaining information about atomic and molecular systems date back to early work for Thomas and Fermi, 1927.[132,133] The Thomas-Fermi model takes into account the kinetic energy in a quantum statistical way while treating the nuclear-electron and electron-electron contributions classically. In this model, the uniform electron gas approximation is used and the energy is given by

$$E_{TF}[\rho(r)] = \frac{3}{10}(3\pi^2)^{2/3}\int \rho^{5/3}(r)dr - Z\int \frac{\rho(r)}{r}dr + \frac{1}{2}\iint \frac{\rho(r_1)\rho(r_2)}{r_{12}}dr_1 dr_2 \quad (22)$$

where ρ(r) is the electron density distribution function. This omits electron exchange and correlation energy correction to the Coulomb term. It is noted that these terms are defined in the wavefunction approach.

2.2 Slater's Approximation of Hartree-Fock Exchange, Xα Method

Another early example is that Slater ignored the correlation energy and added a term identified with the exchange energy from the Hartree-Fock approach:[134]

$$E_{X\alpha}[\rho(r)] = -\frac{9}{8}\left(\frac{3}{\pi}\right)^{1/3}\alpha\int \rho^{4/3}(r)dr \quad (23)$$

where α is a semiempirical parameter introduced to improve the quality of calculated properties. This approach is called the Xα method.

2.3 Hohenberg-Kohn Theorems

In 1964, Hohenberg and Kohn proved two theorems which motivated the development of modern density functional theory.[135] The first theorem states that the external potential $V_{ext}(r)$ is a unique functional of ρ(r); since, in turn $V_{ext}(r)$ fixes H, and then the full many particle ground state is a unique functional of ρ(r). The second theorem demonstrates that the ground state energy is minimized by the ground state electron density:

$$E_0[\rho_0] \leq E[\rho] \tag{24}$$

where the ρ_0 is the electron density of the ground state and the ρ is a trial electron density. This leads to the variational principle. The complete ground state energy is a functional of the ground state electron density:

$$E_0[\rho_0] = T[\rho_0] + E_{ee}[\rho_0] + E_{Ne}[\rho_0] = F_{HK}[\rho_0] + E_{Ne}[\rho_0] \tag{25}$$

where $T[\rho_0]$ is the kinetic energy, $E_{ee}[\rho_0]$ is the electron-electron repulsion, $E_{Ne}[\rho_0]$ is the nuclei-electron attraction, and $F_{HK}[\rho_0]$ is called Hohenberg-Kohn functional which contains the system independent part.

$$E_{ee}[\rho_0] = \frac{1}{2}\iint \frac{\rho_0(r_1)\rho_0(r_2)}{r_{12}} dr_1 dr_2 + E_{ncl}[\rho_0] = J[\rho_0] + E_{ncl}[\rho_0] \tag{26}$$

where $J[\rho_0]$ is the classical Coulomb part and $E_{\text{ncl}}[\rho_0]$ is the non-classical contribution to the electron-electron interaction containing all the effects of exchange and Coulomb correlation. $F_{HK}[\rho_0]$ is an unknown functional.

2.4 Kohn-Sham Equations

Kohn and Sham, in 1965, introduced the orbital approximation to the kinetic energy.[136]

$$T_s = -\frac{1}{2}\sum_i^n \langle \varphi_i | \nabla^2 | \varphi_i \rangle \tag{27}$$

$$F_{HK}[\rho_0] = T_s[\rho_0] + J[\rho_0] + E_{XC}[\rho_0] \tag{28}$$

where E_{XC} is called exchange-correlation energy.

$$E_{XC}[\rho_0] \equiv (T[\rho_0] - T_s[\rho_0]) + (E_{ee}[\rho_0] - J[\rho_0]) = T_C[\rho_0] + E_{ncl}[\rho_0] \tag{29}$$

where $T_C[\rho_0]$ is the residual part of the true kinetic energy which is not covered by $T_S[\rho_0]$ added to the non-classical electrostatic contributions.

With these substitutions, the energy of system is given by:

$$E_0[\rho_0] = T_s[\rho_0] + J[\rho_0] + E_{XC}[\rho_0] + E_{Ne}[\rho_0]$$

$$= T_s[\rho_0] + \frac{1}{2}\iint \frac{\rho_0(r_1)\rho_0(r_2)}{r_{12}} dr_1 dr_2 + E_{XC}[\rho_0] + \int V_{Ne}\rho_0 dr$$

$$= -\frac{1}{2}\sum_i^n \langle\varphi_i|\nabla^2|\varphi_i\rangle + \frac{1}{2}\sum_i^N \sum_j^N \iint |\varphi_i(r_1)|^2 \frac{1}{r_{12}} \left|\varphi_j(r_2)\right|^2 dr_1 dr_2$$

$$+E_{XC}[\rho_0] - \sum_i^N \int \sum_A^M \frac{Z_A}{r_{1A}} |\varphi_i(r_1)|^2 dr_1 \qquad (30)$$

The one-particle equations are:

$$\left\{-\frac{1}{2}\nabla^2 + \left[\int \frac{\rho_0(r_2)}{r_{12}} dr_2 + V_{XC}(r_1) - \sum_A^M \frac{Z_A}{r_{1A}}\right]\right\}\varphi_i = \varepsilon_i \varphi_i \qquad (31)$$

If the exact forms of E_{XC} and V_{XC} were known, the Kohn-Sham equation will lead to the exact energy, the correct eigenvalue of the Hamiltonian H of the Schrödinger equation. But $E_{XC}[\rho_0]$ and V_{XC} are unknown and can only be guessed.

2.5 Local Density Approximation (LDA)

All the approximate exchange and correlation functionals are based on the local density approximation. This approximation uses a uniform electron gas to approximate the exchange-correlation functional.

$$E_{XC}^{LDA}[\rho] = \int \rho(r)\varepsilon_{XC}\big(\rho(r)\big) dr \qquad (32)$$

where the $\varepsilon_{XC}(\rho(r))$ is the exchange-correlation energy per particle of a uniform electron gas of density $\rho(r)$. The quantity $\varepsilon_{XC}(\rho(r))$ can be further split into exchange and correlation contributions,

$$\varepsilon_{XC}\big(\rho(r)\big) = \varepsilon_X\big(\rho(r)\big) + \varepsilon_C\big(\rho(r)\big) \tag{33}$$

The ε_X, so called Slater exchange, represents the exchange energy of an electron in a uniform electron gas as found by Slater:[134]

$$\varepsilon_X = -\frac{3}{4}\sqrt[3]{\frac{3\rho(r)}{\pi}} \tag{34}$$

The correlation part, ε_C, uses the values based on Monté Carlo calculations of the energy of homogeneous electron gases of varying densities.[137-140] When the LDA approximation is used, molecular bond strengths are generally overestimated.[141]

2.6 Generalized Gradient Approximation (GGA)

The generalized gradient approximation improves on the LDA by including the gradient of the density, $\nabla\rho(r)$, to account approximately for the non-homogeneity of the true electron density. The exchange functional is:

$$E_X^{GGA} = E_X^{LDA} - \sum_\sigma \int F(s_\sigma)\rho_\sigma^{4/3}(r)dr \tag{35}$$

The function F is the reduced density gradient for spin σ.

$$s_\sigma(r) = \frac{|\nabla \rho_\sigma(r)|}{\rho_\sigma^{4/3}(r)} \quad (36)$$

where s_σ is a local inhomogeneity parameter which assumes large values not only for parts of ρ(r) with large gradients, but also in regions of small densities. For the function F, Becke developed in 1988:[142]

$$F^{B88} = \frac{\beta s_\sigma^2}{1+6\beta s_\sigma \sin h^{-1} s_\sigma} \quad (37)$$

β is an empirical parameter determined by a least-squares fit to the exactly known exchange energies of the rare gas atoms He through Ru.

2.7 Hybrid Functionals

For more accurate results, the functionals take into account a certain amount of exact exchange energy, which is calculated within Hartree-Fock method, incorporating with the exchange-correlation energy approximated by functional. These functionals are called DFT/HF hybrid functional. Becke's three parameter exchange-correlation functional introduced semiempirical coefficients to determine the weights of the various components:[143]

$$E_{XC}^{B3} = E_{XC}^{LSD} + a(E_{XC}^{HF} - E_X^{LSD}) + bE_X^{B88} + cE_C^{PW91} \quad (38)$$

The three empirical parameters were chosen such that the atomization, ionization energies and some total energies were optimally reproduced which lead to a = 0.20, b = 0.72, and c = 0.81.

The most current popular hybrid functional, B3LYP, was suggested by Stephens et al.[144] In B3LYP functional, the PW91 correlation functional is replaced by the Lee-Yang-Parr (LYP) functional. The B3LYP exchange-correlation energy expression is:

$$E_{XC}^{B3LYP} = (1-a)E_X^{LSD} + aE_{XC}^{HF} + bE_X^{B88} + cE_C^{LYP} + (1-c)E_C^{LSD} \qquad (39)$$

Bibliography

(1) Gurney, R. W. *Proceedings of the Royal Society of London. Series A* **1931**, *134*, 137-154.

(2) Condon, E. *Physical Review* **1926**, *28*, 1182-1201.

(3) Condon, E. *Physical Review* **1928**, *32*, 858-872.

(4) Libby, W. F. *Journal of Physical Chemistry* **1952**, *56*, 863-868.

(5) Miller, R. J. D.; McLendon, G. L.; Nozik, A. J.; Schmickler, W.; Willig, F. *Surface Electron Transfer Processes*; VCH Publishers, Inc.: Cambridge, 1995.

(6) Marcus, R. J.; Zwolinski, B. J.; Eyring, H. *The Journal of Physical Chemistry* **1954**, *58*, 432 - 437.

(7) Marcus, R. A. *Journal of Chemical Physics* **1956**, *24*, 966-978.

(8) Hush, N. S. *Journal of Chemical Physics* **1958**, *28*, 962-972.

(9) Conway, B. E. *Canadian Journal of Chemistry* **1959**, *37*, 178-189.

(10) Bockris, J. O. M.; Matthews, D. B. *Proc. Roy. Soc. London Ser. A* **1966**, *292*, 479.

(11) Libby, W. F. *Annual Review of Physical Chemistry* **1977**, *28*, 105-110.

(12) Anderson, A. B. *The Journal of Chemical Physics* **1975**, *62*, 1187-1188.

(13) Anderson, A. B.; Grimes, R. W.; Hong, S. Y. *Journal of Physical Chemistry* **1987**, *91*, 4245 - 4250.

(14) Anderson, A. B.; Awad, M. K. *Journal of the American Chemical Society* **1985**, *107*, 7854-7857.

(15) Ray, N. K.; Anderson, A. B. *Surface Science* **1983**, *125*, 803-812.

(16) Ray, N. K.; Anderson, A. B. *Journal of Physical Chemistry* **1982**, *86*, 4851-4852.

(17) Mehandru, S. P.; Anderson, A. B. *Journal of Physical Chemistry* **1989**, *93*, 2044-2047.

(18) Anderson, A. B.; Kötz, R.; Yeager, E. *Chemical Physics Letters* **1981**, *82*, 130-134.

(19) Blyholder, G. *The Journal of Physical Chemistry* **1964**, *68*, 2772 - 2777.

(20) Garfunkel, E. L.; Crowell, J. E.; Somorjai, G. A. *The Journal of Physical Chemistry* **1982**, *86*, 310 - 313.

(21) Biberian, J. P.; Hove, M. A. V. *Surface Science* **1982**, *118*, 443-464.

(22) Russell, J. W.; Overend, J.; Scanlon, K.; Severson, M.; Bewick, A. *Journal of Physical Chemistry* **1982**, *86*, 3066-3068.

(23) Ikezawa, Y.; Saito, H.; Matsubayashi, H.; Toda, G. *Journal of Electroanalytical Chemistry* **1988**, *252*, 395-402.

(24) Holloway, S.; Norskov, J. K. *Journal of Electroanalytical Chemistry* **1984**, *161*, 193-198.

(25) Anderson, A. B. *Journal of Electroanalytical Chemistry* **1990**, *280*, 37-48.

(26) Bockris, J. O. M.; Khan, S. U. M. *Surface Electrochemistry: A Molecular Level Approach*; Plenum Press: New York, 1993.

(27) Marcus, R. A.; Sutin, N. *Biochimica Et Biophysica Acta* **1985**, *811*, 265-322.

(28) Anderson, A. B.; Kang, D. B. *Journal of Physical Chemistry A* **1998**, *102*, 5993-5996.

(29) Anderson, A. B.; Albu, T. V. *Electrochemistry Communications* **1999**, *1*, 203-206.

(30) Anderson, A. B.; Albu, T. V. *Journal of the American Chemical Society* **1999**, *121*, 11855-11863.

(31) Anderson, A. B.; Albu, T. V. *Journal of the Electrochemical Society* **2000**, *147*, 4229-4238.

(32) Cai, Y.; Anderson, A. B. *Journal of Physical Chemistry B* **2005**, *109*, 7557-7563.

(33) Roques, R. M.; Anderson, A. B. *Journal of the Electrochemical Society* **2004**, *151*, E85-E91.

(34) Roques, J.; Anderson, A. B. *Journal of Fuel Cell Science and Technology* **2005**, *2*, 86-93.

(35) Schweiger, H.; Vayner, E.; Anderson, A. B. *Electrochemical and Solid State Letters* **2005**, *8*, A585-A587.

(36) Vayner, E.; Schweiger, H.; Anderson, A. B. *Journal of Electroanalytical Chemistry* **2007**, *607*, 90-100.

(37) Sidik, R. A.; Anderson, A. B. *Journal of Physical Chemistry B* **2006**, *110*, 936-941.

(38) Sidik, R. A.; Anderson, A. B.; Subramanian, N. P.; Kumaraguru, S. P.; Popov, B. N. *Journal of Physical Chemistry B* **2006**, *110*, 1787-1793.

(39) Vayner, E.; Sidik, R. A.; Anderson, A. B.; Popov, B. N. *Journal of Physical Chemistry C* **2007**, *111*, 10508-10513.

(40) Norskov, J. K.; Rossmeisl, J.; Logadottir, A.; Lindqvist, L.; Kitchin, J. R.; Bligaard, T.; Jonsson, H. *Journal of Physical Chemistry B* **2004**, *108*, 17886-17892.

(41) Albu, T. V.; Anderson, A. B. *Electrochimica Acta* **2001**, *46*, 3001-3013.

(42) Anderson, A. B.; Neshev, N. M.; Sidik, R. A.; Shiller, P. *Electrochimica Acta* **2002**, *47*, 2999-3008.

(43) Anderson, A. B. *Electrochimica Acta* **2002**, *47*, 3759-3763.

(44) Anderson, A. B.; Neshev, N. M. *Journal of the Electrochemical Society* **2002**, *149*, E383-E388.

(45) Narayanasamy, J.; Anderson, A. B. *Journal of Electroanalytical Chemistry* **2003**, *554*, 35-40.

(46) Narayanasamy, J.; Anderson, A. B. *Journal of Physical Chemistry B* **2003**, *107*, 6898-6901.

(47) Anderson, A. B.; Sidik, R. A.; Narayanasamy, J.; Shiller, P. *Journal of Physical Chemistry B* **2003**, *107*, 4618-4623.

(48) Kostadinov, L. N.; Anderson, A. B. *Electrochemical and Solid State Letters* **2003**, *6*, E30-E33.

(49) Cai, Y.; Anderson, A. B. *Journal of Physical Chemistry B* **2004**, *108*, 9829-9833.

(50) Anderson, A. B.; Cai, Y. *Journal of Physical Chemistry B* **2004**, *108*, 19917-19920.

(51) Anderson, A. B.; Cai, Y.; Sidik, R. A.; Kang, D. B. *Journal of Electroanalytical Chemistry* **2005**, *580*, 17-22.

(52) Cai, Y.; Anderson, A. B.; Angus, J. C.; Kostadinov, L. N. *Electrochemical and Solid State Letters* **2005**, *8*, E62-E65.

(53) Zhang, T. H.; Anderson, A. B. *Journal of Physical Chemistry C* **2007**, *111*, 8644-8648.

(54) Zhang, T.; Anderson, A. B. *Electrochimica Acta* **2007**, *53*, 982-989.

(55) Anderson, A. B. *Electrochimica Acta* **2003**, *48*, 3743-3749.

(56) Frisch, M. J.; Trucks, G. W.; Schlegel, H. B.; Scuseria, G. E.; Robb, M. A.; Cheeseman, J. R.; J. A. Montgomery, J.; Vreven, T.; Kudin, K. N.; Burant, J. C.; Millam, J. M.; Iyengar, S. S.; Tomasi, J.; Barone, V.; Mennucci, B.; Cossi, M.; Scalmani, G.; Rega, N.; Petersson, G. A.; Nakatsuji, H.; Hada, M.; Ehara, M.; Toyota, K.; Fukuda, R.; Hasegawa, J.; Ishida, M.; Nakajima, T.; Honda, Y.; Kitao, O.; Nakai, H.; Klene, M.; Li, X.; Knox, J. E.; Hratchian, H. P.; Cross, J. B.; Bakken, V.; Adamo, C.; Jaramillo, J.; Gomperts, R.; Stratmann, R. E.; Yazyev, O.; Austin, A. J.; Cammi, R.; Pomelli, C.; Ochterski, J. W.; Ayala, P. Y.; Morokuma, K.; Voth, G. A.; Salvador, P.; Dannenberg, J. J.; Zakrzewski, V. G.; Dapprich, S.; Daniels, A. D.; Strain, M. C.; Farkas, O.; Malick, D. K.; Rabuck, A. D.; Raghavachari, K.; Foresman, J. B.; Ortiz, J. V.; Cui, Q.; Baboul, A. G.; Clifford, S.; Cioslowski, J.; Stefanov, B. B.; Liu, G.; Liashenko, A.; Piskorz, P.; Komaromi, I.; Martin, R. L.; Fox, D. J.; Keith, T.; Al-Laham, M. A.; Peng, C. Y.; Nanayakkara, A.; Challacombe, M.; Gill, P. M. W.; Johnson, B.; Chen, W.; Wong, M. W.; Gonzalez, C.; Pople, J. A.; Gaussian 03, Revision C.02 ed.; Gaussian, Inc.: Wallingford CT, 2004.

(57) Saveant, J. M. *Journal of the American Chemical Society* **1987**, *109*, 6788-6795.

(58) Koper, M. T. M.; Voth, G. A. *Chemical Physics Letters* **1998**, *282*, 100-106.

(59) Calhoun, A.; Koper, M. T. M.; Voth, G. A. *Chemical Physics Letters* **1999**, *305*, 94-100.

(60) Calhoun, A.; Koper, M. T. M.; Voth, G. A. *Journal of Physical Chemistry B* **1999**, *103*, 3442-3448.

(61) Decornez, H.; Hammes-Schiffer, S. *Journal of Physical Chemistry A* **2000**, *104*, 9370-9384.

(62) Hammes-Schiffer, S. *Accounts of Chemical Research* **2001**, *34*, 273-281.

(63) Hammes-Schiffer, S.; Iordanova, N. *Biochimica Et Biophysica Acta-Bioenergetics* **2004**, *1655*, 29-36.

(64) Balbuena, P. B.; Altomare, D.; Vadlamani, N.; Bingi, S.; Agapito, L. A.; Seminario, J. M. *Journal of Physical Chemistry A* **2004**, *108*, 6378-6384.

(65) Balbuena, P. B.; Calvo, S. R.; Lamas, E. J.; Salazar, P. F.; Seminario, J. M. *Journal of Physical Chemistry B* **2006**, *110*, 17452-17459.

(66) Taylor, C. D.; Neurock, M. *Current Opinion in Solid State & Materials Science* **2005**, *9*, 49-65.

(67) Filhol, J. S.; Neurock, M. *Angewandte Chemie-International Edition* **2006**, *45*, 402-406.

(68) Ge, Q. F.; Neurock, M. *Journal of Physical Chemistry B* **2006**, *110*, 15368-15380.

(69) Jinnouchi, R.; Anderson, A. B. *Journal of Physical Chemistry C* **2008**, *112*, 8747-8750.

(70) Jinnouchi, R.; Anderson, A. B. *Physical Review B* **2008**, *77*, 2454170_1-245417_18.

(71) Volkening, S.; Bedurftig, K.; Jacobi, K.; Wintterlin, J.; Ertl, G. *Physical Review Letters* **1999**, *83*, 2672-2675.

(72) Tafel, J. Z. *Physical Chemisty* **1905**, *50A*, 641-712.

(73) Butler, J. A. V. *Proceedings of the Royal Society of London. Series A* **1936**, *157*, 423-433.

(74) Lamy-Pitara, E.; El Mouahid, S.; Barbier, J. *Electrochimica Acta* **2000**, *45*, 4299-4308.

(75) Paliteiro, C.; Correia, E. *Journal of the Electrochemical Society* **2000**, *147*, 3445-3455.

(76) Markovic, N. M.; Grgur, B. N.; Ross, P. N. *Journal of Physical Chemistry B* **1997**, *101*, 5405-5413.

(77) Schmidt, T. J.; Ross, P. N.; Markovic, N. M. *Journal of Electroanalytical Chemistry* **2002**, *524*, 252-260.

(78) Lu, K. E.; Rye, R. R. *Journal of Vacuum Science and Technology* **1975**, *12*, 334-337.

(79) Breakspere, R. J.; Eley, D. D.; Norton, P. R. *Journal of Catalysis* **1972**, *27*, 215-221.

(80) Norton, P. R.; Richards, P. J. *Surface Science* **1974**, *41*, 293-311.

(81) Montano, M.; Bratlie, K.; Salmeron, M.; Somorjai, G. A. *Journal of the American Chemical Society* **2006**, *128*, 13229-13234.

(82) Aryanpour, M.; Rai, V.; Pitsch, H. *Journal of the Electrochemical Society* **2006**, *153*, E52-E57.

(83) Gomez, R.; Orts, J. M.; Alvarez-Ruiz, B.; Feliu, J. M. *Journal of Physical Chemistry B* **2004**, *108*, 228-238.

(84) Anderson, A. B.; Roques, J.; Mukerjee, S.; Murthi, V. S.; Markovic, N. M.; Stamenkovic, V. *Journal of Physical Chemistry B* **2005**, *109*, 1198-1203.

(85) Yeager, E. *Electrochimica Acta* **1984**, *29*, 1527-1537.

(86) Toda, T.; Igarashi, H.; Watanabe, M. *Journal of the Electrochemical Society* **1998**, *145*, 4185-4188.

(87) Markovic, N. M.; Schmidt, T. J.; Grgur, B. N.; Gasteiger, H. A.; Behm, R. J.; Ross, P. N. *Journal of Physical Chemistry B* **1999**, *103*, 8568-8577.

(88) Mukerjee, S.; Srinivasan, S.; Soriaga, M. P.; McBreen, J. *Journal of the Electrochemical Society* **1995**, *142*, 1409-1422.

(89) Mukerjee, S.; Srinivasan, S.; Soriaga, M. P.; McBreen, J. *Journal of Physical Chemistry* **1995**, *99*, 4577-4589.

(90) Iwasita, T.; Xia, X. H. *Journal of Electroanalytical Chemistry* **1996**, *411*, 95-102.

(91) Markovic, N. M.; Ross, P. N. *Surface Science Reports* **2002**, *45*, 121-229.

(92) Stamenkovic, V.; Schmidt, T. J.; Ross, P. N.; Markovic, N. M. *Journal of Physical Chemistry B* **2002**, *106*, 11970-11979.

(93) Uribe, F. A.; Zawodzinski, T. A. *Electrochimica Acta* **2002**, *47*, 3799-3806.

(94) Vukmirovic, M. B.; Zhang, J.; Sasaki, K.; Nilekar, A. U.; Uribe, F.; Mavrikakis, M.; Adzic, R. R. *Electrochimica Acta* **2007**, *52*, 2257-2263.

(95) Panchenko, A.; Koper, M. T. M.; Shubina, T. E.; Mitchell, S. J.; Roduner, E. *Journal of the Electrochemical Society* **2004**, *151*, A2016-A2027.

(96) Roques, J.; Anderson, A. B. *Surface Science* **2005**, *581*, 105-117.

(97) Li, X.; Gewirth, A. A. *Journal of the American Chemical Society* **2005**, *127*, 5252-5260.

(98) Li, X.; Heryadi, D.; Gewirth, A. A. *Langmuir* **2005**, *21*, 9251-9259.

(99) Wei, Y. L.; Wu, K. B.; Wu, Y. H.; Hu, S. S. *Electrochemistry Communications* **2003**, *5*, 819-824.

(100) Kajita, M.; Hikosaka, K.; Iitsuka, M.; Kanayama, A.; Toshima, N.; Miyamoto, Y. *Free Radical Research* **2007**, *41*, 615-626.

(101) Bard, A. J.; Parsons, R.; Jordan, J. *Standard Potentials in Aqueous Solution*; Marcel Dekker Inc.: New York and Basel, 1985.

(102) Shao, M. H.; Liu, P.; Adzic, R. R. *Journal of the American Chemical Society* **2006**, *128*, 7408-7409.

(103) Huber, K. P.; Herzberg, G. *Molecular Spectra and Molecular Structure IV. Constants of Diamtomic Molecules*; Van Nostrand Reinhold Company: New York, 1979.

(104) Vayner, E.; Anderson, A. B. *Journal of Physical Chemistry C* **2007**, *111*, 9330-9336.

(105) Schmidt, T. J.; Stamenkovic, V.; Ross, P. N.; Markovic, N. M. *Physical Chemistry Chemical Physics* **2003**, *5*, 400-406.

(106) Sidik, R. A.; Anderson, A. B. *Journal of Electroanalytical Chemistry* **2002**, *528*, 69-76.

(107) Markovic, N. M.; Ross, P. N. In *Interfacial Electrochemistry*; Wieckowski, A., Ed.; Marcel Dekker Inc.: New York and Basel, 1999.

(108) Damjanovic, A.; Sepa, D. B.; Stojanovic, M.; Vracar, L. M.; Vojnovic, M.; Martinovic, J. *Journal of the Electrochemical Society* **1987**, *134*, C508-C508.

(109) Damjanovic, A.; Conway, B. E.; Sepa, D. B. *Berichte Der Bunsen-Gesellschaft-Physical Chemistry Chemical Physics* **1989**, *93*, 510-513.

(110) Damjanovic, A.; Sepa, D. B. *Electrochimica Acta* **1990**, *35*, 1157-1162.

(111) Damjanovic, A.; Walsh, A. T.; Sepa, D. B. *Journal of Physical Chemistry* **1990**, *94*, 1967-1973.

(112) Climent, V.; Gomez, R.; Orts, J. M.; Feliu, J. M. *Journal of Physical Chemistry B* **2006**, *110*, 11344-11351.

(113) Gouy, G. *Journal de Physique* **1910**, *9*, 457-467.

(114) Chapman, D. L. *Philosophical Magazine* **1913**, *25*, 475-481.

(115) Borukhov, I.; Andelman, D.; Orland, H. *Physical Review Letters* **1997**, *79*, 435-438.

(116) Borukhov, I.; Andelman, D.; Orland, H. *Electrochimica Acta* **2000**, *46*, 221-229.

(117) Otani, M.; Sugino, O. *Physical Review B* **2006**, *73*.

(118) Hammer, B.; Hansen, L. B.; Norskov, J. K. *Physical Review B* **1999**, *59*, 7413-7421.

(119) Kelly, C. P.; Cramer, C. J.; Truhlar, D. G. *Journal of Physical Chemistry B* **2006**, *110*, 16066-16081.

(120) Cai, Y.; Zhang, T.; Anderson, A. B.; Angus, J. C.; Kostadinov, L. N.; Albu, T. V. *Diamond and Related Materials* **2006**, *15*, 1868-1877.

(121) Albu, T. V.; Anderson, A. B.; Angus, J. C. *Journal of the Electrochemical Society* **2002**, *149*, E143-E147.

(122) Anderson, A. B.; Kostadinov, L. N.; Angus, J. C. *Physical Review B* **2003**, *67*.

(123) Eaton, S. C.; Anderson, A. B.; Angus, J. C.; Evstefeeva, Y. E.; Pleskov, Y. V. *Electrochemical and Solid State Letters* **2002**, *5*, G65-G68.

(124) Kalish, R.; Saguy, C.; Cytermann, C.; Chevallier, J.; Teukam, Z.; Jomard, F.; Kociniewski, T.; Ballutaud, D.; Butler, J. E.; Baron, C.; Deneuville, A. *Journal of Applied Physics* **2004**, *96*, 7060-7065.

(125) Goss, J. P.; Briddon, P. R.; Sque, S. J.; Jones, R. *Physical Review B* **2004**, *69*.

(126) Hartree, D. R. *Proceedings of the Cambridge Philosophical Society* **1928**, *24*, 426-437.

(127) Fock, V. *Zeitschrift für Physik* **1930**, *61*, 126-127.

(128) Slater, J. C. *Physical Review* **1930**, *36*, 57-64.

(129) Boys, S. F. *Proceedings of the Royal Society of London. Series A* **1950**, *200*, 542-554.

(130) Pople, J. A.; Beveridge, D. L. *Approximate Molecular Orbital Theory*; McGRAW-Hill Inc, 1970.

(131) Moller, C.; Plesset, M. S. *Physical Review* **1934**, *46*, 618-622.

(132) Thomas, L. H. *Proceedings of the Cambridge Philosophical Society* **1927**, *23*, 542-548.

(133) Fermi, E. *Rendiconti Accademia Nazionale dei Lincei* **1927**, *6*, 602-607.

(134) Slater, J. C. *Physical Review* **1951**, *81*, 385-390.

(135) Hohenberg, P.; Kohn, W. *Physical Review* **1964**, *136*, B864-B871.

(136) Kohn, W.; Sham, L. J. *Physical Review* **1965**, *140*, A1133-A1138.

(137) Ceperley, D.; Alder, B. *Science* **1986**, *231*, 555-560.

(138) Ceperley, D. M.; Alder, B. J. *Physical Review Letters* **1980**, *45*, 566-569.

(139) Perdew, J. P.; Wang, Y. *Physical Review B* **1992**, *45*, 13244-13249.

(140) Vosko, S. H.; Wilk, L.; Nusair, M. *Canadian Journal of Physics* **1980**, *58*, 1200-1211.

(141) Kock, W.; Holthausen, M. C. *A Chemist's Guide to Density Functional Theory, Second Eddition*; WILEY-VCH Verlag GmbH: Weinheim, 2001.

(142) Becke, A. D. *Physical Review A* **1988**, *38*, 3098-3100.

(143) Becke, A. D. *Journal of Chemical Physics* **1993**, *98*, 5648-5652.

(144) Stephens, P. J.; Devlin, F. J.; Chabalowski, C. F.; Frisch, M. J. *Journal of Physical Chemistry* **1994**, *98*, 11623-11627.